Towards a method for detecting the potential genotoxicity of nanomaterials

NANOGEN⬤TOX

D4.2: Transmission electron microscopic characterization of NANOGENOTOX nanomaterials

Final report

Key intrinsic physicochemical characteristics of NANOGENOTOX nanomaterials

June
2012

Co-funded by
the Health Programme
of the European Union

NANOGEN⬤TOX   **Grant Agreement n° 2009 21 01**

NANOGENOTOX

Grant Agreement n° 2009 21 01

WP 4 : Physicochemical Characterization of Manufactured Nanomaterials (MNs) and Exposure Media (EMs)

D4.2: Transmission electron characterization of NANOGENOTOX nanomaterials and comparison with and atomic force microscopy

---

Deliverable leader: NRCWE

Keld Alstrup Jensen

The National Research Centre for the Working Environment (NRCWE),

Lersø Parkallé 105, DK-2100 Copenhagen, DENMARK

National Research Centre
for the Working Environment

Co-funded by
the Health Programme
of the European Union

Workflow	
Author(s)	**Reviewer(s)**
Pieter-Jan de Temmeman and Jan Mast (CODA-CERVA) Camille Guiot and Olivier Spalla (CEA) Davy Rousset (INRS) Boris Shivachev and Mihail Tarassov (IMC-BAS)	WP Leader: Keld Alstrup Jensen (NRCWE) Coordinator: Nathalie Thieret (ANSES)

Document status: v.1   first draft   Creation date: 9/01/2012
                   v.1.1   final draft   Creation date: 5/03/2012
                   v.1.2   revised and reviewed by KAJ   Creation date: 1/06/2012
                   v.1.3   revised by coordination team   Creation date: 11/02/2013
                   v.1.4   revised and reviewed by authors   Creation date: 19/03/2013

Confidentiality level of the deliverable		
PU	Public	
CO	Confidential, only for members of the consortium (including the Commission Services)	CO

1 Introduction

This report presents the final results and description of the standard operation procedures (SOPs) for characterization of manufactured nanomaterials regarding their primary size, size-distribution and particle morphology as individual nano-objects and in the aggregated/agglomerated state. In addition to general data presentation, the report also contains an evaluation of the vial to vial and intra-vial variability using transmission electron microscopy. A section also evaluates the comparability between data obtained by transmission electron microscopy (TEM) and atomic force microscopy (AFM).

The results have been generated during the first two years of the Joint Actions project, NANOGENOTOX, which is funded by the EAHC (Executive Agency for Health and Consumers). Temporary results and SOPs have previously been reported in Guiot et al (2010) and Jensen et al., (2010) as well as in power point presentations at the three General Assembly meetings in Rome (September 2010), Nancy (April 2011) and Copenhagen (October 2011), respectively.

This report fulfils the part of deliverable 4 of the project, which concerns the size and size-distribution analysis using electron and atomic force microscopy. The analyses were made by IMC-BAS (Bulgaria), INRS (France) and CODA-CERVA (Belgium). The complete deliverable is submitted in a number of topical reports and a final summary report.

The complete list of final report series on physico-chemical characterization are listed hereafter:

> D4.1: Summary report on primary physiochemical properties of manufactured nanomaterials used in NANOGENOTOX

> D4.2: Transmission electron characterization of NANOGENOTOX nanomaterials and comparison with and atomic force microscopy

> D4.3: Crystallite size, mineralogical and chemical purity of NANOGENOTOX nanomaterials

> D4.4: Determination of specific surface area of NANOGENOTOX nanomaterials

> D4.5: Surface charge, hydrodynamic size and size distributions by zetametry, dynamic light scattering (DLS) and small-angle X-ray scattering (SAXS) in optimum aqueous suspensions for titanium and silicon dioxide)

> D4.6: Dustiness of NANOGENOTOX nanomaterials using the NRCWE small rotating drum and the INRS Vortex shaker

> D4.7: Hydrochemical reactivity, solubility, and biodurability of NANOGENOTOX MN.

TEM remains an important characterization technique in the perspective of NM characterization. Other imaging techniques such as Scanning Electron Microscopy (SEM) and Atomic Force Microscopy (AFM) are possible alternatives with each of their complementary strengths and weaknesses. Recently a regulatory definition of manufactured nanomaterials (MN) was launched by the EC and says that a nanomaterial is solid particulate compound where at least 50% of the particle number is between 1 and 100 nm along at least one dimension. This definition is currently an issue of debate

4

Co-funded by
the Health Programme
of the European Union

[2-4], but it is agreed that such particlulate MN are minute pieces of matter with defined physical boundaries [3, 5]. In aggregates and agglomerates they are referred to as primary particles [6]. The physical and chemical properties of a NM can be different from the properties of the corresponding bulk material because of quantum and surface effects which are size dependent [7]. The influence of a NM on an organism or cell depends on the characteristics of its aggregates or agglomerates as well as on the size of its primary particles [8, 9]. The size of aggregates and agglomerates but also their morphology and the charge, coating and reactivity of their surface were shown to influence their interactions with biological systems [4, 10-17].

Due to its high resolution and wide-spread use, TEM remains an important characterization technique in the perspective of NM characterization and supporting on e.g. the EC definition [18]. For characterization at least one method, like TEM, should be applied that takes in account the 'dimensionality' of a NM. The EC definition explicitly states 'in one dimension'. Techniques based on scattering, like DLS, and on the measurements of the hydrodynamic radius, like centrifugal sedimentation, reduce 3D information to 1D (e.g. radius of hypothetical sphere') which in unequiaxal NM, like fibers, might lead to erroneous conclusions. Taken in account the 1-nm-resolution is aimed for NM characterisation, TEM is one of the few techniques, in addition to SEM and in specific cases AFM (crf. 4.6), with sufficient resolution. TEM yields number-based results, allows size measurements but also specific shape measurements and characterization of surface topologies on a number basis (per particle), it allows making a distinction between the characterizations of primary particles and of aggregates/agglomerates and has successfully been applied to the NM applied in the nanogenotox project.

Qualitative TEM analysis allows visual evaluation of possible measurement artifacts or bias. It was essential to judge the relevance/suitability of quantitative analyses by TEM and by diffraction based techniques (DLS, PIXE) and differential centrifugation.

TEM is further used to determine the primary particle characteristics. These are relatively robust parameters, which compared to aggregate/agglomerate size, are less influenced by environmental conditions like pH, solvent, sonication, presence of proteins). They correlate well with volume-specific surface area (VSSA) [19] and nano-specific properties. Primary particle size is measured manually. Suitable measurands were selected for this method of measurement.

The size, physical form and morphology of aggregates and agglomerates of dispersed NANOGENOTOX NM were investigated by quantitative (semi-automatic) analysis of aggregated/agglomerated NM based on TEM micrographs. Image analysis techniques, allow on the one hand direct visualization of NM and on the other hand analysis of the size, elongation, curvature of the particle corners and smoothness of the particle surface [20-23]. Bright field transmission electron microscopy (BF-TEM) is combined with systematic random imaging and semi-automatic image analysis to obtain an accurate and representative quantification. The general approach of this methodology is based on NIST guide lines [24]. The different parts of this method supports on different guidelines. Subsampling and suspension of samples can be done according to [24-26]. Imaging and image analysis guidelines are given in [27] [28-30], data analysis and representation can be done supporting on [27-29, 31]. Essential basic general principles of this approach are (i) the traceability of information, imaging and results, (ii) analysis and representation of results on the per-particle level, (iii) (for practicality) automating of repetitive tasks. Multiple, arhythmically complex parameters are measured on the same particle.

Artifacts are examined and interpreted supporting on advanced TEM techniques. Electron tomography allows interpretation of projection artifacts, inevitably associated with conventional TEM by visualization and measurement in 3 dimensions [19]. In this study, we examined the feasibility of three-dimensional visualization of SAS NM in suspension using conventional bright field (BF) ET. We examined whether such materials can be defined as a NM based on the measurement of their VSSA from its electron tomographic reconstruction.

Samples were generally prepared in Millipore water, ethanol, or 0.05% w/v BSA-water and characterized following the dispersion and characterization SOPs presented in the NANOGENOTOX SOP-report [1]. In some cases higher probe sonication amplitudes, durations and mediums and dilution were used to improve the ability of characterization.

6

2 Nanomaterials and information given by suppliers

The tested NANOGENOTOX materials include 6 titania-based products, 5 synthetic amorphous silica products and 6 multi-walled carbon nanotubes (Table 1). Synthetic Amorphous Silica NMs is denoted SAS or SiO_2 in accord with a decision in the NANOGENOTOX Consortium. However, amorphous silica usually is oxygen deficient and may contain other elements and is therefore not SiO_2 *senso stricto*. For titania- and carbon nanotube-based NM, the short used forms are TiO_2 and CNT or MWCNT (Multi-walled CNT).

Table 1. Nanomaterials included in the NANOGENOTOX project and information given by suppliers.

JRC Code	Special notes	Phase	application	Purity wt%	Particle size	BET (m^2/g)	impurity / coating
NM-100	Dry-milled	anatase	paper loadings, rubber, cosmetics, adhesives, low cost interior paints	98.5	200-220 nm	-	-
NM-101		anatase	semiconductor catalyst for use in photocatalytic processes	91(99)*	< 10 nm	>250	9%*
NM-102		anatase	photocatalytic	95	-	90	-
NM-103	hydrophobic	rutile	cosmetics (sun care, colour), pharma, food	89	20 nm	60	Al2O3 6%, silicone - Dimethicone 2%
NM-104	hydrophilic	rutile		90	20 nm	60	Al2O3 6% - Dimethicone 2%
NM-105		rutile/anatase	catalysis, heat stabilizer	-	21 nm	50+/-15	-
NM-200	precipitated	PR-A-02	food, processing	-	15 um	220	10 SiO2 1 H2O, 2% soluble salts
NM-201	precipitated	PR-B-01	Rubber reinforcement, mechanical and optical properties and process	-	-	160	10 SiO2 1 H2O, 1,5% soluble salts
NM-202	thermal	PY-AB-03	inks, adhesives, cosmetics, reinforcement, powder process, food, pharmaceuticals	>99,8	-	170-230	-
NM-203	thermal	PY-A-04	food, cosmetics pharma, reinforcement	-	12 nm	200+/-25	hydrates?
NM-204	Precipitated		food	-	-	140	-

www.nanogenotox.eu

Co-funded by
the Health Programme
of the European Union

JRC Code	Special notes	Phase	application	Purity wt%	CNT tube length	BET (m²/g)	impurity / coating
NM-400	CCVD$^€$	MWCNT	structural composite and energy applications	-	~1.5 um long	250-300	10 wt% oxides/coated with pyrogenic carbon
NM-401	CCVD$^€$	MWCNT	structural composite and energy applications	-	5-15 um long	40-300	~2% amorph. carbon
NM-402	CCVD$^€$	MWCNT	structural composite and energy applications	-	0.1-10 um long	-	<10 wt%
NM-403	CCVD$^€$	MWCNT	structural composite and energy applications	-	1->10 µm long	-	-
NRCWE-006	CCVD$^€$	MWCNT	energy / Li-ion battery	>99.5	segments; 3-5 um long	24-28	
NRCWE-007	CCVD$^€$	MWCNT	structural composites etc.	-	8-15 nm OD; 10-50 um long	233	ca. 3.2 wt% C impurties/ < 1.5wt% ash (Al, Cl, S)

* calcination causes loss of 9 wt% and the residual is 99% pure
$^€$ CCVD : Catalytic Chemical Vapour Deposition

8

3 Sample preparation and analytical methods

3.1 Sample preparation

The generic Nanogenotox dispersion protocol for toxicity testing [32] was modified such that the primary physico-chemical data of the examined NM could be measured optimally with the applied methodology. These modifications include variations of the dispersion media, the NM concentration and the sonication energy.

.Specifically, in CODA-CERVA, the NM were brought in the selected dispersion medium (water or water containing BSA) at a concentration optimized for TEM analysis: 2.56 mg/ml for SAS and titanium dioxide NM, 0.512 mg/ml for CNT. and sonicated for 16 minutes using a Vibracell™ 75041 ultrasonifier (750 W, 20 kHZ, Fisher Bioblock Scientific, Aalst, Belgium) equipped with a 13 mm horn (CV33) at 40% amplitude. This setup resulted in an average horn power of about 26 W and a sample specific energy of 2530 ± 20 MJ/m³. During sonication the samples were cooled in icy water to prevent excessive heating. After sonication, the samples were diluted to a concentration of 0.512 mg/ml.

The suspended NM were brought on pioloform- and carbon- coated, 400 mesh copper grids (Agar Scientific, Essex, England) that were pretreated with 1% Alcian blue (Fluka, Buchs, Switserland) to increase hydrophilicity as described [12].

In IMC-BAS, the NMs were transferred onto carbon-coated copper grids without Alcian blue pretreatment using a special tool - Pt wire loop (0.2 mm Pt wire, one end of which is bent as loop with external diameter of 2.5-3.0 mm). The following operations are carried out during the transferring a suspension onto EM grids:

   (i)   catching a grid by tweezers with reverse action;
   (ii)   disposing the tweezers on a table surface in a way ensuring direct contact of the grid and the filter paper;
   (iii)   careful sinking and extracting the Pt loop in/from the vessel with suspension of nanoparticles in a liquid media (in this stage, a thin film of nanoparticles suspension is formed in the loop space due to the surface tension);
   (iv)   careful touching the Cu grid placed on the filter paper by the Pt loop (in this operation, the whole surface of Cu grid in contact with the Pt loop is covered by nanoparticles while liquid media is absorbed by the filter paper);

NB : (iii-iv) operation can be performed 1 or 2 times (the covered by nanoparticles Cu grid is ready for observation immediately or after a few seconds of drying at an ambient temperature).

For AFM measurements at CEA, stock suspensions are prepared by 20 min sonication at 40 % amplitude of suspensions of respectively, 3.41 g/L NM in HNO_3 10^{-2} mol/L for TiO_2 nanomaterials and 6.82 g/L NM in Millipore water for SiO_2 nanomaterials. For TiO_2 nanomaterials, nanoparticles are deposited on freshly clived mica by dipping it 30s in a 100-fold diluted suspension followed by rinse in pure water. For SiO_2 nanomaterials, mica sheets are preliminary coated with alcian blue before dipping in suspension (25-fold diluted, 2 to 5 min). See appendix for more details.

9

3.2 Recording of electron micrographs

In IMC-BAS, well-contrasted BF images of NM irrespective of their composition were obtained using:

    (i)   a Philips TEM420 at 120 kV acceleration voltage;

    (ii) EM grids with holey carbon support film

    (iii) well calibrated regimes in EM for recording images on photo plates (Kodak electron image film SO-163);

    (iv) appropriate developing of EM films;

    (v) high-resolution scanner technique for transferring the image from EM film into digital file,

    (vi) image processing.

In CODA-CERVA, the samples were imaged in bright field (BF) mode using a Tecnai Spirit TEM (FEI, Eindhoven, The Netherlands) with Biotwin lens configuration operating at 120 kV at spot size 3.

The condenser lens current was chosen such that the beam was parallel and images were taken approximately 500 nm below minimal contrast conditions, where Fresnel fringes were minimal and contrast was judged to be optimal. Microgaphs were recorded using a 4*4 K CCD camera (Eagle, FEI).To achieve maximal traceability of information, each micrograph was stored together with its administrative and sample preparation information and with the information related to its imaging conditions in a dedicated database integrated in the iTEM software (Olympus, Münster, Germany). At several levels, modifications of the TIA image acquisition software (FEI) and of the iTEM software were made to transfer the micrographs and their associated microscope data efficiently in the iTEM database :

    (i)   The TIA protocol for batch conversion of the software-specific SER- and EMI-formats was adjusted to avoid over long file names.

    (ii)   (An imaging C- and libtiff library-based module, referred to as the TIA-TAG module, was developed in iTEM. This module reads the information relevant for image analysis and quality control in the private tags of the TIF image files and renders it accessible in a new information tab of the iTem software. In addition, the TIA TAG module facilitates calibration of images by automatically converting the pixel size from mm scale to nm scale.

    (iii)   New fields were defined in the iTEM database specifying the sample and sample preparation characteristics. Where applicable, drop lists were foreseen to avoid typing errors.

3.3 Qualitative TEM characterization and measurement of the primary particle characteristics

A qualitative description of the NM is provided based on conventional BF electron microscopy. This description includes

    (i)   representative and calibrated micrographs,

    (ii)   the agglomeration- and aggregation status,

    (iii)   the general morphology [4],

    (iv)   the surface topology, (v) the structure (crystalline, amorphous, …)

    (v)   the presence of contaminants and aberrant particles.

To measure the characteristics of primary particles of a NM, the Feret Min and Feret Max were measured in CODA-CERVA following a systematic random sampling based on stereology at an appropriate magnification. Briefly: Micrographs were taken at 10 fixed positions determined by the microscope stage. On these micrographs a grid with a mesh of 100 nm by 100 nm was placed at random. The primary particle on each tenth intersection, counted from left to right was measured. When no particle was located at this intersection, the horizontal grid lines were followed until a primary particle was located on an intersection (Figure 1).

3.4 Quantitative analysis of aggregated/agglomerated NM based on TEM micrographs.

To avoid subjectivity in the selection of particles by the microscopist, the positions on the EM grid where micrographs were taken, were selected randomly and systematically. The grid was placed randomly into the holder and positions distributed evenly over the entire area were predefined by the microscope stage. When the field of view was obscured, e.g. by a grid bar or an artifact, the stage was moved sideways to the nearest suitable field of view.

For NM-200, NM-201, NM-202, NM-203 and for NM-103 and NM-104, three independent samples were analyzed. Per sample, five micrographs were made with a 4*4 k Eagle CCD camera (FEI) at a magnification of 18500 times. For the given microscope and camera configuration, this magnification corresponds with a pixel[1] size of 0.60 nm and a field of view of 2.45 μm by 2.45 μm. This implies a lower particle size detection limit of approximately 6 nm, supporting on the criterion of Merkus [13] that large systematic size deviations can be avoided if the particle area is at least hundred pixels. The field of view limits the upper size detection limit to 245 nm, one tenth of the image size as recommended [27]. To estimate the number of particles required for the estimation of the mean particle diameter with a confidence level, it is assumed that the particle size distribution follows a log-normal size distribution. The minimal number of particles can then be calculated according Matsuda and Gotoh [15, 27]. Their equation allows to calculate the sample size required for the estimation of mean particle diameter with an uncertainty of 5 percent.
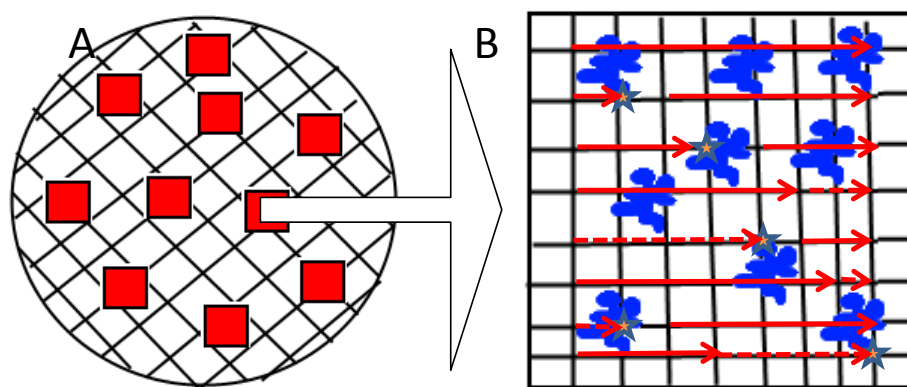

Figure 1 Schematic overview of the systematic random sampling. A) TEM grid with 10 fixed positions

---

[1] A **pixel (picture element)** is a physical point in a raster image, the smallest addressable element in micrograph.

Co-funded by
the Health Programme
of the European Union

indicated by red squares. B) TEM micrograph with a 100 nm by 100 nm mesh grid. Primary particles on the intersections of the grid were measured. The stars indicate the measured primary particles, Full red lines: Counting procedure from left to right until each 10th intersection. Dashed red line: the horizontal grid lines were followed until a primary particle was located on an intersection.

The Feret Max and Feret Min were measured as indicated in Figure 2. The Feret Mean of the particle was calculated as the mean of Feret Min and Feret Max. The aspect ratio was calculated as the ratio of Feret Max and Feret Min.
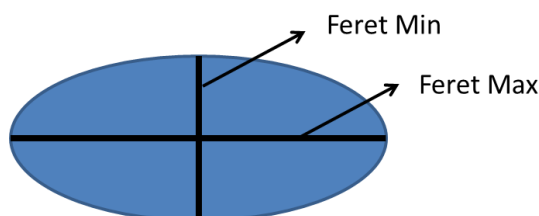

Figure 2 Schematic view of the Feret Min and Feret Max measurements on a primary particle.

The 'Detection module' of iTEM was used for threshold-based detection of the NM. Briefly, the contrast and brightness of the micrographs were optimized, the involved particles were enclosed in a pre-defined frame or region of interest and thresholds were set to separate particles from the background based on their electron density and size. Particles consisting of less than fifty pixels and particles on the border of the frame were omitted from analysis. For each particle, twenty-three quantitative parameters, described in Table 13, are measured and considered relevant for its characterization. Each particle detected in a micrograph was identified by a unique number, written in the overlay of the image. This allowed the selection of data of individual particles and the post-analysis deletion of erroneously detected particles. In general, artifacts were characterized by their morphology and a grey value lower than the mean grey value of the background plus three times its standard deviation. Particles fulfilling this criterion were identified and deleted automatically and particles with an unusual morphology, judged to be artifacts based on visual inspection on the micrographs, were omitted manually from analysis.

In addition to the micrograph related information, the intermediate and annotated images obtained during image analysis and the results and reports of these analyses were stored in the database, linked to the original micrograph.

Descriptive statistics and histograms were calculated in Sigmaplot (Systat, Cosinus computing, Drunen, The Netherlands). The normality of the distributions of the measured parameters was tested with the Shapiro-Wilk and Kolmogorov-Smirnov tests, while the homogeneity of variances was tested with Spearman rank correlation test. Since these assumptions were not met, the non-parametric Kruskal-Wallis one way ANOVA was performed and data were compared pairwise with Dunn's Method to determine the micrograph and sample effects, and to determine the effect of sonication on the number of particles per grid area. The normality of the distributions and the homogeneity of variances were met for the mean values of the median mean diameter, the median sphericity and the median shape factor of the different SAS NM that were obtained in independent analyses. Hence, a one way analysis of variance (ANOVA) was performed and data were compared pairwise with the Tukey test. The measured parameters were classified by principle component analysis using the SAS statistical software (SAS Institute Inc., Cary, NC, USA).

12

Descriptive statistics and histograms were calculated in Sigmaplot (Systat, Cosinus Computing, Drunen, The Netherlands). The normality of the distributions of the measured parameters was tested with the Shapiro-Wilk and the Kolmogorov-Smirnov tests, while the homogeneity of variances was tested with the Spearman rank correlation test. Since these assumptions were not met, the non-parametric Kruskal-Wallis one-way ANOVA was performed and data were compared pairwise with the Dunn's Method to determine the micrograph and sample effects, and to determine the effect of sonication on the number of particles per grid area.

3.5 Transmission electron tomography

The method to characterize SAS NM by ET is described in detail in [19]. Briefly, particle coated grids, mounted in a tomography holder were analyzed using a Tecnai Spirit TEM (FEI) with a BioTWIN lens configuration and a LaB6-filament operating at an acceleration voltage of 120 kV. Series of micrographs (tilt-series) were recorded semi-automatically over a tilt range of at least 65°, or highest angle possible, at intervals of 1 degree. Shift and focus changes were corrected at every interval. Electron micrographs were acquired with a 4*4 k Eagle CCD-camera (FEI) at magnifications of 26,500 times. The tilt series were aligned by iterative rounds of cross correlation. Reconstructions were made using the Simultaneous Iterative Reconstruction Technique (SIRT) algorithm. For visualization in 3D, isosurface rendering and pseudo-coloring was used to visualize the NM surface. This allowed measurement of the surface area of the reconstructed 3D objects and of their enclosed volume.

4 Results

4.1 Sample preparation

By adjusting the charge of the grid, the attachment of the negatively charged SAS NM to the EM grid could be assured (Figure 7). Alcian blue pretreatment introduced positive charges on the surface of pioloform- and carbon-coated grids that tend to have a negative or neutral charge. In our hands, this approach is experienced easier than the alternative based on glow discharging EM-grids with air [33] to introduce negative charges and subsequent Mg^{2+} treatment, introducing positive charges.

In IMC-BAS, the NM were transferred onto carbon-coated grids without Alcian blue treatment using a Pt wire loop (cfr. 3.1).

To obtain homogenous and stable suspensions and a sufficient number of particles per grid surface, the examined SAS and titanium dioxide NM required sonication and dilution.

In a preliminary experiment, the number of particles of representative SAS and titanium dioxide NM (NM-201 and NM-104, respectively) per grid area increased proportionally with sonication time (Figure 3 and Figure 4). For eight and 16 minutes of sonication of NM-201, the total number of detected aggregates was 1564 and 1674, respectively. This was higher than 1366, the number of particles allowing an estimation of the geometric mean particle size with an error of maximum five percent [15, 27]. The corresponding median mean particle diameters were 40 and 39 nm, respectively, and did not differ significantly. For zero, two and four minutes of sonication, the total number of detected aggregates too low (17, 905 and 1220, respectively), such that the median mean diameter for these sonication times could not be evaluated reliably.

For NM-104 (Figure 4) very similar results were obtained. For five and 10 minutes of sonication of NM-104, the total number of detected aggregates was 814 and 927, respectively. This was higher than 795, the number of particles allowing an estimation of the geometric mean particle size with an error of maximum five percent [15, 27]. The corresponding median mean particle diameters were 65 and 67 nm, respectively, and did not differ significantly. Only 17 aggregates were measured for NM-104, therefore the median mean diameter for the unsonicated sample could not be evaluated reliably.

To examine the intrinsic properties of SAS and titanium dioxide NM, samples were diluted in double distilled water allowing high adsorption of the fraction of nano-sized particles to the grid surface. For SAS NM dispersed in water, fifteen to thirty percent of the grid surface was covered by the SAS NM, the particles were homogenously distributed over the grid surface and were well separated with only occasional overlap (Figure 7).

To examine the intrinsic properties of SAS NM, samples were diluted in double distilled water because this medium allowed maximal adsorption of the fraction of nano-sized particles to the grid surface. Moderate salt concentrations, like 10 mM phosphate and 137 mM NaCl in PBS, as well as proteins, provided as 0.05 % BSA or 10 % fetal calf serum, resulted in a reduced number of particles per surface area (Figure 5A), although the size distributions remained unchanged (Figure 5B). This possibly results in the formation of agglomerates that precipitate.
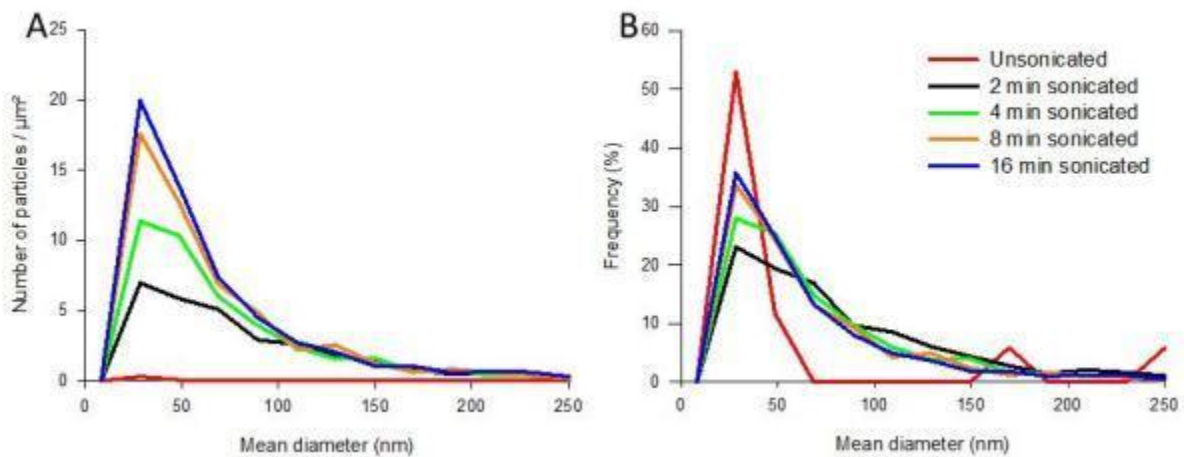
Figure 3 Effect of sonication on the size distribution of the precipitated SAS NM-201. The number of particles per µm² of grid area for a concentration of 0.512 mg/ml (A) and the corresponding frequencies (B) are represented as a function of their mean diameter.

Figure 4 Effect of sonication on the size distribution of the TiO$_2$ NM-104. The number of particles per µm² of grid area for a concentration of 1 mg/ml (A) and the corresponding frequencies (B) are represented as a function of their mean diameter.

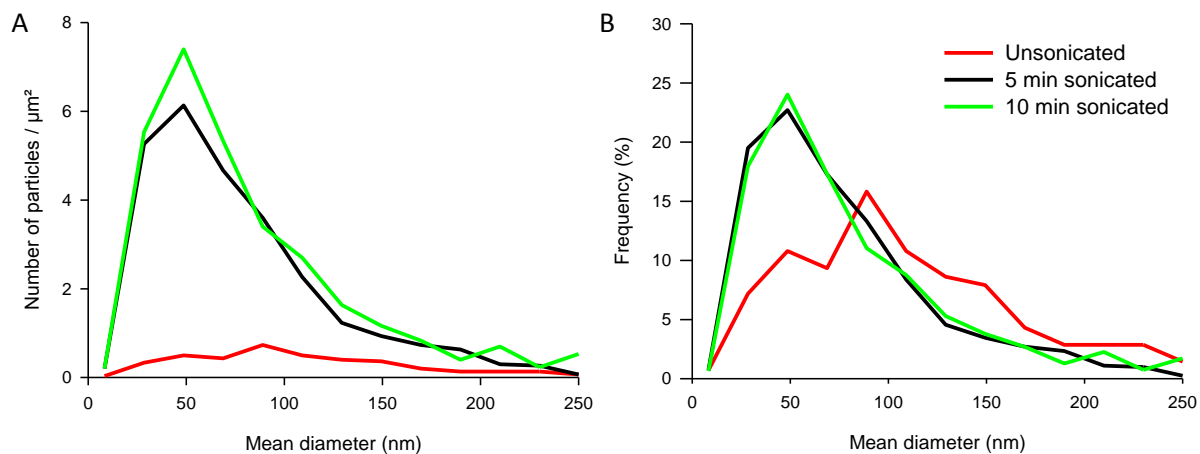*Figure 5 Effect of medium on the size distribution of the precipitated SAS NM-200. The number of particles per µm² of grid area for a concentration of 0.512 mg/ml (A) and the corresponding frequencies (B) are represented as a function of their mean diameter.*
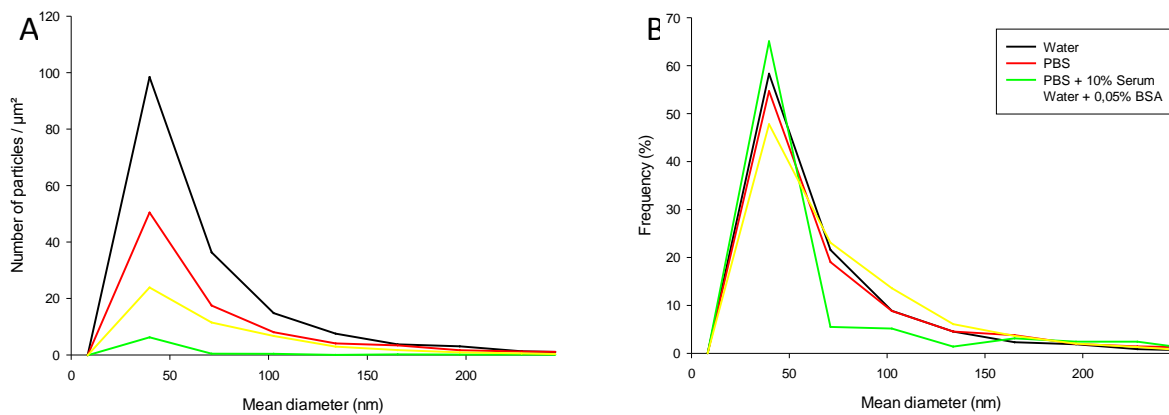
Using this methodology a NMdispersion stable for more than 1 hour were obtained in water and in water containing 0.05 % BSA for SiO_2 NM-200, NM-201, NM-202, NM-203, NM-103 and NM-104 but not for NM-102 and NM-105 (Table 1).

Table 1 Summary of the stabilities* of the dispersions and of the realised TEM analyses of the NM in diverse media

	NM-200	NM-201	NM-202	NM-203	NM-102	NM-103	NM-104	NM-105	NM-400	NM-401	NM-402	NM-403	NRCWE-006	NRCWE-007
Water (glass vial)	green	green	green	green	yellow	green	green	yellow	yellow	yellow	yellow	yellow	yellow	yellow
Water + 0.05 % BSA	green	green	green	green	yellow	yellow	yellow	yellow	green	green	green	green	green	green
Water + 0.05 % BSA + ethanol	green	green	green	green	yellow	yellow	yellow	yellow	white	white	white	white	white	white

* Visible inspection suggested sonication during 16 minutes resulted in a stable dispersion. Prepared dispersions were inspected over a period of 1 hour and did not show alterations.
Green coloured cells represent samples and media where a stable dispersion was obtained. Qualitative and quantitative TEM analyses were realised.
Yellow coloured cells represent samples and media where no stable dispersion was obtained. Only qualitative TEM analyses were realised.
White coloured cells represent samples and media that were not analysed.

4.2 Recording, storage and analysis of micrographs

Because of their relatively low molecular mass and their amorphous structure, the contrast between SAS NM and the background tends to be relatively low when using conventional BF TEM.

In IMC-BAS, well-contrasted BF images of NM could successfully be made irrespective of their composition using: a Philips TEM420 at 120 kV acceleration voltage. The images were recorded on photo plates and scanned using a high-resolution scanner.

In CODA-CERVA, the combination of a Tecnai Spirit TEM (FEI) operating at 120 kV equipped with a Biotwin lens configuration, an objective aperture of 150 nm and a 4*4 k Eagle CCD camera (FEI) allowed recording images of SAS NM in BF mode with a contrast suitable for semi-automatic particle detection and analysis (Figure 7). Because of their relatively high electron density, titanium dioxide NM could readily be distinguished from the background.

A complete traceability of information was obtained by storing the micrographs in a dedicated iTEM database accompanied with their administrative and sample preparation information, with the information related to their imaging conditions and with the (intermediate) results from their analysis. Adaptations of the TIA and iTEM software made the transfer of the micrographs and their associated information to the iTEM database efficient and easy.

For all NM that could be brought into a stable dispersion (Table 1), aggregates and agglomerates could be detected semi-automatically in the micrographs, based on their electron density and analyzed quantitatively. Under the applied imaging conditions the useful range where the particle size can be measured with a precision of 95% [15] contained from 95% to 98% of the detected particles for SAS NM. Two to five percent of the detected particles were larger than the upper boundary of the useful range. Hardly any of the detected particles (< 0.1 %) were smaller than the lower boundary of the useful range.

Differences in the size of primary particles, as illustrated in Figure 7C and Figure 7D for SAS could not be measured. The raw data resulting from such image analyses consist of two-dimensional matrices containing up to multiple thousands of rows (one for each detected particles) by twenty-four columns (particle identification number and twenty-three measured parameters). The corresponding descriptive statistics of twenty-three parameters considered most relevant are presented in

Table 19, Table 20, Table 21,

Table 22,

Table 23 and

Co-funded by
the Health Programme
of the European Union

Table 24.

A representative micrograph of NM-103 was analyzed in CODA-CERVA using three image analysis softwares, namely iTEM, Visilog and ImageJ. Particles in the same micrograph were detected and analyzed semi-automatically (Figure 6). For selected micrograph 130 to 162 particles were detected depending on filters and the exclusion criteria of the particles available in the software.

To be able to compare results between programs, the ECD was selected because this was defined and calculated the same way in all programs. No significant differences in ECD were found between the Image analysis softwares (Table 2).
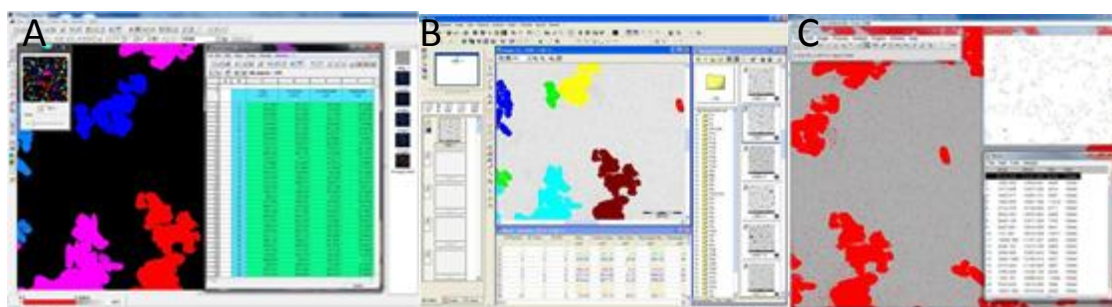

Figure 6 Illustration of the detection and analysis of aggregates with the TEM image analysis software used in the Nanogenotox project. A) Visilog (Noesis, Saint Aubin, France); B) iTEM (Olympus, Münster, Germany) and C) ImageJ (NIH, Berthesda, United States)

Table 2 Qualitative TEM analysis with the iTEM, Visilog and ImageJ software of titanium dioxide NM-103.

Sample	ECD (nm) (N)*
iTEM	64[a] (133)
Visilog	70[a] (130)
Image J	60[a] (162)

* Median Area equivalent circular diameter with the analysed number of particles (N).
[a, b] Different letters indicate significantly different mean values by Kruskal-Wallis One Way Analysis of Variance on Ranks (p < 0,05)
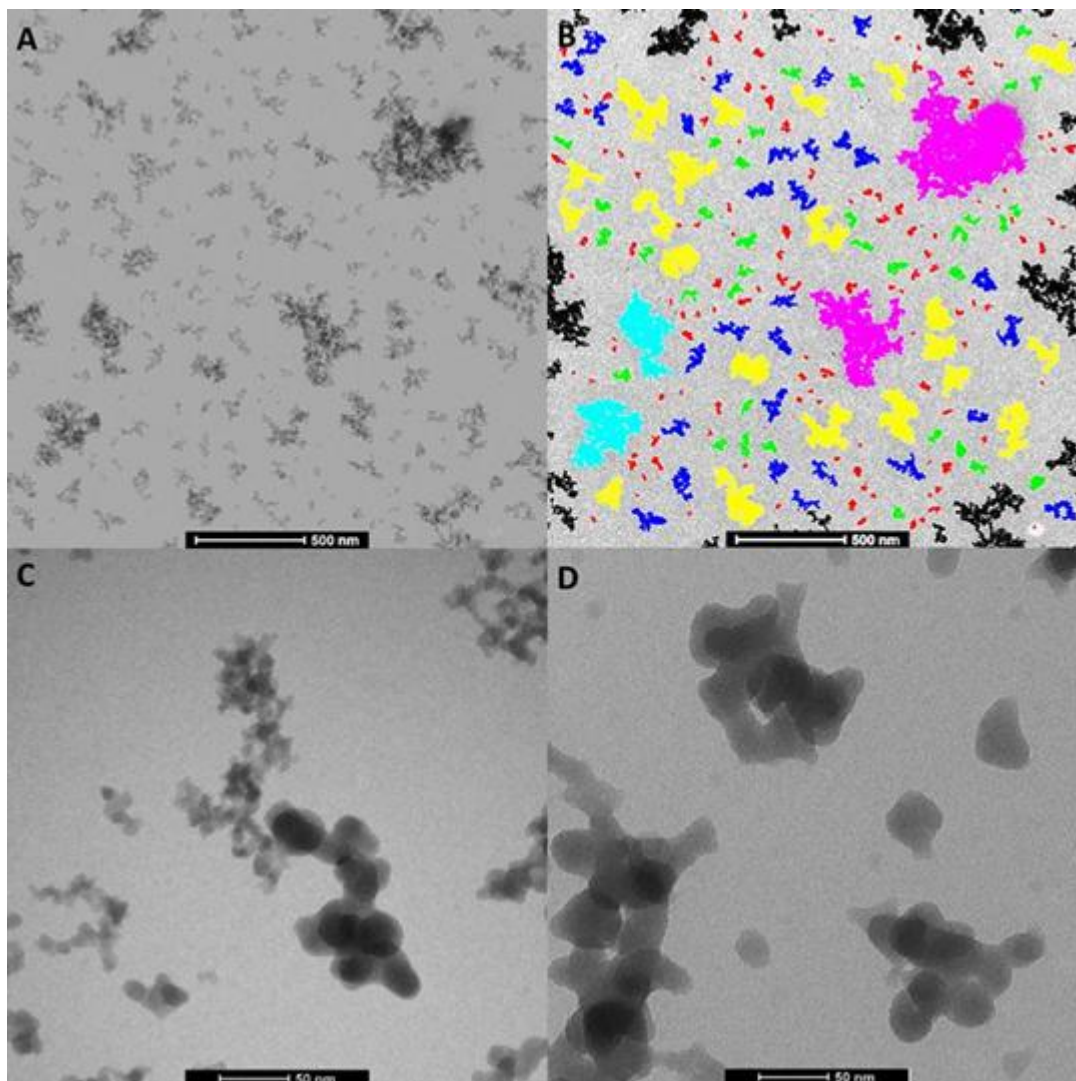
Figure 7 Illustration of the detection of SAS NM-201 based on electron density and detail of the primary particles of NM-201 and NM-203. The NM in the representative electron micrograph (A) are detected, classified by mean diameter and false colour-coded in the corresponding annotated image (B). Red: <50 nm, green: 50 - 70 nm, blue: 70 - 100 nm, yellow: 100 - 200 nm, cyan: 200 - 300, pink: 300 -500 nm and brown: > 500 nm. Particles at the borders of detection region are black and are omitted from analysis. Bar 500 nm. The selected electron micrographs illustrate the primary particles of NM-203 (C) and NM-201 (D). Bar 50 nm.

4.3 Qualitative TEM characterization and measurement of primary particles characteristics

4.3.1 Titanium dioxide

4.3.1.1 Representative micrographs

Representative images of the titanium dioxide nanomaterials are shown in Figure 8, Figure 9, Figure 10, Figure 11, Figure 12 and Figure 13. IMC-BAS prepared samples using the generic NANOGENOTOX dispersion protocol and INRS made dispersion in ethanol [1]. The titanium dioxide particles mainly occur in branched aggregates, with a fractal-like morphology, and minor amounts of singlet spheroidal particles. NM100 contains the largest primary particles and the material consist of mainly aggregated euhedral ca. 50 to 200 nm-size anatase crystals (Figure 8). The average primary particle size of NM100 is on the order of 50 to 150 nm, depending on the laboratory (Table 3).
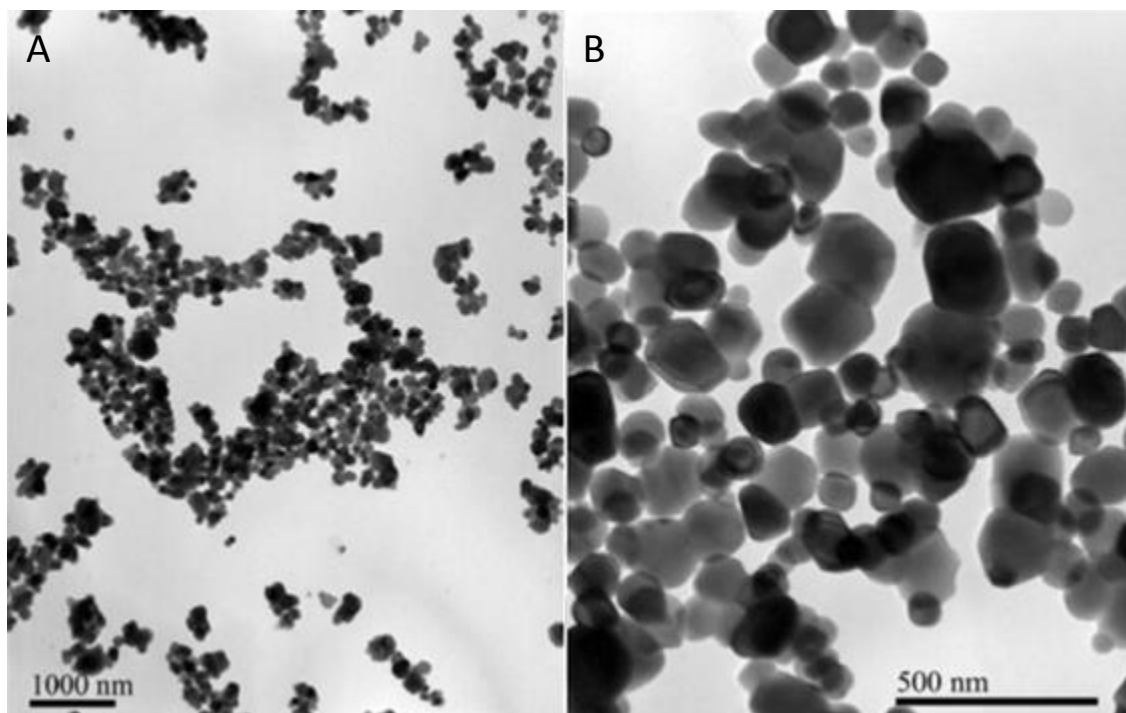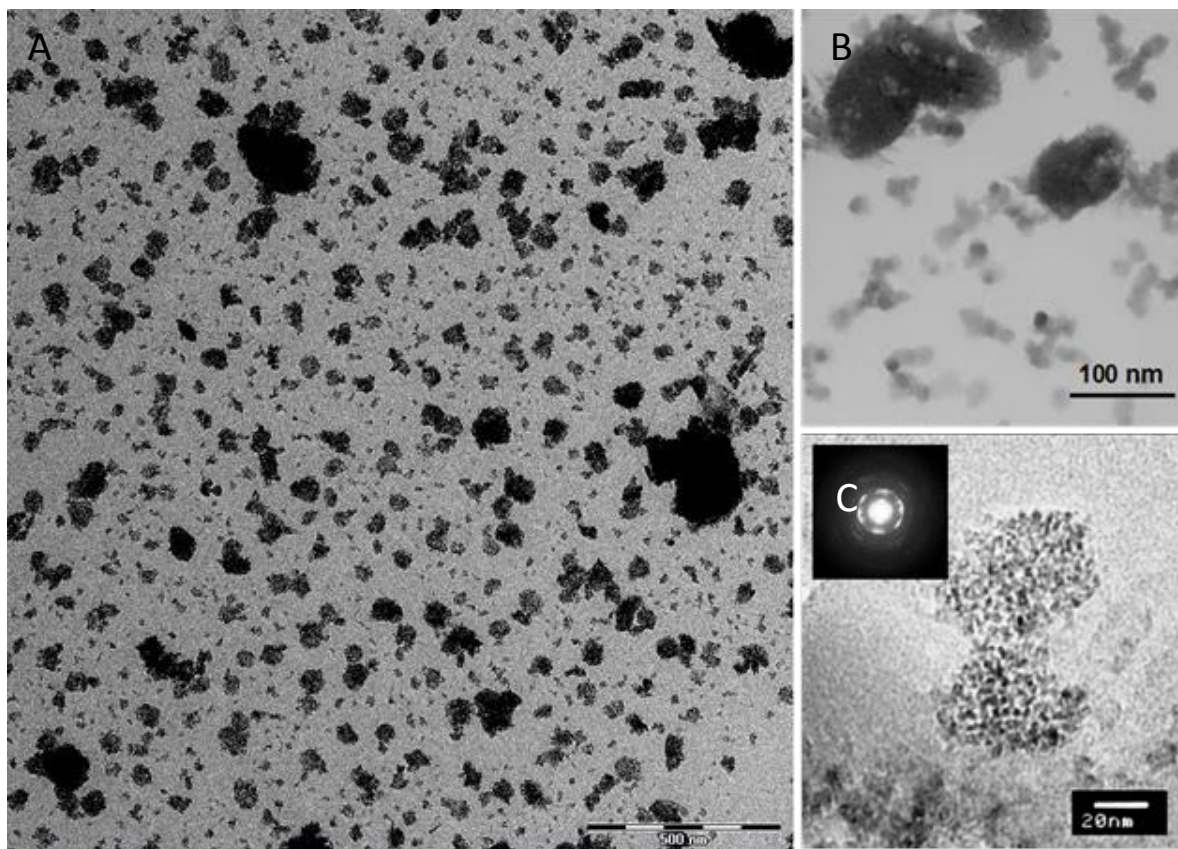

Figure 8 NM100: A) Representative TEM-micrograph showing the range in agglomerate and aggregate sizes and typical euhedral morphology of the individual crystallites in the sample. B) selected TEM-micrograph taken at higher resolution illustrating the aggregates are mainly aggregates sintered at crystal facets.

23

Co-funded by
the Health Programme
of the European Union

Figure 9 NM101: A) Representative TEM-micrograph showing the range in agglomerate and aggregate sizes B) Selected TEM-micrograph showing that the sample contains two different aggregate types. One type consists of aggregates of 10-20 nm-size primary particles. The second type consists of coarser ca. 100 nm or larger, dense and rounded aggregates. B) Image taken at higher resolution showing that the aggregates consist of ca. 5 nm-size crystallites. Insert shows the electron diffraction pattern of anatase.

4.3.1.2 Primary particle measurements

NM101 contains the smallest primary crystallites among the titanium dioxide NM (Figure 9). The average crystallite size was 5 to 6 nm, depending on the laboratoryTable 3.In addition, NM101 contains two types of particles of which one type is 10-20 nm size and occurs in small aggregates and the other are coarser aggregates of very small crystallites (5 nm).

The aggregate texture and particle morphology in NM-102, NM-103 and NM-104 is quite comparable to the one observed in NM101. The only difference is the larger sizes of the primary particles (21 to 26 nm) (Table 3, Table 4 and Table 5) and the presence of only one general particle type. A fraction of the crystallites in NM103 and NM-104, however, has a more elongated morphology, where NM-104 may be even more elongated than NM-103. This difference may be due to crystallographic differences between rutile (NM-103 and NM-104) and anatase (NM-100, NM-101 and NM-102).

NM105 consist of a mixture between anatase and rutile. The sample reveals two particle size-populationsTable 3. Rutile has been found to have a smaller crystallite size (15 nm) than anatase (21 nm) with an average size on the order of 21 to 24 nmTable 3.
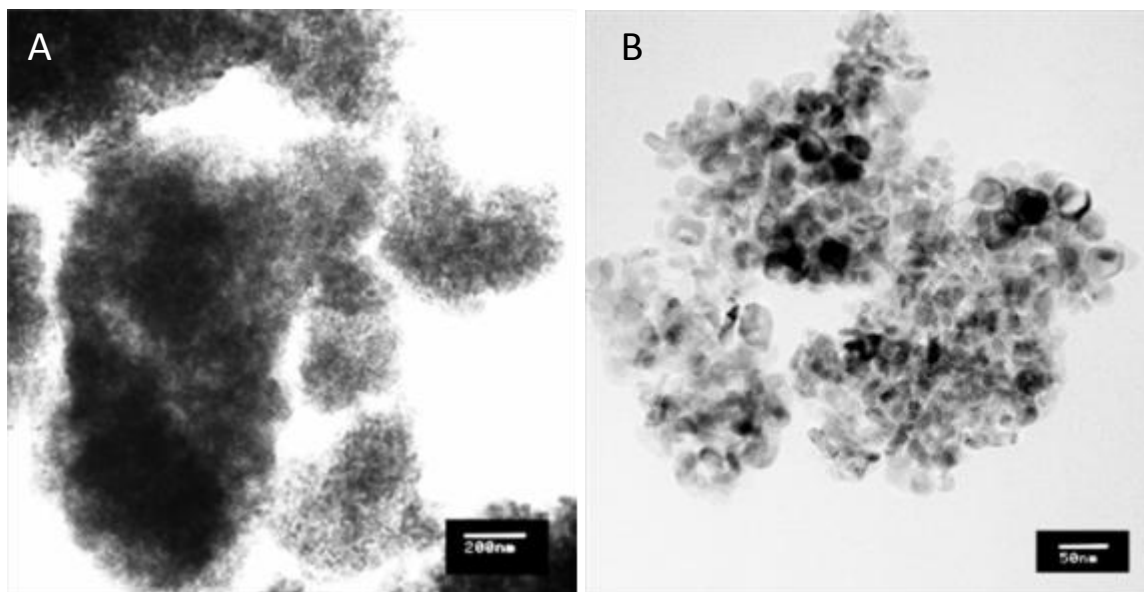
Figure 10 NM102: A) Selected TEM image showing the typical 100 to 500 nm-size aggregates/agglomerates in the sample. B) Selected Higher resolution TEM-image showing the nanocrystalline anatase aggregates with individual crystallite sizes typically smaller than 50 nm.
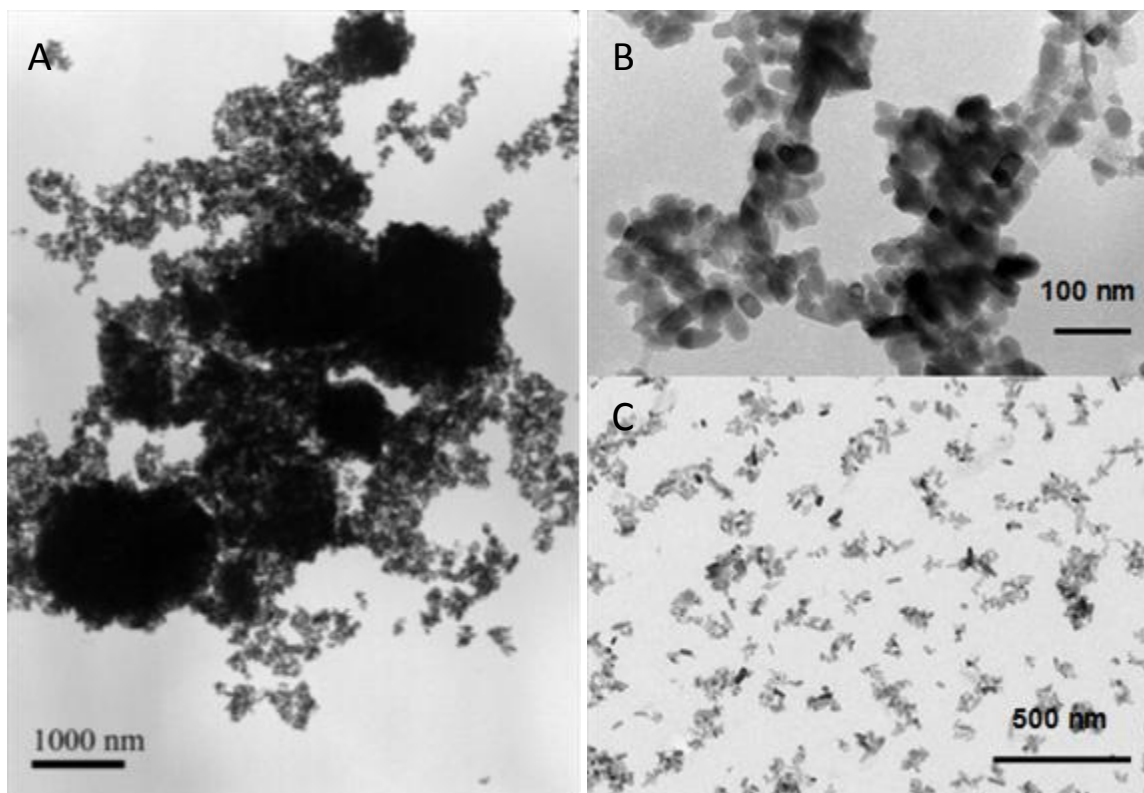

Figure 11 NM103: Selected TEM micrographs showing the range from coarse μm-size aggregates (A) to small nanosize (B) in the sample. C) Representative TEM-Micrograph illustrating well-dispersed titanium dioxide aggregates showing typical aggregate/agglomerate size of 100 to 200 nm. Individual single nanoparticles are also present. Primary particles are typically smaller than 20 nm along the shortest dimensions. Note the elongated morphology of several particles.
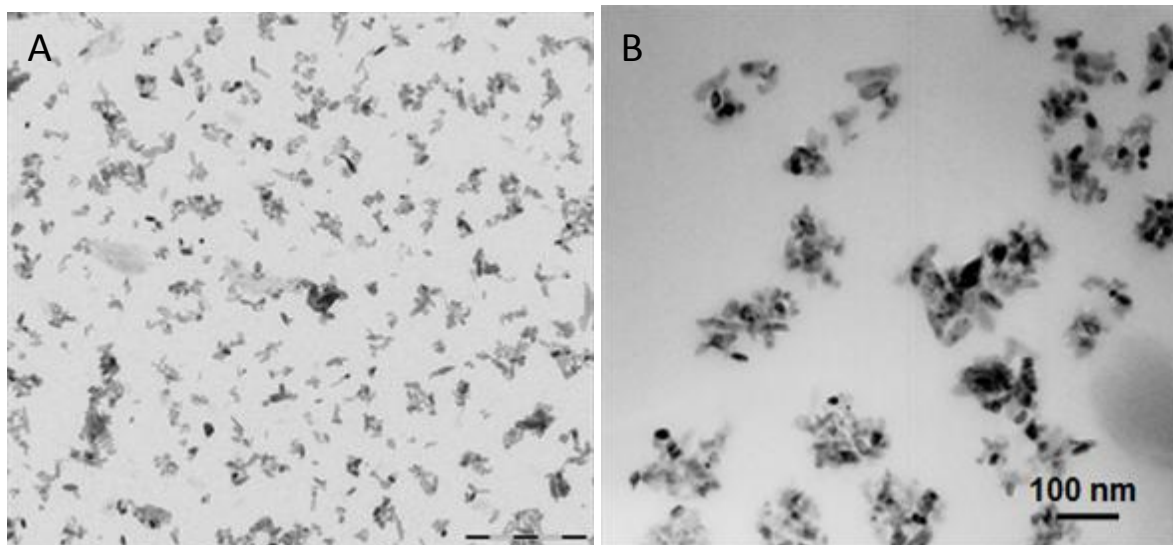
25

Figure 12 NM104: A) Representative TEM micrograph showing the typical aggregate/agglomerate size in the sample (Bar is 500nm). B) TEM micrograph showing a close-up of the aggregates showing the presence of equidimensional euhedral and some elongated crystals of rutile.
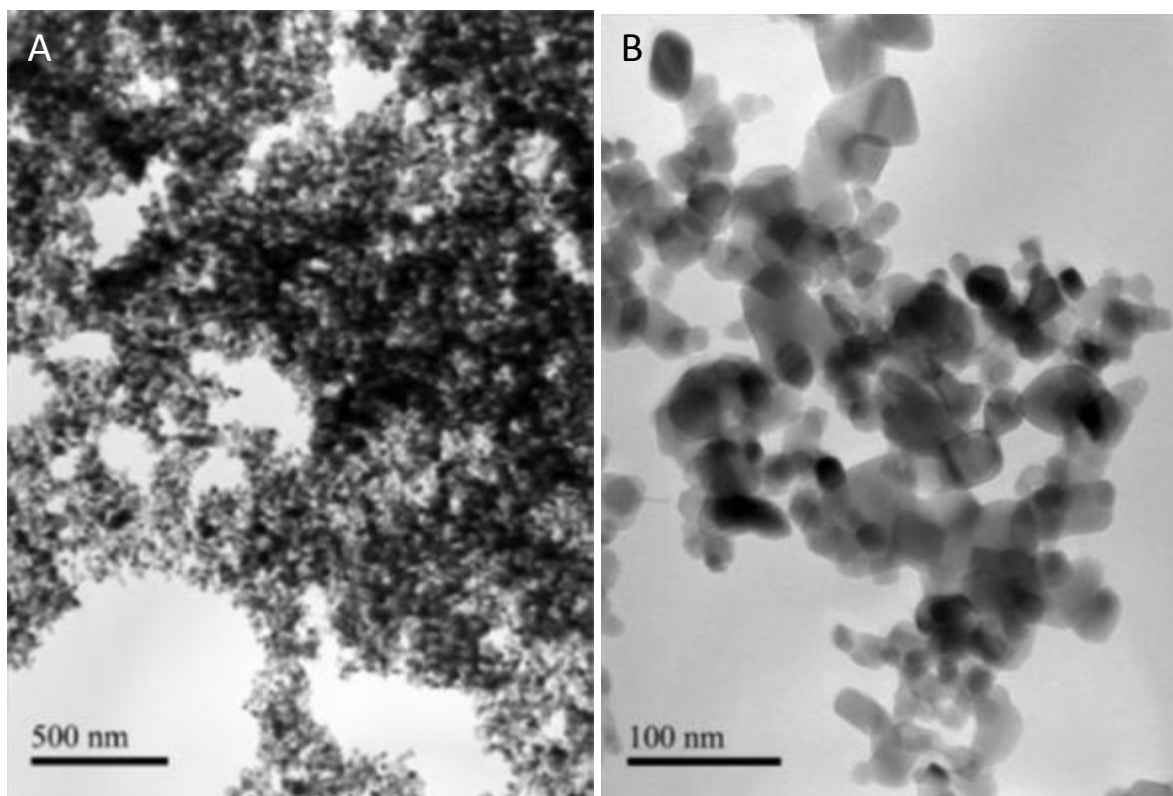

Figure 13 NM105: A) TEM micrograph showing a higly agglomerated and aggregated titanium dioxide. (Bar is 500nm). B) Close-up of an aggregate showing that it mainly consists of equidimensional to weakly elongated euhedral of rutile.

26

Table 3 Primary particle area equivalent circular diameter of the titanium dioxide NM analysed by different partners.

Sample	ECD (nm) ± SD (N); CODA-CERVA	ECD (nm) ± SD (N); INRS	Diameter (nm); IMC-BAS
NM-100	50-90*		116.9 $\pm$ 36.8**
NM-101	6*		4.5 $\pm$ 0.6**
NM-102	21 ± 10 (1395)	22 ± 6 (100)	~22*
NM-103	26 ± 10 (1317)	26 ± 6 (101)	23.7 $\pm$ 5.9**
NM-104	26 ± 10 (1099)	26 ± 7 (100)	~23*
NM-105	21 ± 9 (1421)	24 ± 5 (105)	Anatase 20.5 $\pm$ 8.6** Rutile ~ 15*

* Manual measurement
** Manual measurement using ImageJ software.

4.3.1.3 Interlaboratory comparison of primary particle characteristics

NM-103 contains small elongated prismatic primary particles with an aspect ratio of 1,7 - 1.8 measured in their projection in EM images and a short size (Feret Min) of 19 - 24 nm, depending on the used methodology. All analyzed primary particles were smaller than 100 nm (Table 4). The Feret Mean and Feret Max of these particles were lognormal distributed, Feret min and Aspect ratio were lognormal distributed for semi-automatic measurements but not for manual measurements (Figure 14) (CODA-CERVA). Significant differences were found between manual and semi-automatic measurements (p = 0.02). The Feret min, Feret Max, Feret Mean and Aspect ratio of these particles manually measured in IMC-BAS were found to be lognormal distributed.

Table 4 Primary particle Feret Min, Feret Max, Feret Mean, percentage of particles with a Feret Min lower than 100 nm and Aspect ratio of NM-103

Lab	Feret Min ± SD (nm)*	Feret max ± SD (nm)*	Feret mean ± SD (nm)*	< 100 nm	Aspect ratio ± SD *	n
CODA-CERVA (Man)	21,9 ± 1,4 [a]	37,9 ± 1,6 [a]	30,1 ± 1,5 [a]	100 %	1,7 ± 1,3 [a]	40
CODA-CERVA (Auto)	19,2 ± 1,4 [b]	32,5 ± 1,6 [b]	27,1 ± 1,5 [a]	100 %	1,7 ± 1,3 [a]	1317
IMC-BAS (Man)	23.7 $\pm$ 5.9**	42.8 $\pm$ 15.0**	33.3 $\pm$ 9.4**	100 %	1.82+0.53**	440

* Geometric mean ± the geometric standard deviation (SD) [15]
[a, b] Different letters indicate significantly different mean values by Kruskal-Wallis One Way Analysis of Variance on Ranks (p < 0,05)
** Arithmetic mean ± the standard deviation

NM-105 contains small ellipsoidal primary particles with an aspect ratio of 1,3 and a size of 17 - 19 nm, depending on the used methodology. All analyzed primary particles were smaller than 100 nm (Table 5). The Feret Min (Figure 15), Feret Mean and Feret Max of these particles were lognormal distributed, Aspect ratio were lognormal distributed for semi-automatic measurements but not for

27

manual measurements. No significant (p < 0,05) differences were found between manual and semi-automatic measurements.

Table 5 Primary particle Feret Min, Feret Max, Feret Mean, percentage of particles with a Feret Min lower than 100 nm and Aspect ratio of NM-105.

Lab	Feret Min ± SD (nm)	Feret max ± SD (nm)	Feret mean ± SD (nm)	< 100 nm	Aspect ratio	n
CODA-CERVA (Man)	19,0 ± 1,5 [a]	25,8 ± 1,4 [a]	22,6 ± 1,4 [a]	100 %	1,36 ± 1,3 [a]	47
CODA-CERVA (Auto)	17,3 ± 1,5 [a]	24,2 ± 1,4 [a]	21,6 ± 1,5 [a]	100 %	1,36 ± 1,2 [a]	1421

* Geometric mean ± the geometric standard deviation (SD) [15]

[a, b] Different letters indicate significantly different mean values by Kruskal-Wallis One Way Analysis of Variance on Ranks (p < 0,05)
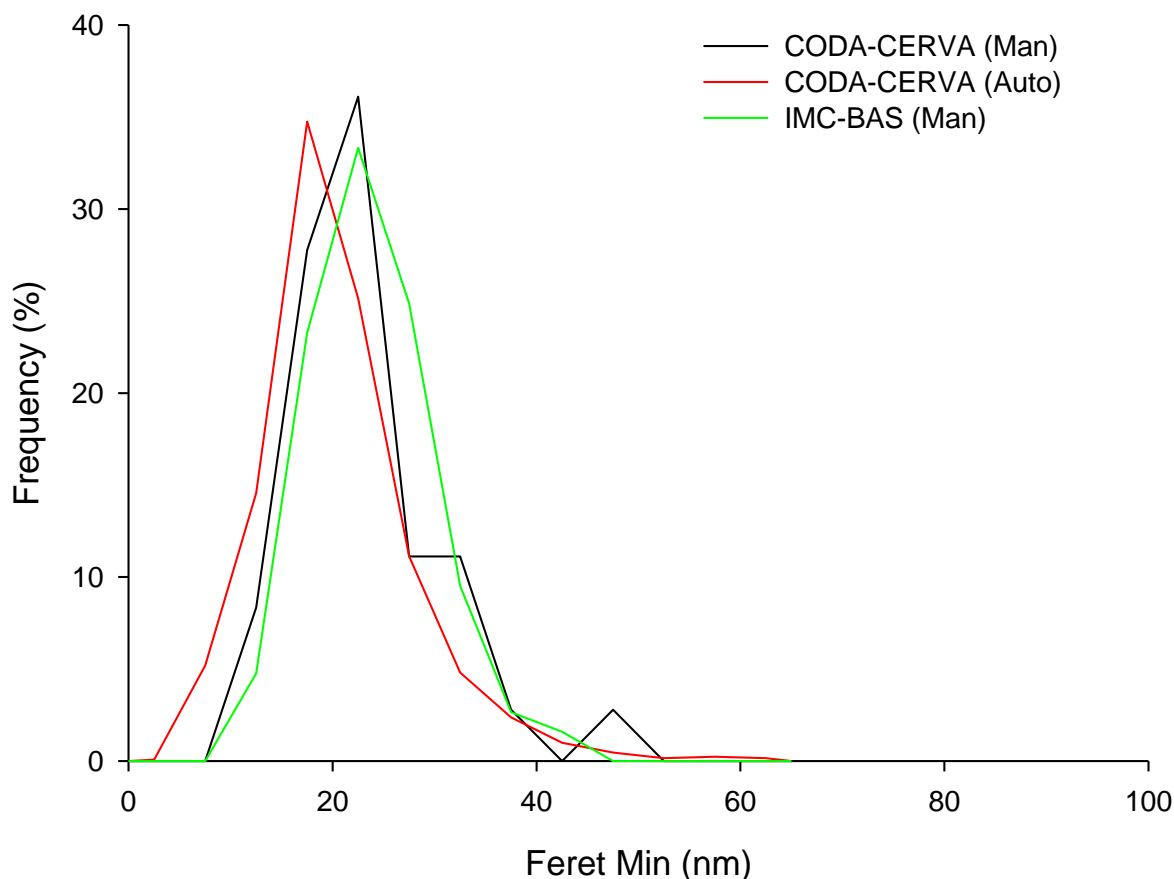
Figure 14 Qualitative TEM image analysis of TiO2 NM-103. Graph illustrates the primary particle Feret Min size distribution in function of the frequency. The manual measurements (IMC-BAS (Man) and CODA-CERVA (Man)) and the semi-automatic measurement (CODA-CERVA (Auto))are given.
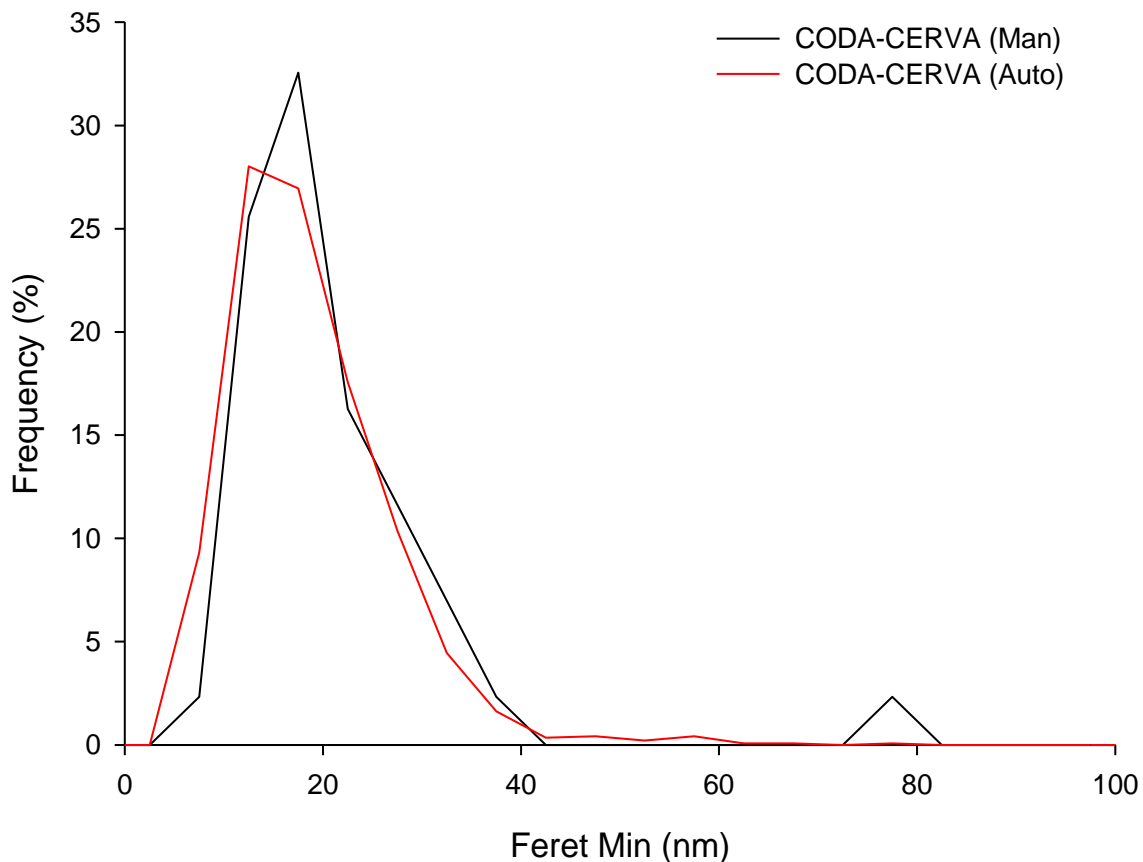
Figure 15 Qualitative TEM image analysis of TiO2 NM-105. Graph illustrates the primary particle Feret Min size distribution in function of the frequency. The manual measurement (CODA-CERVA (Man)) and the semi-automatic measurement (CODA-CERVA (Auto))are given.

4.3.2 SAS nanomaterials

Representative TEM overview images of the SAS particles dispersed in water are shown in Figure 16, Figure 17, Figure 18, Figure 19 and Figure 20. IMC-BAS prepared samples using the generic NANOGENOTOX dispersion protocol and INRS made dispersion in ethanol [1].

4.3.2.1 Representative micrographs

Figure 16 NM-200: A) Representative TEM micrograph of well-dispersed sample taken for quantitative TEM-analysis (Scale bar is 500nm). B) selected TEM micrograph showing the complex structure of SAS aggregated (Scale bar is 100 nm).

Figure 17 NM-201: A) Representative TEM micrograph of well-dispersed sample taken for quantitative TEM-analysis (Scale bar is 500nm). B) TEM micrograph showing the complex open network structure in the SAS aggregates (Scale bar is 100 nm).

Figure 18 NM-202: A) Representative TEM micrograph of well-dispersed sample taken for quantitative TEM-analysis (Scale bar is 500nm). B) TEM micrograph showing the complex open network structure in the SAS aggregates (Scale bar is 100 nm).
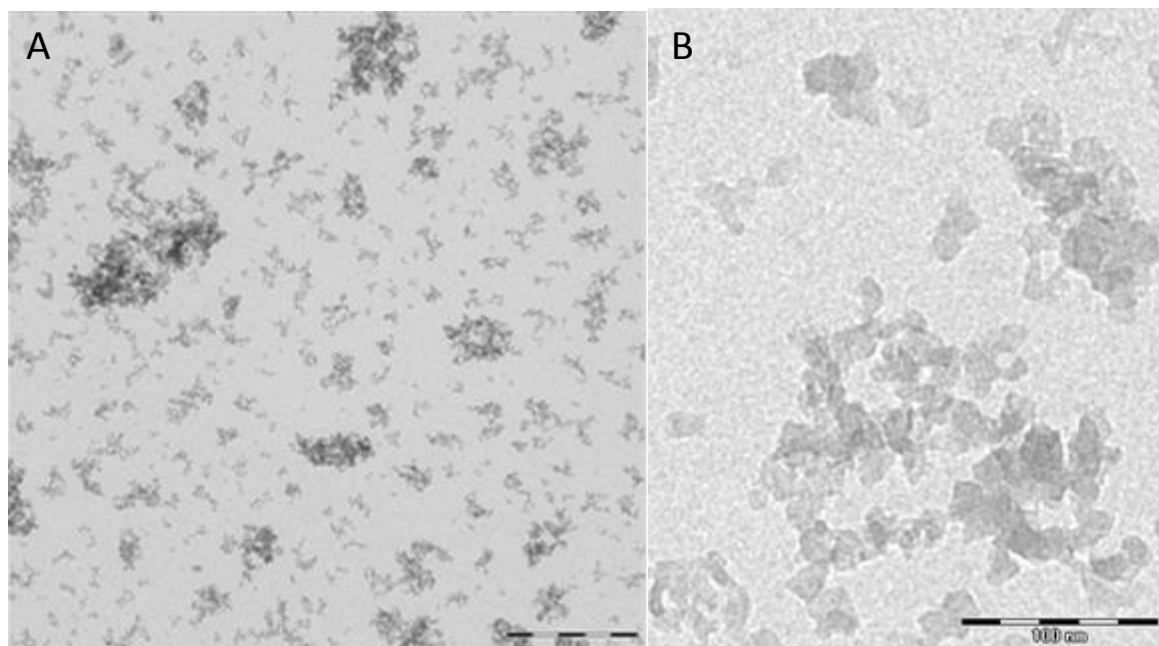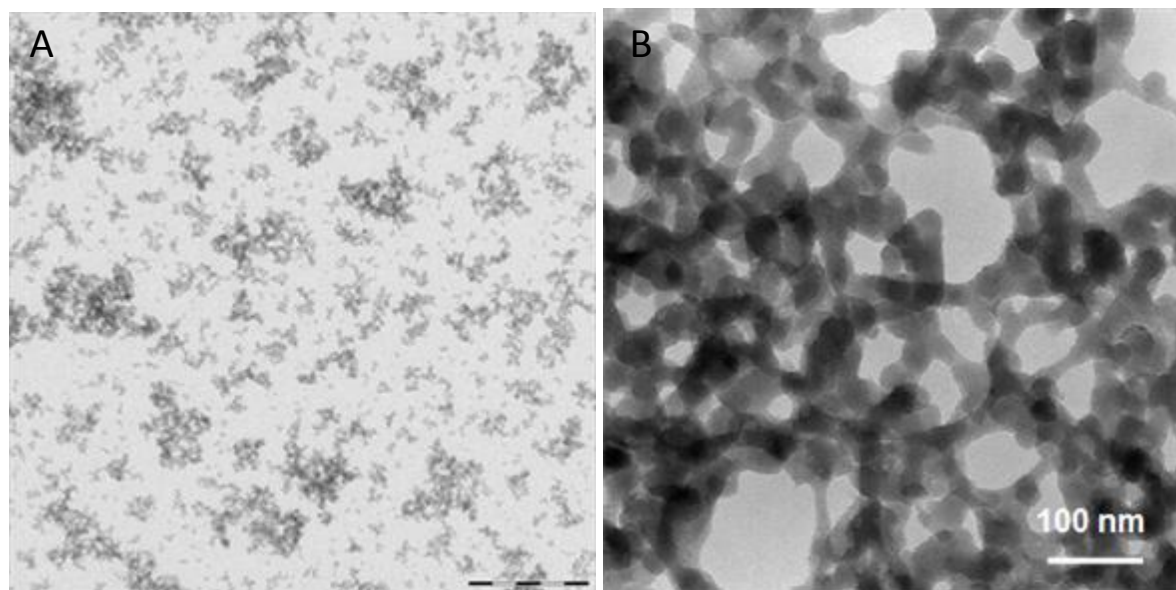

Figure 19 NM-203: A) Representative TEM micrograph of well-dispersed sample taken for quantitative TEM-analysis (Scale bar is 500nm). B) TEM micrograph showing the complex open network structure in the SAS aggregates (Scale bar is 100 nm).
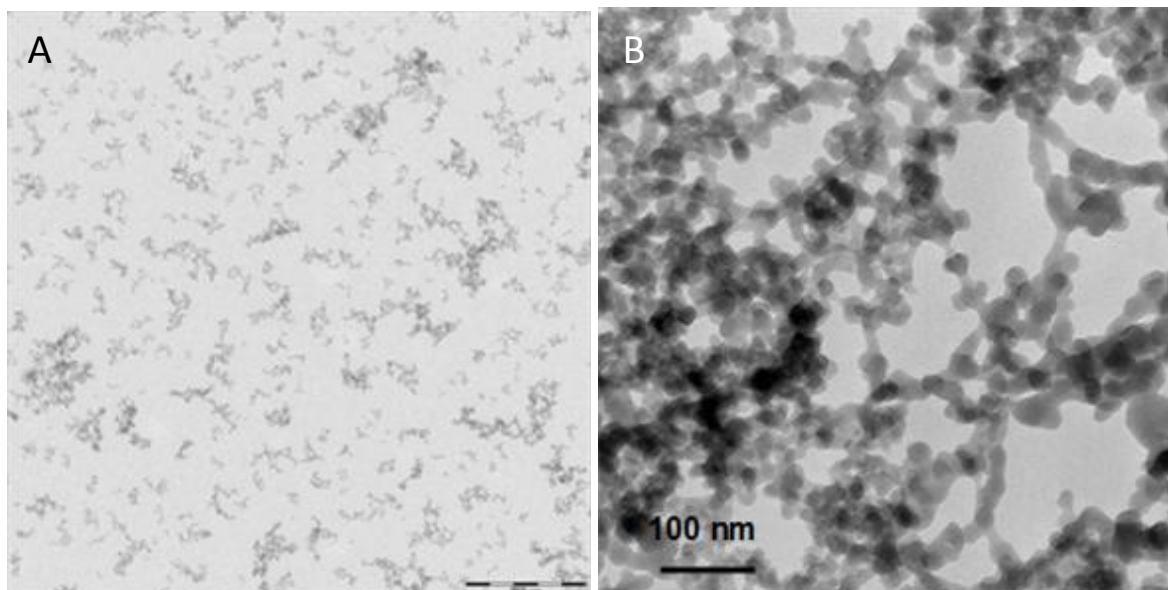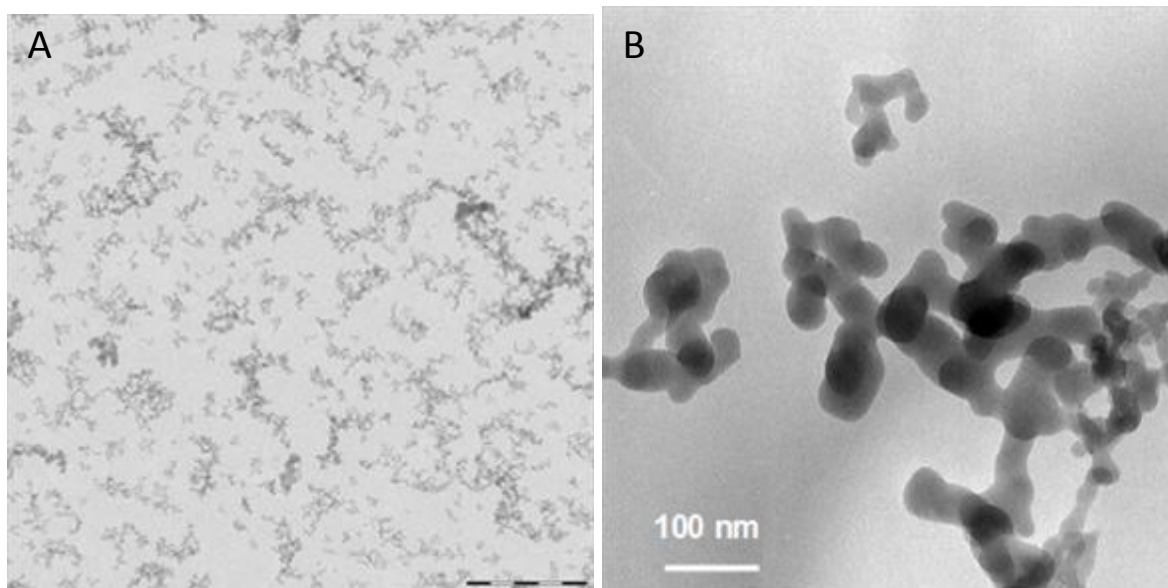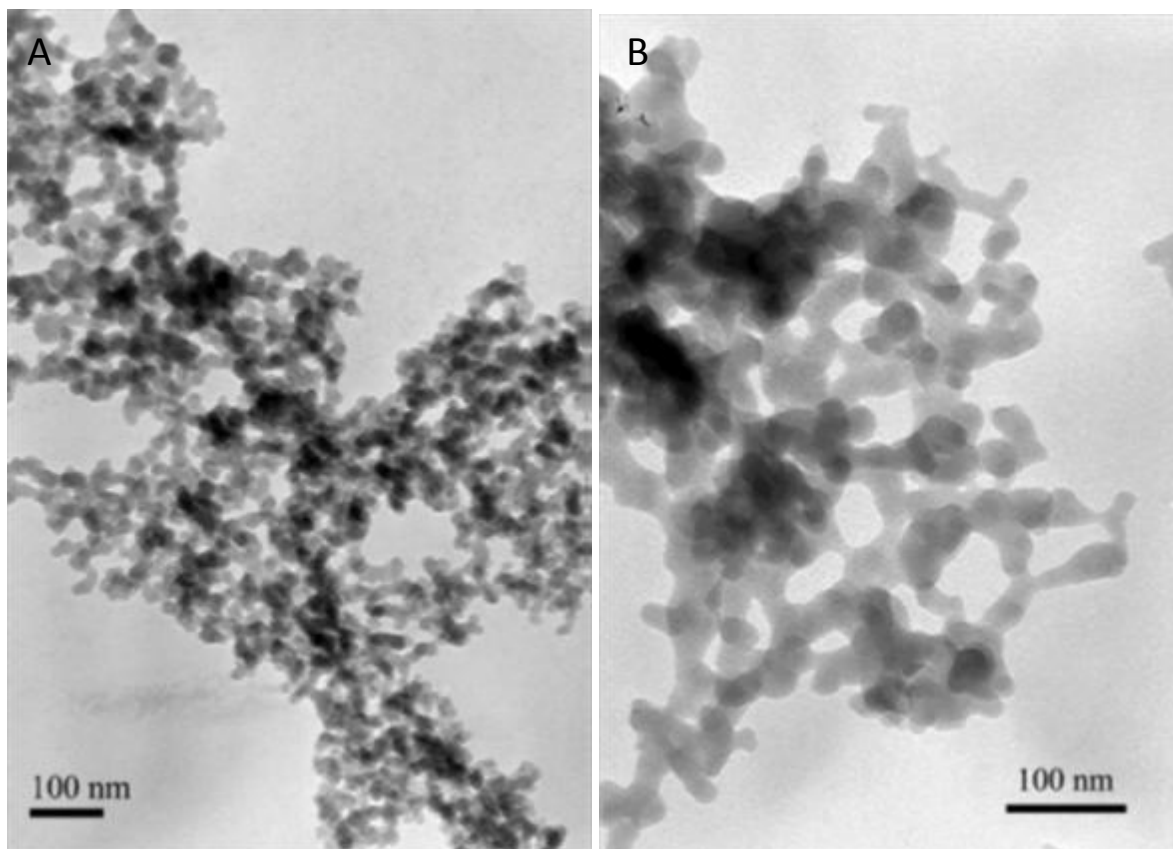
Figure 20 NM-204: A) Representative TEM micrograph of typical SAS aggregate (Scale bar is 500nm). B) TEM micrograph showing the complex open structure of the SAS nanomaterials (Scale bar is 100 nm).

4.3.2.2 Primary particle measurements

Table 6 Primary particle size of the SAS NM analysed by different partners

Sample	ECD (nm) ± SD (N); CODA-CERVA	ECD (nm) ± SD (N); INRS	Diameter (nm); IMC-BAS
NM-200	14 ± 7 (1876)	23 ± 8 (100)	18
NM-201	17 ± 8(1726)	19 ± 4 (100)	18
NM-202	15 ± 7 (401)	18 ± 3 (105)	20
NM-203	13 ± 6 (448)	16 ± 3 (105)	45
NM-204	10 – 15*		19

* Manual measurement

4.3.2.3 Interlaboratory comparison

NM-201 contains small ellipsoidal primary particles with an aspect ratio of 1,4 and a size of 13 - 14 nm, depending on the used methodology. All analyzed primary particles were smaller than 100 nm (Table 7). The Feret Min (Figure 21), Feret Mean, Feret Max and Aspect Ratio of these particles were lognormal distributed, were lognormal distributed for manual measurements but not for semi-

automatic measurements. No significant (p < 0,05) differences were found between manual and semi-automatic measurements.

Table 7 Primary particle, Feret Min, Feret Max, Feret Mean, percentage of particles with a Feret Min lower than 100 nm and Aspect ratio of NM-201

Lab	Feret Min ± SD (nm)	Feret max ± SD (nm)	Feret mean ± SD (nm)	< 100 nm	Aspect ratio	n
CODA-CERVA (Man)	12,7 ± 1,3 [a]	17,9 ± 1,4 [a]	15,4 ± 1,3 [a]	100 %	1,4 ± 1,3 [a]	42
CODA-CERVA (Auto)	13,9 ± 1,5 [a]	19,4 ± 1,6 [a]	17,0 ± 1,6 [a]	100 %	1,4 ± 1,2 [a]	1726

* Geometric mean ± the geometric standard deviation (SD) [15]
[a, b] Different letters indicate significantly different mean values by Kruskal-Wallis One Way Analysis of Variance on Ranks (p < 0,05)

NM-203 contains small ellipsoidal primary particles with an aspect ratio of 1,4 – 1,5 and a size of 10 - 11 nm, depending on the used methodology. All analyzed primary particles were smaller than 100 nm (Table 8). The Feret Min (Figure 22), Feret Mean, Feret Max and Aspect Ratio of these particles were lognormal distributed, were lognormal distributed for manual measurements but not for semi-automatic measurements. No significant (p < 0,05) differences were found between manual and semi-automatic measurements.

Table 8 Primary particle, Feret Min, Feret Max, Feret Mean, percentage of particles with a Feret Min lower than 100 nm and Aspect ratio of NM-203

Lab	Feret Min ± SD (nm)	Feret max ± SD (nm)	Feret mean ± SD (nm)	< 100 nm	Aspect ratio	n
CODA-CERVA (Man)	10,4 ± 1,5 [a]	16,3 ± 1,5 [a]	13,5 ± 1,5 [a]	100 %	1,5 ± 1,4 [a]	44
CODA-CERVA (Auto)	10,8 ± 1,5 [a]	15,6 ± 1,5 [a]	13,5 ± 1,5 [a]	100 %	1,4 ± 1,2 [a]	448

* Geometric mean ± the geometric standard deviation (SD) [15]
[a, b] Different letters indicate significantly different mean values by Kruskal-Wallis One Way Analysis of Variance on Ranks (p < 0,05)

Figure 21 Qualitative TEM image analysis of TiO2 NM-201. Graph illustrates the primary particle Feret Min size distribution in function of the frequency. The manual measurement (CODA-CERVA (Man)) and the semi-automatic measurement (CODA-CERVA (Auto))are given.
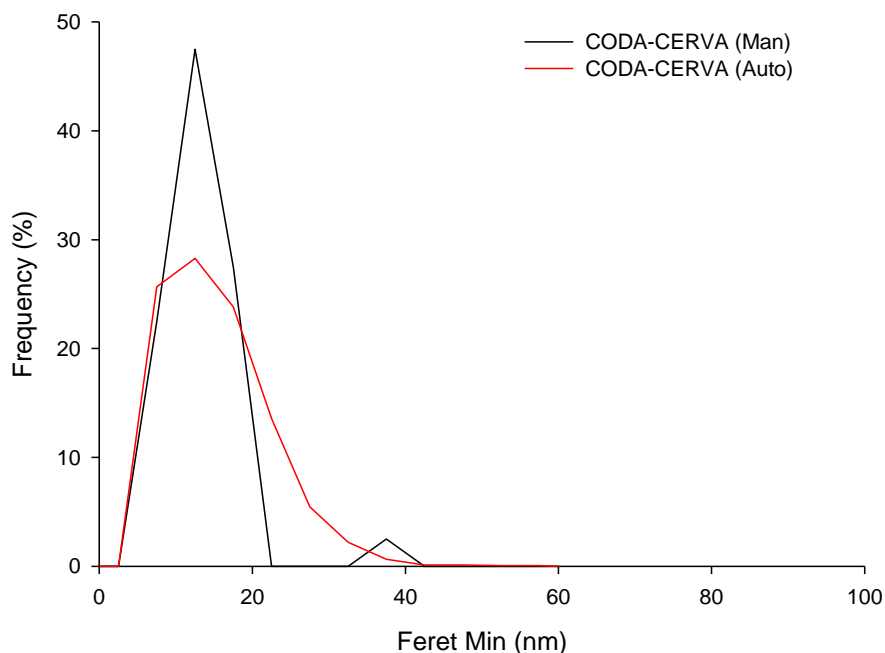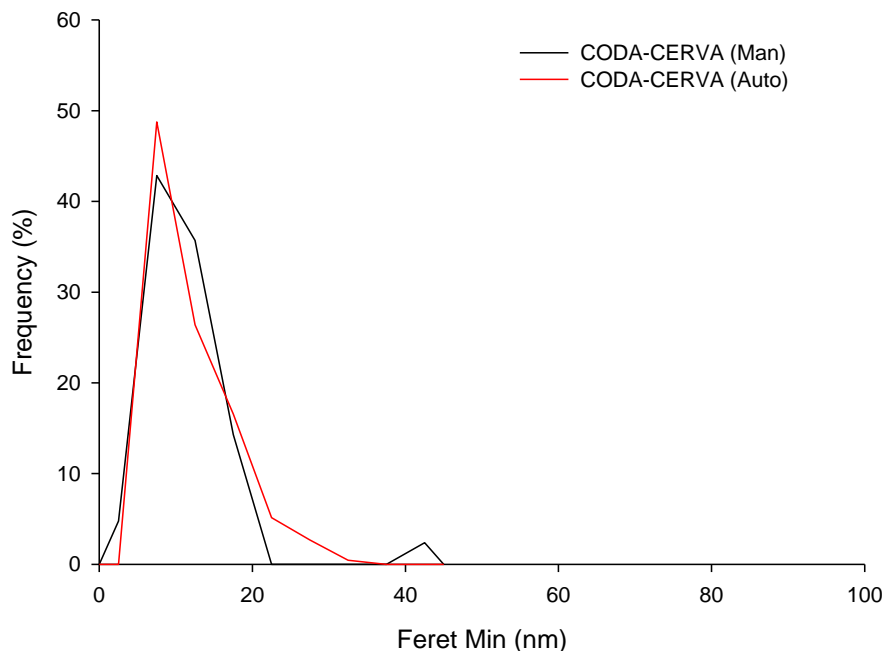

Figure 22 Qualitative TEM image analysis of TiO2 NM-203. Graph illustrates the primary particle Feret Min size distribution in function of the frequency. The manual measurement (CODA-CERVA (Man)) and the semi-automatic measurement (CODA-CERVA (Auto))are given.

34

4.3.3 MWCNT Nanomaterials

Representative images of the MWCNT nanomaterials are shown inFigure 23, Figure 24, Figure 25, Figure 26, Figure 27 and Figure 28. Samples were prepared in 0.05% w/v BSA-water following the principles of the NANOGENOTOX dispersion protocol [1].

In addition to these principal features, it should be noted that the MWCNT nanomaterials show great variation in the types and contents of impurities. All CNT samples appear to contain a fraction of μm-size particles identified in NM400 as corundum crystals (catalyst support material). Inorganic catalyst particles are abundant in the sidewalls of NM401 and NRCWE-006 and appear to occur mainly at the tube ends in NM402. It is important to extend the in situ characterization of all CNT materials beyond size analysis to fully understand these materials and their potential hazard.

4.3.3.1 Representative micrographs
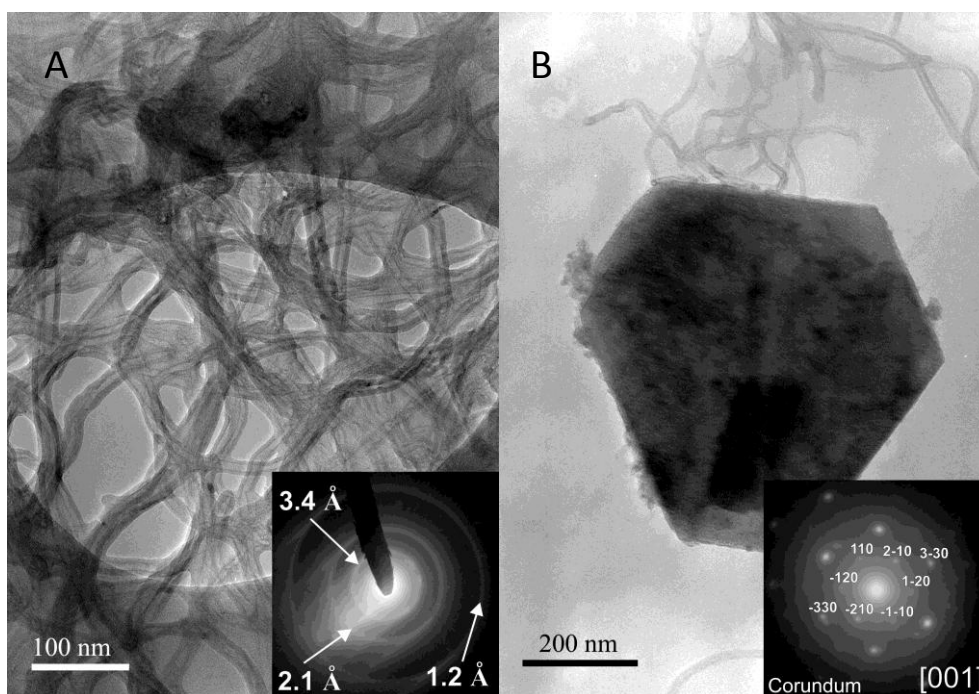
Figure 23. NM400: A) Representative TEM micrograph of NM-400 (Scale bar 100 nm). Typical SAED pattern is shown in insert. B) Example of euhedral foreign particles - catalyst support corundum viewed down [001]. SAED pattern is shown in insert (Scale bar 200 nm).
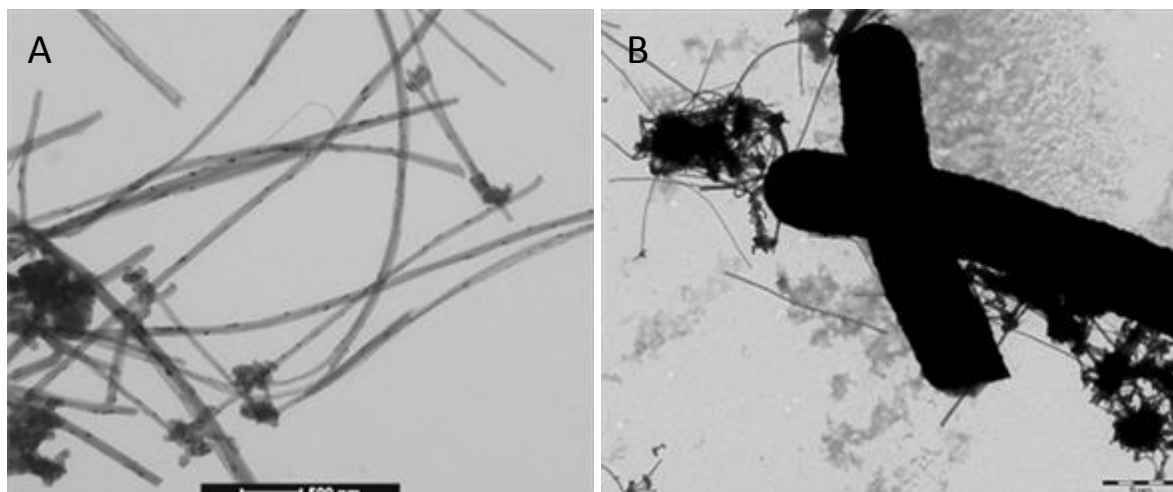
Figure 24 NM401: A) Representative TEM micrograph of NM-401. Dark spots in the CNT sidewall are catalyst impurities (scale bar 500 nm). B) Example of "megatubes" and µm-size dense aggregates and agglomerates(?) in the sample (Scale bar 2 µm)
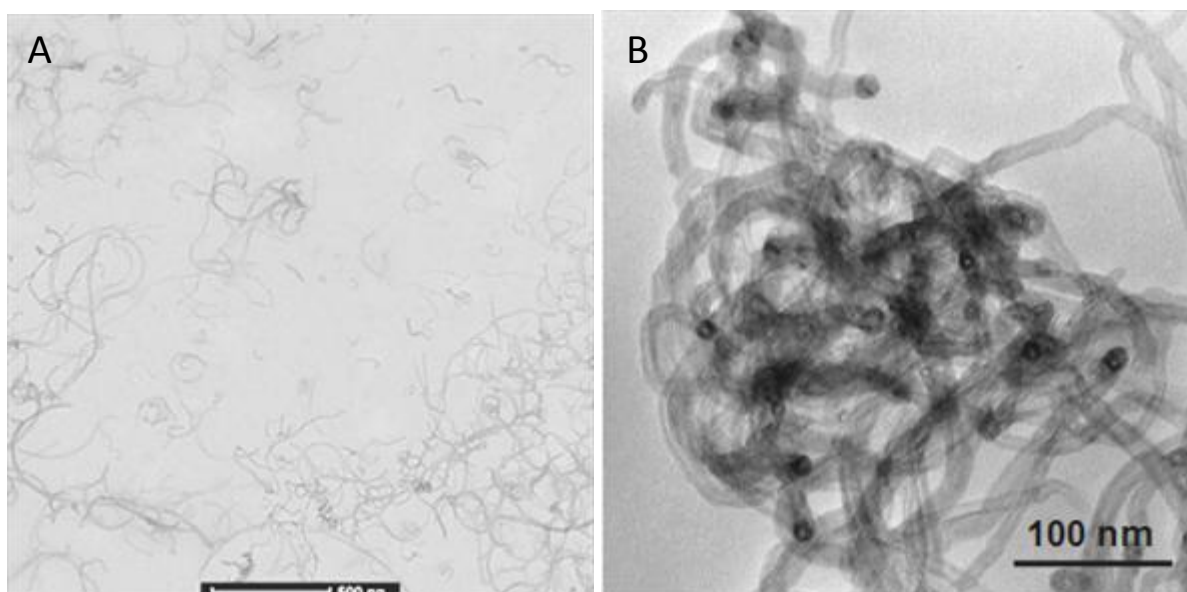
Figure 25 NM402: A) Representative TEM micrograph of highly dispersed CNT in NM-402. B) Image showing the structure of dense "particle" areas, which consist of highly entangled CNT.

Co-funded by
the Health Programme
of the European Union
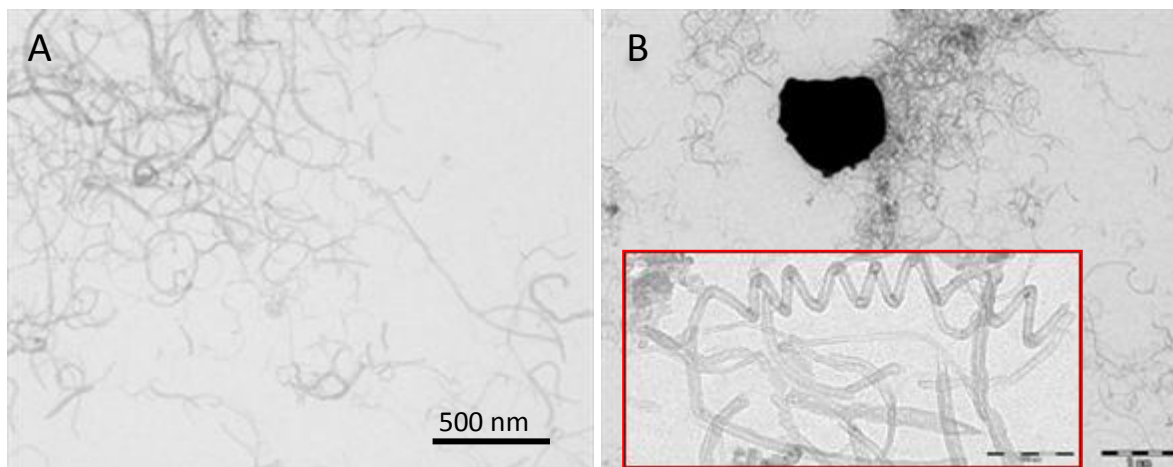
Figure 26 NM403: A) Representative TEM micrograph of NM-403. B) Example of µm-size dense un-identified impurity particles (Scale bar 1 µm) and insert showing different morphologies with bend and spiral shaped CNT (Scale Bar 100 nm).
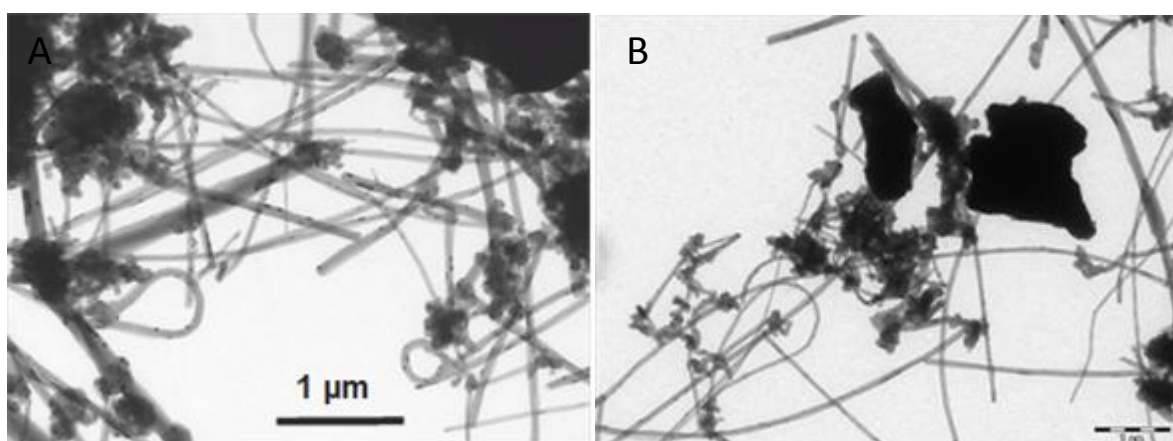
Figure 27 NRCWE-006: Representative TEM micrograph of NRCWE-006. Dark spots in the CNT sidewall are catalyst impurities (Scale Bar 500 nm). B) Example of µm-size dense un-identified impurity particles (Scale bar 1 µm)
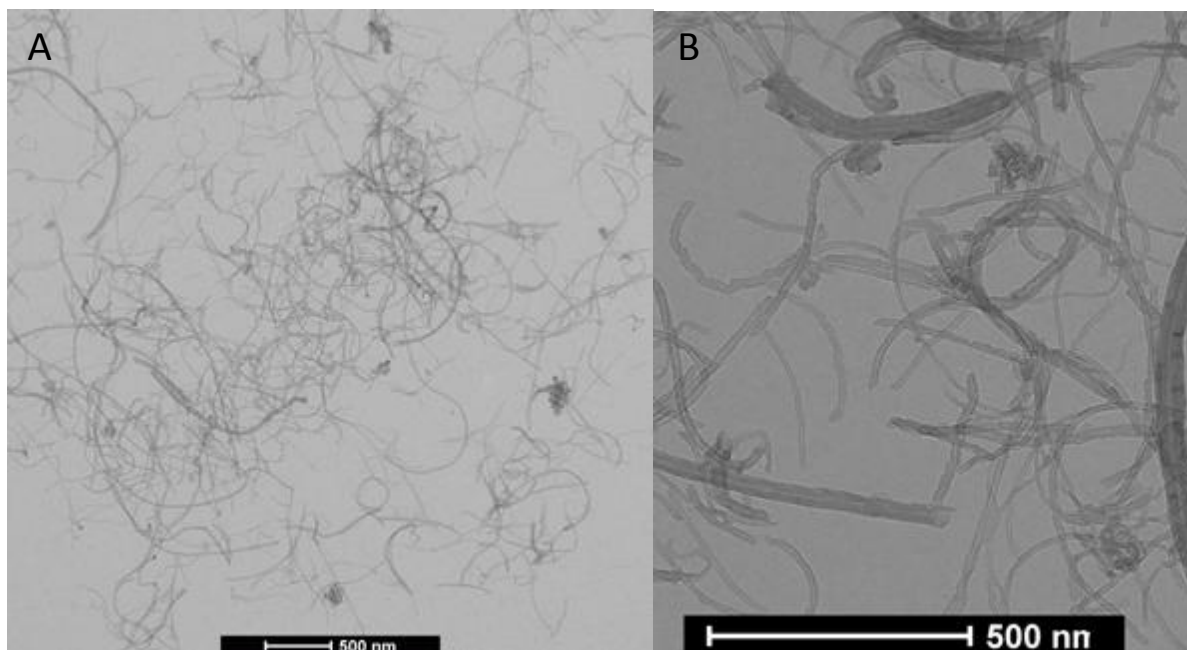
Figure 28 NRCWE-007: Representative TEM micrograph of NRCWE-007. A) representative TEM micrograph (Scale Bar 500 nm). B) Selected micrograph illustrating the different size classes of the MWCNTs (Scale bar 500 nm)

4.3.3.2 Interlaboratory comparison

TEM-analysis shows that by the morphology of the tubes the different CNT materials may be grouped into two principally different types. The general morphology of the MWCNTs within these groups was quite comparable.

- Group 1: Highly bend MWCNT (NM-400, NM-402, NM-403 and NRCWE_007)

- Group 2: Straight-wall MWCNT (NM-401 and NRCWE_006)

Quantitative   size   analysis   of   the   CNT   is   shown   in

Co-funded by
the Health Programme
of the European Union

Table 9 and Table 10. NM401 and NRCWE-006 are classified as large-diameter MWCNT (ca. 70 to 80 nm average diameter), whereas NM400, NM402, and NM403 are low-diameter MWCNT (ca. 10 to 17 nm average diameter). The number based thickness distribution is given in Figure 21. The large – diameter MWCNTs have a wide size distribution while the low-diameter MWCNT have a narrow size distribution (Figure 21). The large majority (87-90%) of the large-diameter MWCNTs had a thickness of less than 100 nm.

For the low diameter MWCNT all analyzed tubes had a thickness of less than 100 nm. Due to the generally high degree of entanglement, it was only possible to complete manual analysis of tube lengths. The average lengths vary from 443 nm (NM403) to 5.73 µm (NRCWE-006). Ordered by length NM403 < NRCWE_007 < NM400 < NM402 < NM401 < NRCWE-006. The lengths of NM401 and NRCWE-006 are the ones that have the greatest similarity with the CNT lengths given by venders.

Table 9 Thickness, Geodesic length, percentage of particles with a Thickness lower than 100 nm and Aspect ratio of NM-400, NM-401, NM-402, NM-403, NRCWE_006 and NRCWE_007 (CODA-CERVA, Belgium).

Lab	Thickness ± SD (nm)*[1]	Geodesic length ± SD (nm)*[2]	< 100 nm	Aspect ratio*	n
NM-400	11 ± 3	846 ± 446	100%	79 ± 50	20
NM-401	67 ± 24	4048 ± 2371	90%	66 ± 46	43
NM-402	11 ± 3	1372 ± 836	100%	125 ± 66	20
NM-403	12 ± 7	443 ± 222	100%	42 ± 29	50
NRCWE-006	74 ± 28	5730 ± 3674	87%	85 ± 63	56
NRCWE-007	17 ± 7	465 ± 340	100%	30 ± 22	50

* Mean ± standard deviation (SD)
1,2: Thickness and Geodesic length as described in [29]

Table 10 Manually measured dimensions of the CNT nanomaterials (IMC-BAS, Bulgaria)

Lab	Thickness of nanotube ± SD (nm)	Thickness of nanotube wall ± SD (nm)	n
NM-400	16.2 ± 3.5	5.1+1.0	36
NM-401	61.4 ± 24.4	-	358
NM-402	14.3+2.7	5.4+1.2	135
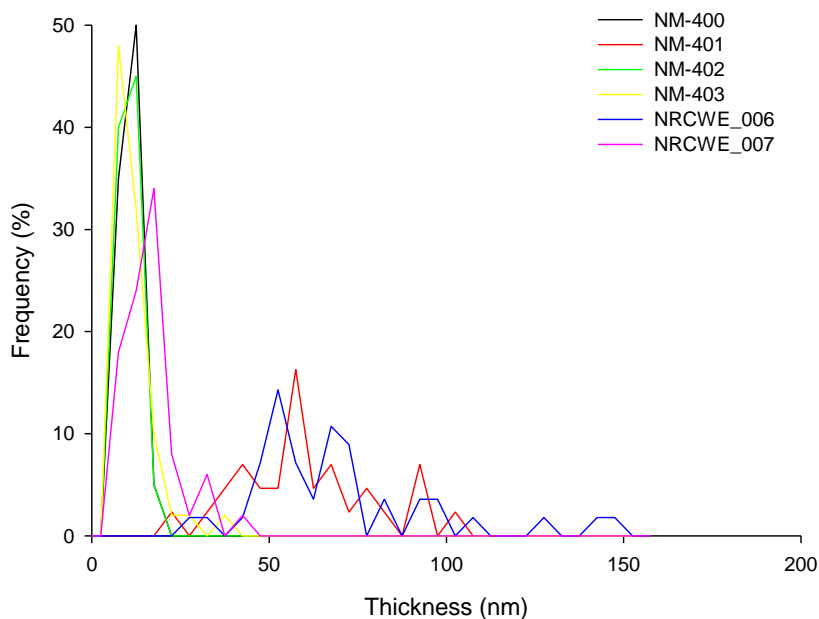
Figure 29 Qualitative TEM image analysis of MWCNT. Graph illustrates the primary Thickness in function of the frequency. Highly bend MWCNT: NM-400, NM402, NM-203 and NRCWE_006; Straight-wall MWCNT: NM-401 and NRCWE_006 are illustrated in the graph.
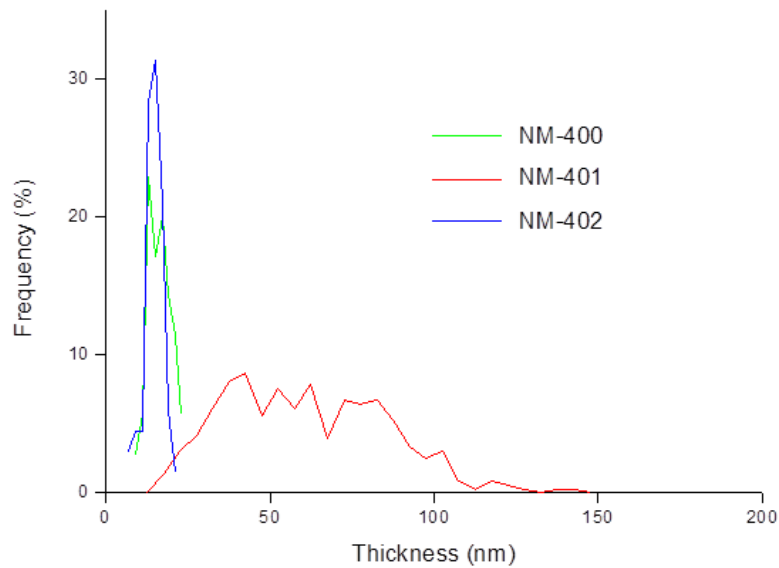
Figure 30 a Qualitative TEM image analysis of MWCNT (IMC-BAS). Graph illustrates the primary Thickness in function of the frequency. Highly bend MWCNT: NM-400 and NM402 and Straight-wall MWCNT: NM-401 are illustrated in the graph.

4.3.4 Printex 90

4.3.4.1 Representative micrographs
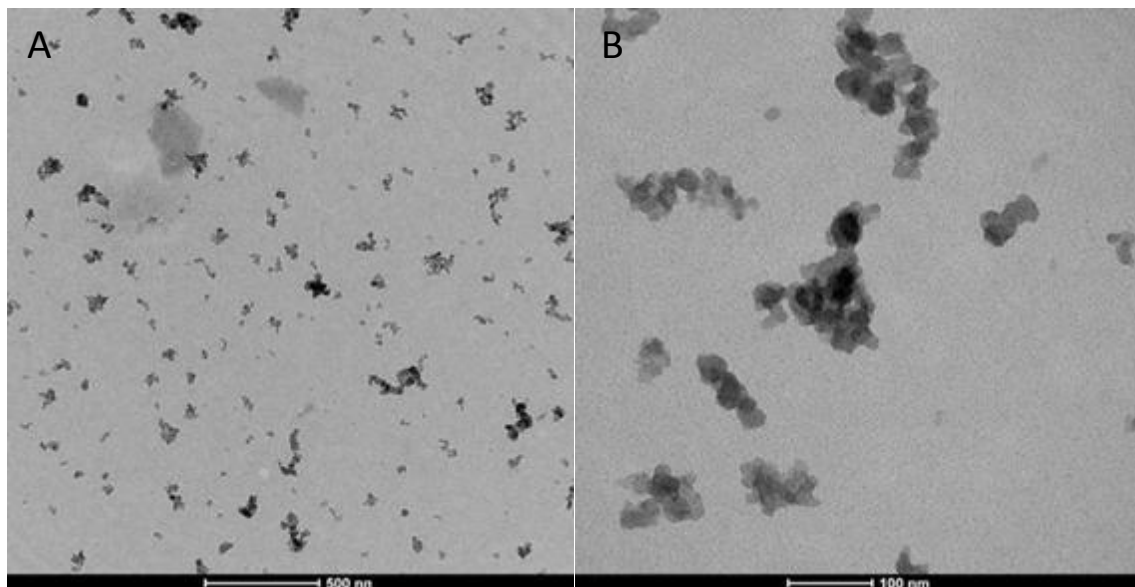
Figure 31 A) Representative TEM micrograph of Carbon black NM (Scale bar is 500 nm). B) TEM micrograph showing the complex open structure of the carbon black aggregates (Scale bar is 100 nm).

4.3.4.2 Primary particle size distribution

Printex 90 contains small ellipsoidal primary particles with an aspect ratio of 1,4 – 1,5 and a size of 19 nm, depending on the used methodology. All analyzed primary particles were smaller than 100 nm (Table 11). The Feret Min (Figure 32) Feret Mean, Feret Max and Aspect Ratio of these particles were lognormal distributed, were lognormal distributed for manual measurements but not for semi-automatic measurements. No significant (p < 0,05) differences were found between manual and semi-automatic measurements.

Table 11 Primary particle Feret Min, Feret Max, Feret Mean, percentage of particles with a Feret Min lower than 100 nm and Aspect ratio of NM-103

Lab	Feret Min ± SD (nm)*	Feret max ± SD (nm)*	Feret mean ± SD (nm)*	< 100 nm	Aspect ratio ± SD *	n
CODA-CERVA (Man)	19,5 ± 1,4 [a]	28,9 ± 1,4 [a]	24,4 ± 1,3 [a]	100 %	1,5 ± 1,3 [a]	32
CODA-CERVA (Auto)	19,3 ± 1,6 [a]	27,0 ± 1,6 [a]	23,6 ± 1,6 [a]	100 %	1,4 ± 1,2 [a]	219

* Geometric mean ± the geometric standard deviation (SD) [15]
[a, b] Different letters indicate significantly different mean values by Kruskal-Wallis One Way Analysis of Variance on Ranks (p < 0,05)
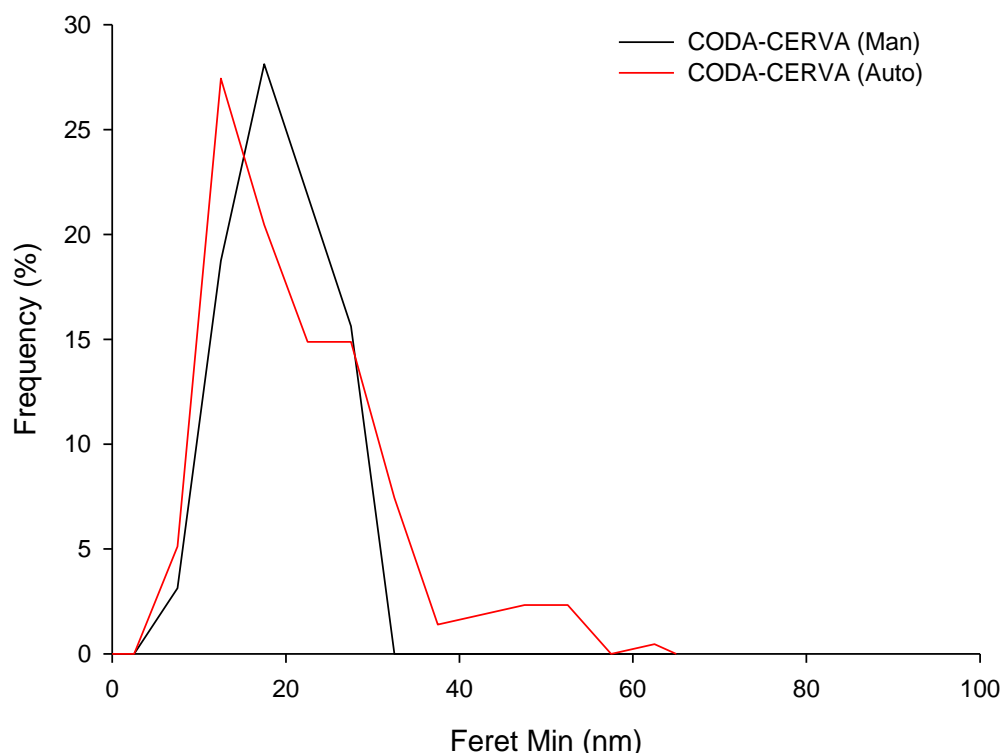
Figure 32 Qualitative TEM image analysis of Carbon Black NM Printex 90. Graph illustrates the primary particle Feret Min size distribution in function of the frequency. The manual measurement (CODA-CERVA (Man)) and the semi-automatic measurement (CODA-CERVA (Auto)) are given.

42

4.4 Quantitative analysis of aggregated and agglomerated NM based on TEM micrographs.

4.4.1 Classification of the parameters into classes by principle component analysis

PCA of the dataset consisting of the twenty-three parameters obtained by quantitative TEM analysis (Table 13) allowed classifying these parameters in three uncorrelated principle components (PC) explaining approximately 93% of the variability in the samples (

www.nanogenotox.eu

Co-funded by
the Health Programme
of the European Union

Table 12). Examination of the component pattern profiles of this PCA, given in Figure 33 for NM-104 and NM-202 shows that PC 1 basically consists of direct size measures and 2D size measurements. The direct size measures include the Feret max, Feret mean, Feret min, central distance max, central distance mean, diameter max, diameter mean and diameter min, The 2D size measurements include area, convex area, rectangle max, rectangle mean, rectangle min, ECD, convex perimeter and perimeter. PC 2 is importantly determined by the aspect ratio, the elongation and the sphericity, which reflect the shape of the particles. PC 3 is mostly determined by the convexity and shape factor, parameters reflecting the surface topology of the particles.

One representative parameter was selected from each of the classifications based on PCA to describe and compare the examined SAS NM. The mean diameter was chosen as a size measure, the sphericity was chosen as a shape measure and the shape factor was chosen as a measure for surface topology.
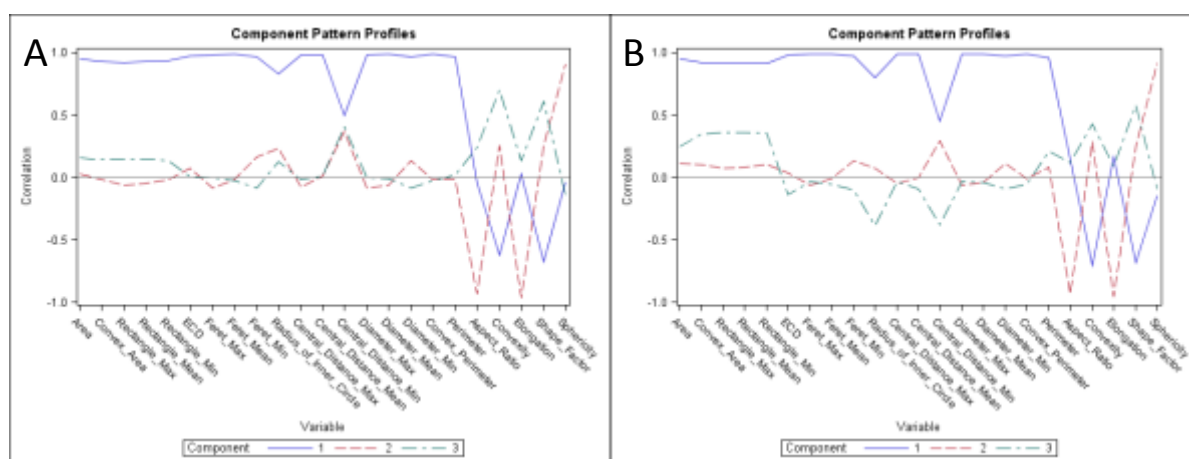
Figure 33 Representative examples of component pattern profiles of quantitative TEM analysis of NM-104 (A) and NM-202 (B) categorized into three principle components (blue line, red dashed line and green dashed line)

Table 12 Representation of the proportion of the eigenvalues of the correlation matrix in each principle component.

	PC1 [x]	PC2 [x]	PC3 [x]	Cumulative [x]
NM-103	73,5 ± 0,5 %	13,3 ± 0,3 %	5,1 ± 0,3 %	91,9 ± 0,2 %
NM-104	73,1 ± 0,8 %	13,2 ± 0,1 %	5,6 ± 0,4 %	91,9 ± 0,5 %
NM-200	73,4 ± 0,7 %	13,5 ± 0,1 %	6,6 ± 0,5 %	93,6 ± 0,3 %
NM-201	73,7 ± 0,4 %	13,7 ± 0,1 %	6,8 ± 0,1 %	94,2 ± 0,5 %
NM-202	73,5 ± 0,3 %	12,9 ± 0,2 %	6,5 ± 0,2 %	92,9 ± 0,2 %
NM-203	74,1 ± 0,4 %	12,9 ± 0,1 %	6,4 ± 0,1 %	93,0 ± 0,3 %

[x] *Mean values of medians ± SD are represented for 3 independent analyses*

4.4.1.1 Characterisation of titanium dioxide NM based on quantitative measures

Table 19 and Table 20 give the descriptive statistics of the measured 23 parameters of Titaniumdioxode NM-103 and NM-104, based on TEM micrographs.

Based on the number-based distributions of the mean diameter (Figure 34A) and on the comparison of the median mean diameters (Table 14) of the aggregates and agglomerates, nanomaterial's NM-103 and NM-104 can be distinguished. Although the number-based size distribution of NM-103 is different to the curves of NM-104, Figure 34B and Figure 34C show that the number-based sphericity and shape factor distributions of NM-103 and NM-104 are very similar. TEM analysis showed that the general morphology of the TiO$_2$ nanomaterials, described based on the guidelines of [30] was quite comparable (

Table 15). All samples consist of high porosity nanostructured materials, which may be considered aggregates of primary euhedral TiO2 particles.
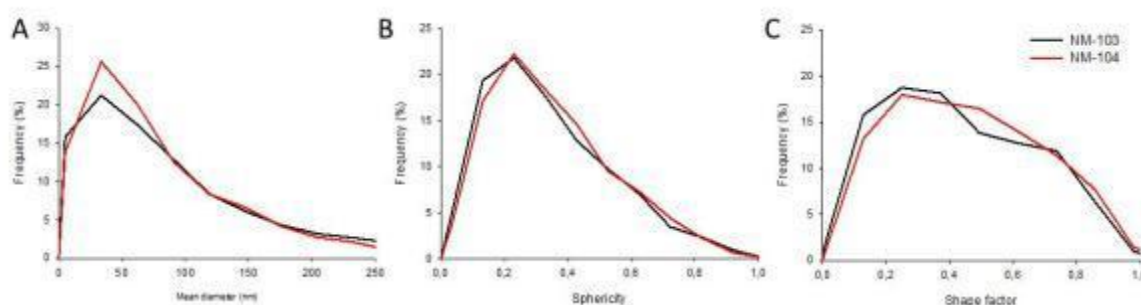
Figure 34 Number-based distributions of the mean diameter (A), sphericity (B) and shape factor (C) of agglomerates and aggregates of TiO$_2$ NMs. The frequency of the agglomerates and aggregates of TiO$_2$ NM are represented as a function of mean diameter, sphericity and shape factor.

Table 13 Quantitative parameters and their description as described in the iTEM software

Measured parameter[1]	Description
Area[4,3] (nm²)	Projection area
Convex Area[3] (nm²)	The area of the convex hull (envelope) bounding the measured object.
Rectangle Max (nm²)	The area of the biggest rectangle whose sides consist of tangents to the measured object borders.
Rectangle Mean (nm²)	The area of the mean rectangle whose sides consist of tangents to the measured object borders.
Rectangle Min[5] (nm²)	The area of the smallest rectangle whose sides consist of tangents to the measured object borders.
ECD[6] (nm)	The equivalence refers to the area of the measured object. The ECD is the diameter of a circle that has an area equal to the area of the measured object.
Feret Max[4] (nm)	The maximum distance of parallel tangents at opposing measured object borders.
Feret Mean[7] (nm)	The mean distance of parallel tangents at opposing measured object borders.
Feret Min[4] (nm)	The minimum distance of parallel tangents at opposing measured object borders.
Radius of Inner Circle (nm)	Radius of the maximal circle inside the measured object.
Central Distance Max (nm)	The maximum distance between the center and the border of a measured object.
Central Distance Mean (nm)	The mean distance between the center and the border of a measured object.

Central Distance Min (nm)	The minimum distance between the center and the border of a measured object.
Diameter Max (nm)	The maximum diameter of a measured object (for angles in the range 0° through 179° with step width 1°).
Diameter Mean (nm)	The mean diameter of a measured object (for angles in the range 0° through 179° with step width 1°).
Diameter Min (nm)	The minimum diameter of a measured object (for angles in the range 0° through 179° with step width 1°).
Convex Perimeter[3] (nm)	The length of the perimeter of the convex hull (envelope) bounding the particle.
Perimeter[3] (nm)	The sum of the pixel distances along the closed boundary.
Aspect Ratio [8]	The maximum ratio of width and height of a bounding rectangle for the measured object.
Convexity [9]	The fraction of the measured object's area and the area of its convex hull.
Elongation	The elongation of the measured object can be considered as lack of roundness. It results from the sphericity.
Shape Factor [10]	The shape factor provides information about the "roundness" of the measured object. For a spherical measured object the shape factor is 1; for all other measured objects it is smaller than 1.
Sphericity	Describes the sphericity or 'roundness' of the measured object by using central moments.

1 These parameters are used in the iTEM software and are described in the iTEM help files
2 The descriptor between brackets gives the synonym for the iTEM parameter as described in ISO
3 As described in ISO 9276-6:2008
4 As described in ISO 13322-1:2004
5 Feret box area[3]
6 Area equivalent diameter[4]
7 Angle-average Feret diameter
8 Shape factor[4,3]
9 Solidity[3]
10 Form Factor[3]

Table 14 Characterization of aggregated titanium dioxide NM by quantitative TEM.

	Mean diameter (nm)[x]	Sphericity [x]	Shape factor [x]	% < 100 nm [x,y]
NM-103	67 ± 1 [a]	0,40 ± 0,01 [a]	0,29 ± 0,02 [a]	66,0 ± 2,0 [a]
NM-104	60 ± 2 [b]	0,44 ± 0,02 [a]	0,32 ± 0,01 [a]	70,7 ± 0,4 [b]

[x] Mean values of medians ± SD are represented for 3 independent analyses
[y] The percentage of aggregates with a minimal Feret diameter smaller than 100 nm is represented.
[a, b] Different letters indicate significantly different mean values by One Way Analysis of Variance and pairwise compared with Tukey test.

Table 15 Summarizing table describing the morphology of aggregates/agglomerates of TiO$_2$ NM according to [30]

Sample	Sphericity	Shape factor	General morphology
NM-103	Low sphericity	Very angular to sub-angular	Angular, low sphericity
NM-104	Low sphericity	Angular to sub-rounded	Sub-angular, low sphericity

4.4.1.2 Characterisation of SAS NM based on quantitative measures

Table 21,

Co-funded by
the Health Programme
of the European Union

Table 22,

The NANOGENOTOX Joint Action is co-funded by the Executive Agency for Health and Consumers (Grant Agreement n°2009 21 01) under the European Union 2ⁿᵈ Health Programme.

www.nanogenotox.eu

Co-funded by
the Health Programme
of the European Union

Table 23 and

Table 24 give the descriptive statistics of the measured 23 parameters of SAS NM-200, NM-201, NM-203 and NM-204, based on TEM micrographs.

Based on the number-based distributions of the mean diameter (Figure 35A) and on the comparison of the median mean diameters of the aggregates and agglomerates, the precipitated NM-200 and NM-201 cannot unambiguously be distinguished from the pyrogenic NM-202 and NM-203. Although the number-based size distribution of NM-200 is different to the curves of NM-202 and NM-203, and its median mean diameter is significantly different from that of the pyrogenic NM-202 and NM-203, the number-based size distribution of NM-201 is comparable to the curves of NM-202 and NM-203, and its median mean diameter is not significantly different from that of the pyrogenic NM-202 and NM-203.

Figure 35B and Figure 35C show that the number-based sphericity and shape factor distributions of the precipitated NM-200 and NM-201 are very similar, as are the corresponding distributions of the pyrogenic NM-202 and NM-203. However, the curves of the precipitated and pyrogenic NM tend to diverge. Table 16 confirms that the median sphericities and shape factors of the pyrogenic and precipitated NM are significantly different, whereas within the precipitated and pyrogenic NM no significant differences were found.

TEM analysis showed that the general morphology of the SAS nanomaterials was quite comparable (Table 17). All samples consist of high porosity nanostructured materials, which may be considered aggregates of primary SAS particles. However, when looking into the detail, the pyrogenetic SAS (NM-202 and NM-203) may have a more complex and branched structure than the precipitated SAS. These differences were very clear in the quantitative morphology analysis, which showed much higher angularity of spheroidal SAS aggregates in NM202 and NM203 as compared to NM200 and NM201.
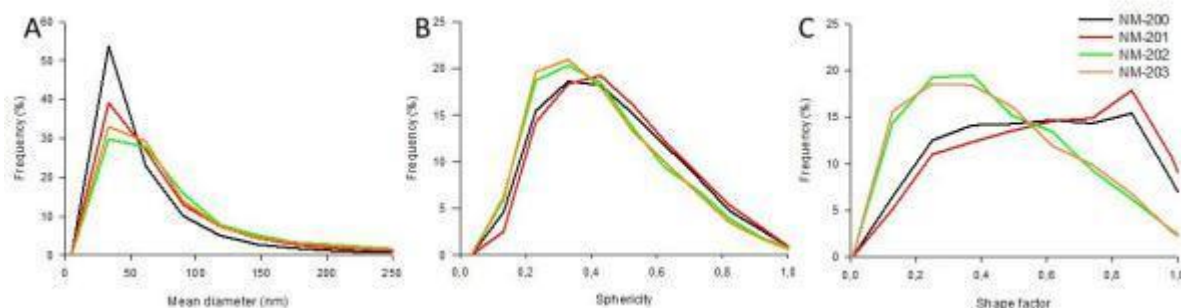
Figure 35 Number-based distributions of the mean diameter (A), sphericity (B) and shape factor (C) of agglomerates and aggregates of SAS NMs. The frequency of the agglomerates/aggregates of SAS NM are represented as a function of mean diameter, sphericity and shape factor.

Table 16 Characterization of aggregated SAS NM by quantitative TEM.

	Mean diameter (nm)[x]	Sphericity [x]	Shape factor [x]	% < 100 nm [x,y]
NM-200	31 ± 3 [a]	0,39 ± 0,01 [a]	0,51 ± 0,02 [a]	94 ± 1 [a]
NM-201	43 ± 4 [a,b]	0,4 ± 0,01 [a]	0,56 ± 0,05 [a]	91 ± 2 [a,b]

| NM-202 | 53 ± 9 [b] | 0,36 ± 0,01 [b] | 0,35 ± 0,01 [b] | 87 ± 2 [b] |
| NM-203 | 48 ± 4 [b] | 0,35 ± 0,02 [b] | 0,35 ± 0,02 [b] | 88 ± 2 [b] |

[x] *Mean values of medians ± SD are represented for 3 independent analyses*
[y] *The percentage of particles with a minimal Feret diameter smaller than 100 nm is represented.*
[a, b] *Different letters indicate significantly different mean values by One Way Analysis of Variance and pairwise compared with Tukey test.*

Table 17 Summarizing table describing the morphology of aggregates/agglomerates of SAS NM according to [30].

.Sample	Sphericity	Shape_factor	General morphology
NM-200	Low to medium sphericity	Sub-angular to rounded	Sub-rounded, low to medium sphericity
NM-201	Medium sphericity	Rounded to well-rounded	Rounded, medium sphericity
NM-202	Low sphericity	Very angular to sub-angular	Angular, low sphericity
NM-203	Low sphericity	Very angular to sub-angular	Angular, low sphericity

4.4.1.3 Characterisation of carbon black printex 90 based on quantitative measures

Figure 36 gives the number based distributions of mean diameter, sphericity and shape factor of the agglomerates and aggregates of Printex 90. The aggregates and agglomerates have a median mean diameter of 58 nm, a Sphericity of 0,39 and a shape factor of 45. Furthermore, 96 percent of the analysed particles have a Feret Min lower than 100 nm.
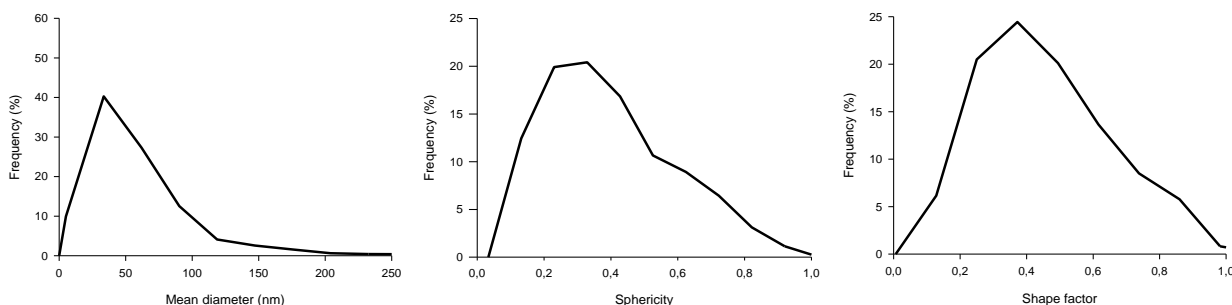
Figure 36 Number-based distributions of the mean diameter (A), sphericity (B) and shape factor (C) of agglomerates and aggregates of carbon black Printex 90. The frequency of the agglomerates and aggregates of varbon black are represented as a function of mean diameter, sphericity and shape factor.

Table 18 Characterization of carbon black printex 90 by quantitative TEM

	Mean diameter (nm)[x]	Sphericity [x]	Shape factor [x]	% < 100 nm [x,y]
Printex 90	58	0,39	0,45	96

[x] *Median values for 1 analysis*
[y] *The percentage of particles with a minimal Feret diameter smaller than 100 nm is represented.*

Table 19. Descriptive statistics of titanium dioxide NM-103

Column	n	Mean	SD	SEM	Max	Min	Median	25%	75%
Area (nm²)	2641	6071	10848	211	152667	36	2101	502	6685
Convex Area (nm²)	2641	9535	19529	380	259709	37	2591	588	9413
Rectangle Max (nm²)	2641	16665	35586	692	479884	58	4340	1020	15754
Rectangle Mean (nm²)	2641	14918	31447	612	412611	52	3942	900	14289
Rectangle Min (nm²)	2641	12660	26442	515	383118	43	3427	731	12244
ECD (nm)	2641	66,9	57,0	1,1	440,9	6,8	51,7	25,3	92,3
Feret Max (nm)	2641	109,9	107,3	2,1	895,0	8,0	75,9	37,3	145,6
Feret Mean (nm)	2641	89,9	85,8	1,7	663,1	7,2	63,7	30,6	120,7
Feret Min (nm)	2641	64,0	60,3	1,2	451,7	3,6	46,5	19,8	87,0
Next Neighbor Distance (nm)	2641	99,9	56,2	1,1	479,0	5,4	96,5	57,9	134,5
Radius of Inner Circle (nm)	2641	22,5	14,4	0,3	129,0	2,1	20,7	12,3	30,9
Central Distance Max (nm)	2641	59,0	58,4	1,1	463,9	3,8	40,5	19,2	78,6
Central Distance Mean (nm)	2641	35,3	31,6	0,6	253,6	3,1	26,6	13,1	47,4
Central Distance Min (nm)	2641	10	9	0	111	0	8	3	14
Diameter Max (nm)	2641	110	107	2	894	8	76	37	145
Diameter Mean (nm)	2641	97,1	94,4	1,8	775,4	7,2	67,2	33,0	128,7
Diameter Min (nm)	2641	67	64	1	460	4	48	20	92
Convex Perimeter (nm)	2641	295	284	6	2185	21	208	99	397
Perimeter (nm)	2641	469	637	12	6728	21	233	103	560
Aspect Ratio	2641	1,794	0,584	0,011	6,280	1,055	1,660	1,389	2,015
Convexity	2641	0,772	0,128	0,002	0,988	0,362	0,780	0,683	0,874
Elongation	2641	2,013	0,796	0,016	8,829	1,008	1,823	1,464	2,321
Shape Factor	2641	0,431	0,233	0,005	0,980	0,030	0,401	0,237	0,620

Table 20. Descriptive statistics of titanium dioxide NM-104

Column	n	Mean	SD	SEM	Max	Min	Median	25%	75%
Area (nm²)	3739	4368	7741	127	149999	36	1667	530	5072
Convex Area (nm²)	3739	6699	14019	229	274061	37	2045	593	6889
Rectangle Max (nm²)	3739	11602	24948	408	454934	58	3424	1004	11898
Rectangle Mean (nm²)	3739	10421	22173	363	425922	54	3100	908	10649
Rectangle Min (nm²)	3739	8909	18572	304	370845	43	2706	761	9107
ECD (nm)	3739	58,5	46,3	0,8	437,0	6,8	46,1	26,0	80,4
Feret Max (nm)	3739	94,4	85,1	1,4	863,9	7,7	68,7	37,7	125,9
Feret Mean (nm)	3739	77,6	68,8	1,1	667,4	7,3	56,2	30,6	104,6
Feret Min (nm)	3739	56,0	49,9	0,8	465,9	4,2	41,2	20,3	76,0
Next Neighbor Distance (nm)	3739	89,2	44,6	0,7	574,5	8,5	86,5	58,3	117,6
Radius of Inner Circle (nm)	3739	20,8	12,4	0,2	103,6	2,1	19,0	12,3	28,3
Central Distance Max (nm)	3739	50,8	46,8	0,8	483,8	3,8	36,3	19,4	68,1
Central Distance Mean (nm)	3739	30,7	25,4	0,4	241,1	3,1	23,5	13,3	41,3
Central Distance Min (nm)	3739	9	8	0	79	0	8	3	12
Diameter Max (nm)	3739	94	85	1	864	8	69	38	126
Diameter Mean (nm)	3739	83,5	75,1	1,2	739,4	7,3	60,5	33,0	111,6
Diameter Min (nm)	3739	58	53	1	506	4	43	21	80
Convex Perimeter (nm)	3739	254	228	4	2227	22	184	99	344
Perimeter (nm)	3739	376	493	8	8553	22	207	103	457
Aspect Ratio	3739	1,741	0,496	0,008	4,630	1,034	1,627	1,384	1,966
Convexity	3739	0,783	0,125	0,002	1,000	0,388	0,793	0,695	0,884
Elongation	3739	1,934	0,668	0,011	6,280	1,011	1,777	1,456	2,233
Shape Factor	3739	0,457	0,229	0,004	0,984	0,020	0,439	0,265	0,636

Table 21. Descriptive statistics of SAS NM-200

Column	n	Mean	SD	SEM	Max	Min	Median	25%	75%
Area (nm²)	8005	2112	6730	75	174446	17	438	146	1443
Convex Area (nm²)	8005	3385	12076	134	328677	18	553	168	2011
Rectangle Max (nm²)	8005	5674	20452	228	565985	30	910	273	3323
Rectangle Mean (nm²)	8005	5134	18383	205	503770	26	832	250	3026
Rectangle Min (nm²)	8005	4434	15721	175	424206	22	727	220	2623
ECD (nm)	8005	35,7	37,5	0,4	471,2	4,7	23,6	13,6	42,8
Feret Max (nm)	8005	56,2	66,4	0,7	883,1	6,0	34,5	18,8	66,0
Feret Mean (nm)	8005	47,2	54,9	0,6	717,9	5,1	29,0	15,9	55,4
Feret Min (nm)	8005	35,6	41,1	0,4	524,7	3,9	21,9	12,2	42,1
New Radius of Inner Circle (nm)	8005	9,00	5,96	0,06	89,42	1,49	7,47	5,08	11,66
Central Distance Max (nm)	8005	30,1	36,3	0,4	518,6	2,7	18,2	9,7	35,3
Central Distance Mean (nm)	8005	18,6	20,4	0,2	266,3	2,1	12,0	6,7	22,0
Central Distance Min (nm)	8005	6,13	6,55	0,07	120,10	0,07	4,39	2,57	7,36
Diameter Max (nm)	8005	56,1	66,4	0,7	883,0	5,6	34,4	18,7	65,8
Diameter Mean (nm)	8005	50,0	59,1	0,6	775,1	5,0	30,6	16,6	59,0
Diameter Min (nm)	8005	36,8	42,9	0,4	541,0	3,7	22,4	12,3	43,4
Convex Perimeter (nm)	8005	153	182	2	2392	14	93	50	181
Perimeter (nm)	8005	254	520	5	12079	15	101	52	235
Aspect Ratio	8005	1,556	0,349	0,003	3,607	1,040	1,480	1,298	1,733
Convexity	8005	0,789	0,123	0,001	1,000	0,362	0,803	0,699	0,895
Elongation	8005	1,722	0,508	0,005	5,055	1,000	1,603	1,351	1,968
Shape Factor	8005	0,512	0,249	0,002	1,007	0,010	0,516	0,303	0,728
Sphericity	8005	0,414	0,196	0,002	0,989	0,039	0,389	0,258	0,548

Table 22. Descriptive statistics of SAS NM-201

Column	n	Mean	SD	SEM	Max	Min	Median	25%	75%
Area (nm²)	2573	3896	13175	259	420592	35	1021	342	2908
Convex Area (nm²)	2573	6158	21840	430	609588	36	1270	377	4089
Rectangle Max (nm²)	2573	10152	34949	689	898373	52	2039	599	6772
Rectangle Mean (nm²)	2573	9255	32209	634	862557	51	1857	550	6152
Rectangle Min (nm²)	2573	8116	28913	570	826460	46	1638	486	5327
ECD (nm)	2573	50,0	49,5	0,9	731,7	6,7	36,0	20,8	60,8
Feret Max (nm)	2573	77	86	1	1150	7	51	27	93
Feret Mean (nm)	2573	65	71	1	938	7	43	23	79
Feret Min (nm)	2573	49	55	1	740	4	33	18	59
New Radius of Inner Circle (nm)	2573	12,20	7,50	0,10	151,60	2,0	11,0	7,40	15,20
Central Distance Max (nm)	2573	41,7	47,5	0,9	641,9	3,5	26,9	14,2	49,9
Central Distance Mean (nm)	2573	25,8	26,4	0,5	371,8	2,9	18,1	10,3	31,2
Central Distance Min (nm)	2573	8,38	8,90	0,17	200,52	0,03	6,39	3,72	9,98
Diameter Max (nm)	2573	77	86	1	1150	7	50	27	93
Diameter Mean (nm)	2573	69	76	1	985	7	45	24	83
Diameter Min (nm)	2573	51	57	1	748	4	34	18	61
Convex Perimeter (nm)	2573	214	238	4	3139	20	141	75	259
Perimeter (nm)	2573	360	708	13	13479	21	155	76	347
Aspect Ratio	2573	1,529	0,317	0,006	3,388	1,023	1,461	1,296	1,714
Convexity	2573	0,799	0,122	0,002	0,993	0,338	0,812	0,713	0,907
Elongation	2573	1,683	0,457	0,009	4,343	1,000	1,590	1,342	1,924
Shape Factor	2573	0,518	0,259	0,005	1,004	0,013	0,523	0,298	0,747
Sphericity	2573	0,424	0,193	0,003	0,983	0,053	0,395	0,270	0,555

Table 23. Descriptive statistics of SAS NM-202

Column	n	Mean	SD	SEM	Max	Min	Median	25%	75%
Area (nm²)	4248	4039	9319	142	177792	35	1127	422	3335
Convex Area (nm²)	4248	7375	20734	318	445959	37	1536	531	5086
Rectangle Max (nm²)	4248	12683	36710	563	817213	58	2549	874	8562
Rectangle Mean (nm²)	4248	11409	32793	503	737974	53	2305	798	7764
Rectangle Min (nm²)	4248	9785	28110	431	671026	46	2014	697	6673
ECD (nm)	4248	53,2	48,0	0,7	475,7	6,7	37,8	23,1	65,1
Feret Max (nm)	4248	90	96	1	1006	7	58	33	107
Feret Mean (nm)	4248	74	78	1	865	7	48	28	88
Feret Min (nm)	4248	55,1	56,7	0,8	675,9	4,1	37,2	21,5	65,8
New Radius of Inner Circle (nm)	4248	11,24	5,97	0,09	51,74	2,09	9,87	6,87	14,05
Central Distance Max (nm)	4248	48,4	52,9	0,8	590,2	3,7	31,0	17,5	57,6
Central Distance Mean (nm)	4248	28,3	27,5	0,4	289,7	3,1	19,3	11,7	34,2
Central Distance Min (nm)	4248	6,94	6,64	0,10	84,15	0,03	5,23	2,86	8,59
Diameter Max (nm)	4248	89	96	1	1006	7	58	33	107
Diameter Mean (nm)	4248	79	85	1	914	7	51	29	94
Diameter Min (nm)	4248	57,3	59,8	0,9	714,8	4,2	38,5	22,1	68,3
Convex Perimeter (nm)	4248	245	259	3	2849	21	158	91	291
Perimeter (nm)	4248	468	865	13	17955	21	197	99	453
Aspect Ratio	4248	1,596	0,367	0,005	3,811	1,032	1,518	1,327	1,793
Convexity	4248	0,726	0,128	0,001	0,991	0,302	0,730	0,635	0,823
Elongation	4248	1,805	0,548	0,008	5,474	1,000	1,679	1,403	2,081
Shape Factor	4248	0,386	0,231	0,003	0,966	0,006	0,354	0,192	0,557
Sphericity	4248	0,383	0,193	0,002	0,988	0,033	0,355	0,231	0,508

Table 24. Descriptive statistics of SAS NM-203

Column	n	Mean	SD	SEM	Max	Min	Median	25%	75%
Area (nm²)	4889	3426	8413	120	161619	35	928	362	2740
Convex Area (nm²)	4889	6467	19253	275	454517	37	1314	450	4243
Rectangle Max (nm²)	4889	11063	33198	474	741224	56	2180	740	7163
Rectangle Mean (nm²)	4889	9987	29909	427	692283	53	2001	673	6474
Rectangle Min (nm²)	4889	8598	25731	368	611812	42	1734	597	5586
ECD (nm)	4889	48,5	44,7	0,6	453,6	6,7	34,3	21,4	59,0
Feret Max (nm)	4889	83	90	1	986	7	53	31	98
Feret Mean (nm)	4889	69	74	1	838	7	45	26	81
Feret Min (nm)	4889	51,0	54,4	0,7	641,1	4,9	33,5	19,7	60,2
New Radius of Inner Circle (nm)	4889	10,03	5,26	0,07	48,75	1,49	9,27	6,28	12,26
Central Distance Max (nm)	4889	44,7	49,5	0,7	531,1	3,6	28,3	16,4	52,8
Central Distance Mean (nm)	4889	26,1	26,1	0,3	277,2	3,0	17,6	10,9	31,2
Central Distance Min (nm)	4889	6,10	5,96	0,08	76,76	0,02	4,48	2,48	7,60
Diameter Max (nm)	4889	83	90	1	986	7	53	31	98
Diameter Mean (nm)	4889	73	80	1	880	7	47	27	87
Diameter Min (nm)	4889	53,3	57,3	0,8	678,8	4,0	34,9	20,3	62,7
Convex Perimeter (nm)	4889	226	245	3	2818	21	147	84	266
Perimeter (nm)	4889	439	839	12	18139	21	182	91	411
Aspect Ratio	4889	1,599	0,357	0,005	3,565	1,039	1,533	1,328	1,794
Convexity	4889	0,717	0,135	0,001	1,000	0,331	0,722	0,622	0,822
Elongation	4889	1,810	0,536	0,007	5,008	1,000	1,700	1,408	2,095
Shape Factor	4889	0,384	0,234	0,003	0,991	0,006	0,354	0,190	0,554
Sphericity	4889	0,379	0,190	0,002	0,981	0,039	0,346	0,228	0,504

4.5 Transmission electron tomography (ET)

4.5.1 Three dimensional visualisation and measurement of SAS NM

In preliminary experiments (not shown) spherical and branched were visualized in three dimensions. From the isosurface based volume rendering of the ET reconstructions, the total surface area and volume of their composing gold particles could be measured, such that VSSA could be calculated. A high correlation between the calculated and measured volume and surface area was found.
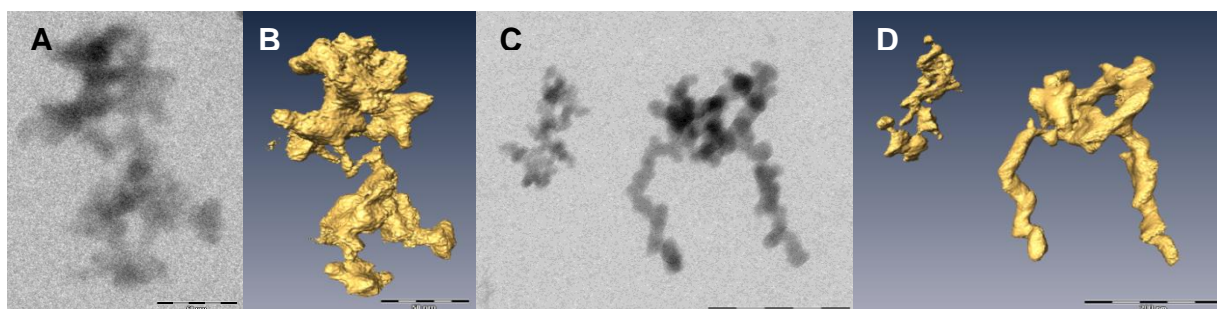
Figure 37 Electron tomographic analyses of SAS NM. The micrographs, taken at 0°, show one (Figure 37 A) and two aggregates (Figure 37C) consisting of multiple primary subunits of NM-200 and NM-203, respectively. Figure 37B and Figure 37D show the corresponding ET reconstructions. Bars: 200 nm.

It is not evident to envisage the structure of the SAS materials NM-200 and NM-203 appropriately by conventional bright field TEM (Figure 37A and Figure 37C). Their relatively low molar mass results in a low contrast, while their complex morphology results in blurring of ultrastructural details due to superposition of projected features. Electron tomographic reconstruction in three dimensions circumvents these difficulties. Figure 37B and Figure 37D, illustrate that both the precipitated SAS NM-200 and the pyrogenic SAS NM-203 consist of aggregates of very complex morphology composed of a variable number of interconnected primary subunits. Although the site where an aggregate interacts with the grid can be found in the 3D reconstruction as a relatively flat surface, structures of primary subunits remain extended in the z-direction, resulting in similar dimensions along the three axes. This suggests a limited flexibility of the material.

Table 25 Mean volume specific surface area of different nanomaterials based on electron tomographic reconstructions

Type of nanomaterial	n	Volume specific surface area (m²/cm³)[a]
Precipitated SAS (NM-200)	5	342 ± 36
Pyrogenic SAS (NM-203)	5	219 ± 23

[a] Values represent mean VSSA ± standard error of mean

Measurement in 3D space showed that individual aggregates in both NM-200 and NM-203 are composed of similarly sized primary subunits. The size of the subunits of the aggregates of NM-200 is relatively constant: they measure approximately 20 nm in diameter. The size of the subunits of different aggregates of NM-203 is variable: the subunits of the left aggregate shown in Figure 37D measure, for example, 8 to 12 nm in diameter, while the subunits of the right aggregate measure approximately 20 nm in diameter. In any of the tilt series of NM-200 and NM-203, diffraction contrast was observed, confirming their amorphous structure. The surface area and volume of NM-200 and NM-203 were measured for five ET reconstructions and the VSSA was calculated (Table 1). For both materials, the mean VSSA were significantly different (P<0.05) from 60 m²/cm³.

4.6 Combination of the results of quantitative AFM and TEM analyses

Results of quantitative AFM and TEM analyses are highly complementary. Quantitative TEM allows determining the minimal and maximal size of aggregates in the X-Y plane, measured as Feret min and Feret Max. AFM estimates the third dimension of a NM, measured as Z-max (Figure 38D, Figure 39D, Figure 40D, Figure 41D, Figure 42D and Figure 43D). The combination of the results of both techniques gives an insight in the 3D properties of the NM. A direct link can be made between the Feret Min and Feret Max on a per particle level. Their ratio, as the aspect ratio, is a measure for aggregate morphology. Regrettably, no direct link can be made between AFM and TEM results at the per-particle-level because different particles are analyzed. Therefore, results can only be compared at the population level, matching (statistical) characteristics of size distributions. The visualization of NM in TEM micrographs can assist in the interpretation of the values measured by AFM.

Figure 38C and Figure 39C show that the aggregates of the titanium dioxide NM-103 and NM-104 are fractal-like. Combining the AFM result (Figure 38A and Figure 39A) with primary particle dimensions (Table 4 and Table 5) tend to confirm the observation Figure 38C and Figure 39C) that most aggregates are approximately 1.5 primary particles thick. The aggregates of NM-103 and NM-104 are wider (Feret min) than high (Z-max) and longer (Feret max) than wide (Feret min) (

Table 19, Table 20, Figure 38B and Figure 39B).

It must be stressed however that for the titanium dioxide NM, the preparation protocols are different from AFM to TEM samples. Indeed, the sonication in acidic medium performed for AFM samples is likely to lead to better dispersed and more stable suspensions, and therefore smaller aggregates. This, and possible preferential orientation towards the grid, explains why the AFM distributions in Figure 38 and Figure 39 are less polydisperse than the corresponding TEM distributions.

Figure 40C and Figure 41C show that the aggregates of the precipitated SAS NM-200 and NM-201 have similar height (Z-max) and width (Feret min) and are 50 % longer than wide (Figure 40B and Figure 41B). Combining the AFM result (Figure 40A and Figure 41A) with primary particle dimensions (*Table 6*) confirms the observation (Figure 40C and Figure 41C) that most aggregates are approximately 1.5 primary particles thick.

Figure 42C and Figure 43C show that the aggregates of the pyrogenic SAS NM-202 and NM-203 are fractal-like while the primary particle size between aggregates is highly variable. Combining the AFM results (Figure 42A and Figure 43A) with primary particle dimensions (*Table 6*) confirms the observation (Figure 42C and Figure 43C) that most aggregates are approximately 1.5 primary particles thick. The aggregates of NM-202 are as high (Z-max) and longer (Feret max) than wide (Feret min). The aggregates of NM-203 are wider (Feret min) than high (Z-max) and longer (Feret max) than wide (Feret min) (

Co-funded by
the Health Programme
of the European Union

Table 23,

Co-funded by
the Health Programme
of the European Union

Table 24, Figure 42Band Figure 43B).

Table 26 Characterization of Titanium dioxide NM-103 in three dimensions

Lab	Technique	Parameter	Median (N)
CEA	AFM	Z max	22,3 (466)
CODA-CERVA	TEM	Feret Min	46,5 (2641)
CODA-CERVA	TEM	Feret Max	75,9 (2641)
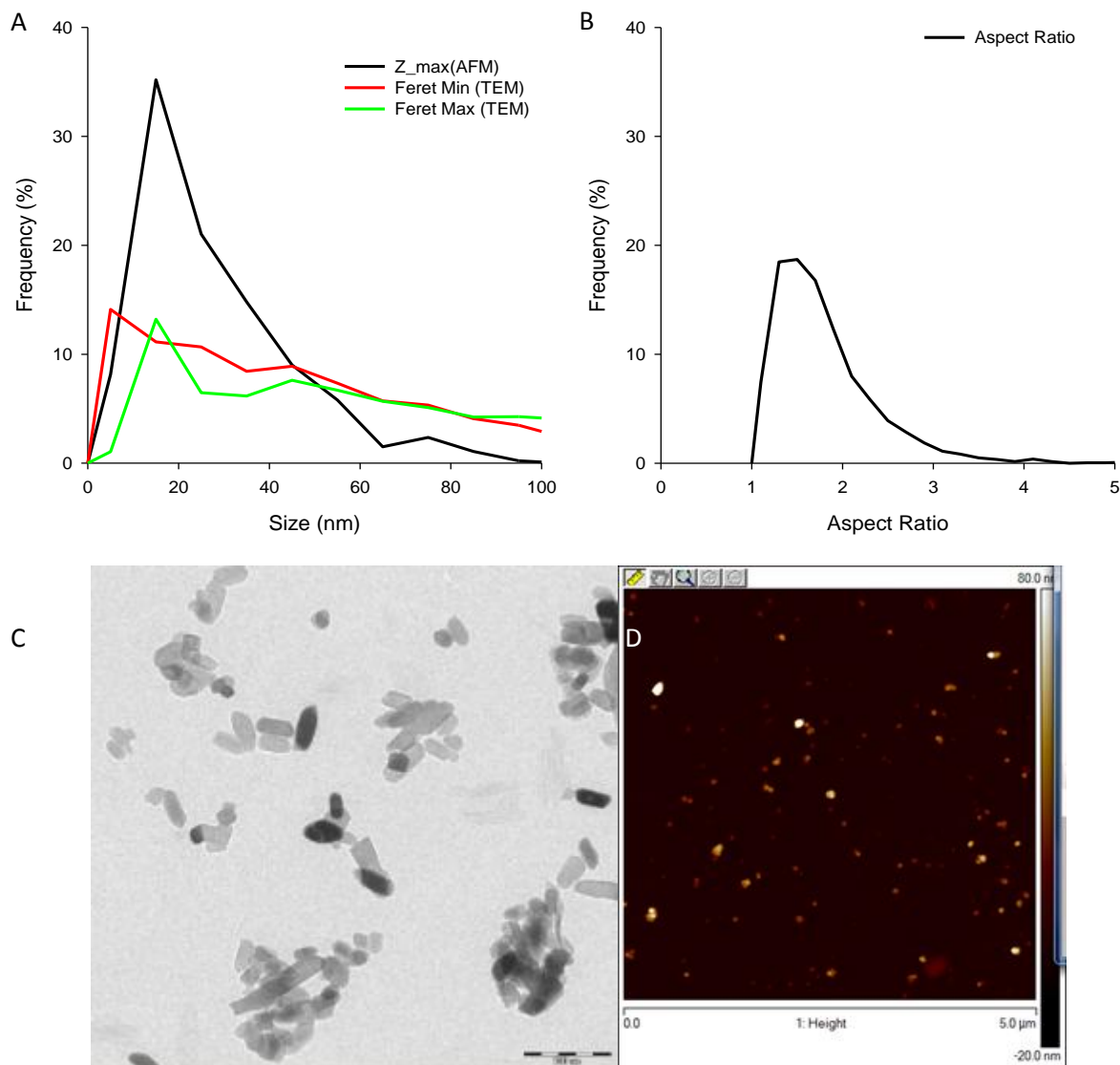
Figure 38 Characterization of the aggregates of TiO₂ NM-103 in three-dimensions by combination of TEM and AFM. A) Number based size distributions of Feret Min, Feret max and Z_max. B) Number based distribution of the aspect ratio. Representative TEM (C) and AFM (D) micrographs visualizing the morphology of the aggregates.

Table 27 Characterization of Titanium dioxide NM-104 in three dimensions

Lab	Technique	Parameter	Median (N)
CEA	AFM	Z max	21,8 (458)
CODA-CERVA	TEM	Feret Min	41,2 (3739)
CODA-CERVA	TEM	Feret Max	68,7 (3739)
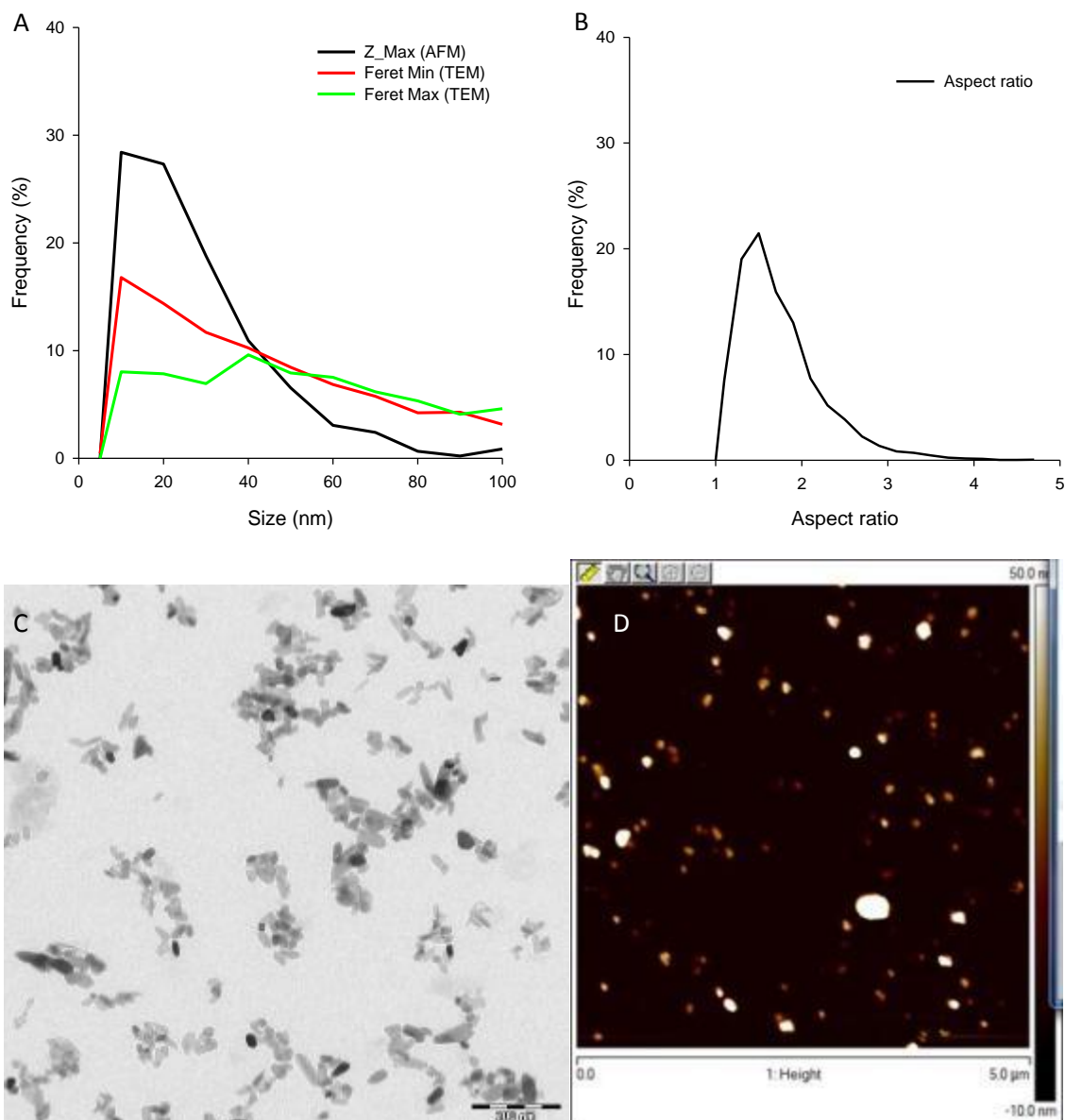
Figure 39 Characterization of the aggregates of TiO₂ NM-104 in three-dimensions by combination of TEM and AFM. A) Number based size distributions of Feret Min, Feret max and Z_max. B) Number based distribution of the aspect ratio. Representative TEM (C) and AFM (D) micrographs visualizing the morphology of the aggregates.

Table 28 Characterization of SAS NM-200 in three dimensions

Lab	Technique	Parameter	Median (N)
CEA	AFM	Z max	21,9 (1382)
CODA-CERVA	TEM	Feret Min	21,9 (8005)
CODA-CERVA	TEM	Feret Max	34,5 (8005)
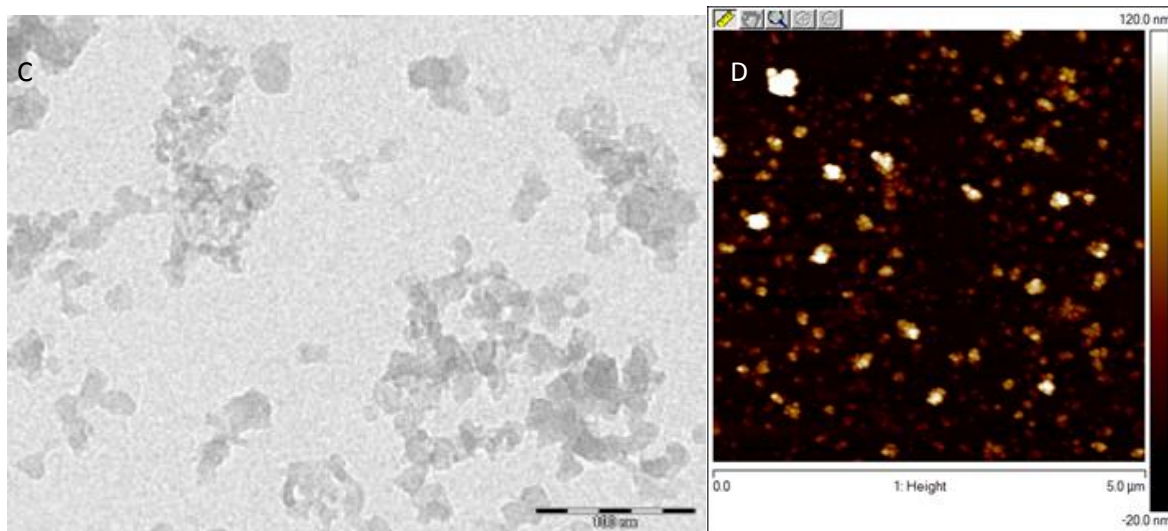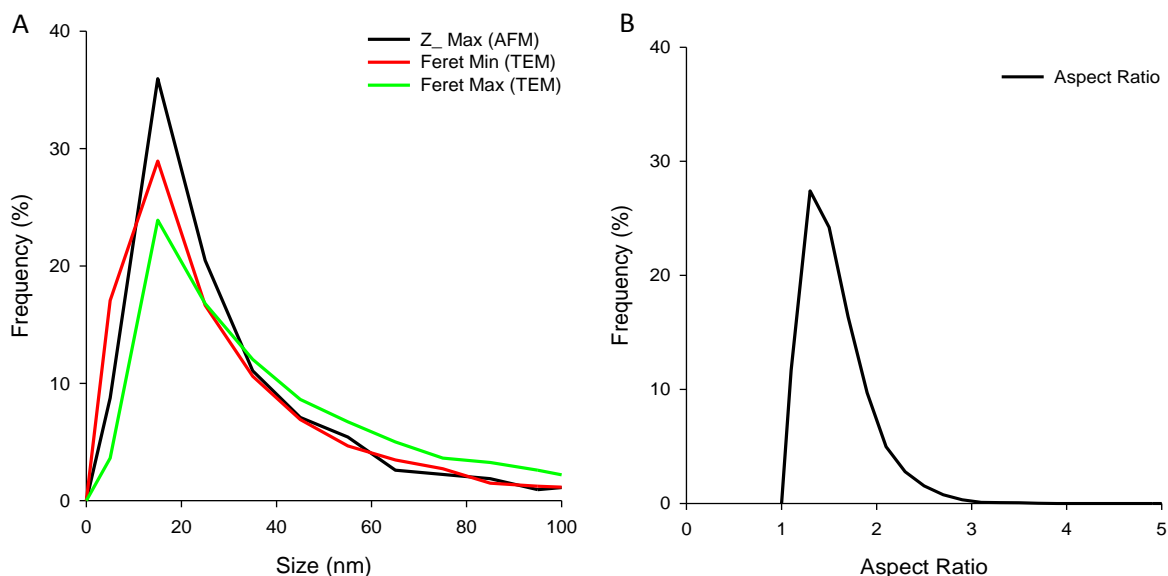
Figure 40 Characterization of the aggregates of SAS NM-200 in three-dimensions by combination of TEM and AFM. A) Number based size distributions of Feret Min, Feret max and Z_max. B) Number based distribution of the aspect ratio. Representative TEM (C) and AFM (D) micrographs visualizing the morphology of the aggregates.

Table 29 Characterization of SAS NM-201 in three dimensions

Lab	Technique	Parameter	Median (N)
CEA	AFM	Z max	33,5 (1275)
CODA-CERVA	TEM	Feret Min	25,4 (5311)
CODA-CERVA	TEM	Feret Max	38,5 (5311)
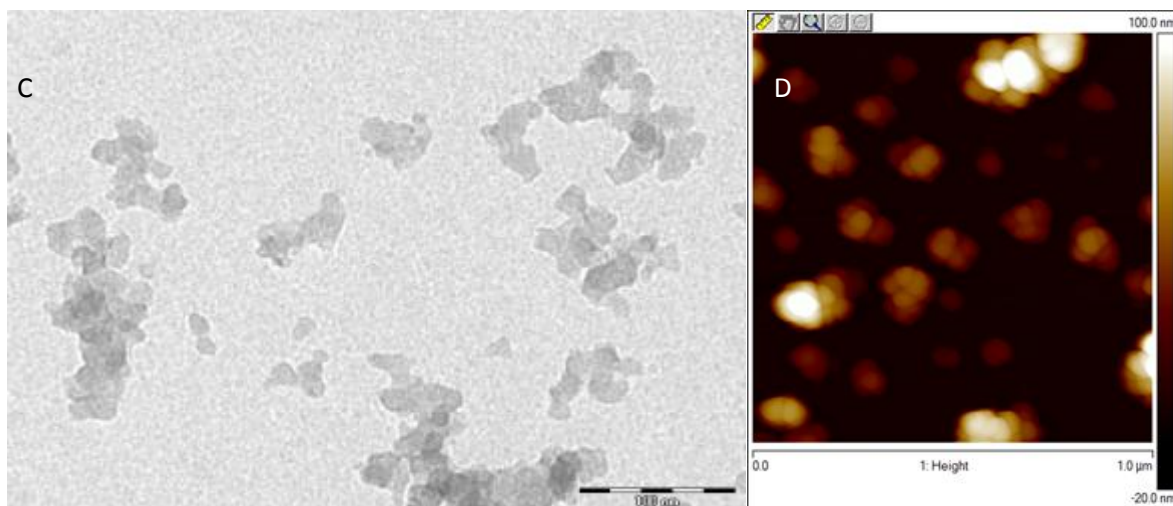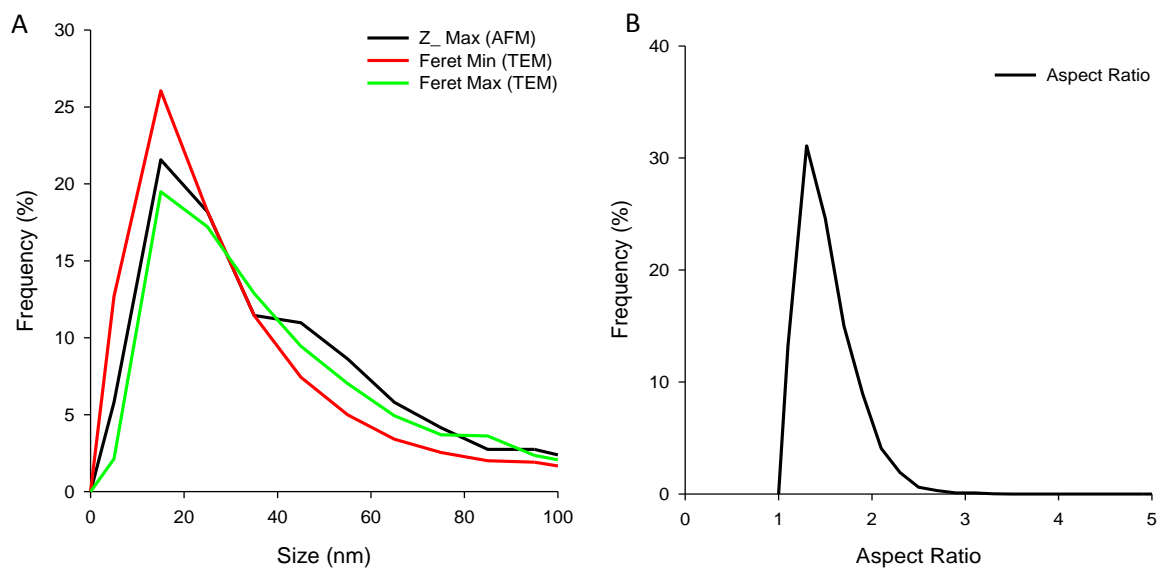
Figure 41 Characterization of the aggregates of SAS NM-201 in three-dimensions by combination of TEM and AFM. A) Number based size distributions of Feret Min, Feret max and Z_max. B) Number based distribution of the aspect ratio. Representative TEM (C) and AFM (D) micrographs visualizing the morphology of the aggregates.

Table 30 Characterization of SAS NM-202 in three dimensions

Lab	Technique	Parameter	Median (N)
CEA	AFM	Z max	38,2 (1103)
CODA-CERVA	TEM	Feret Min	37,2 (4248)
CODA-CERVA	TEM	Feret Max	58,4 (4248)
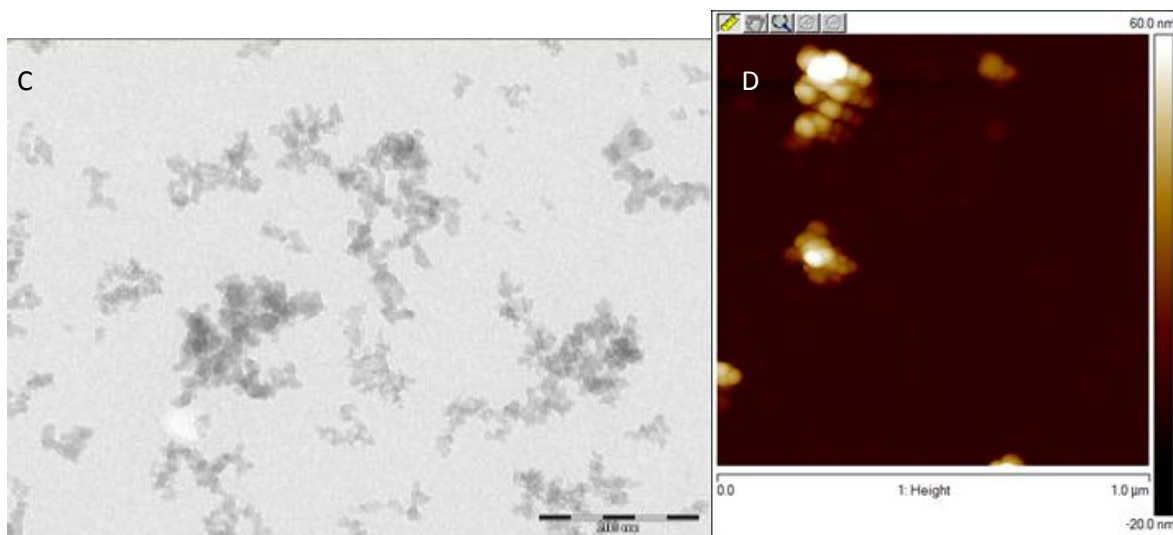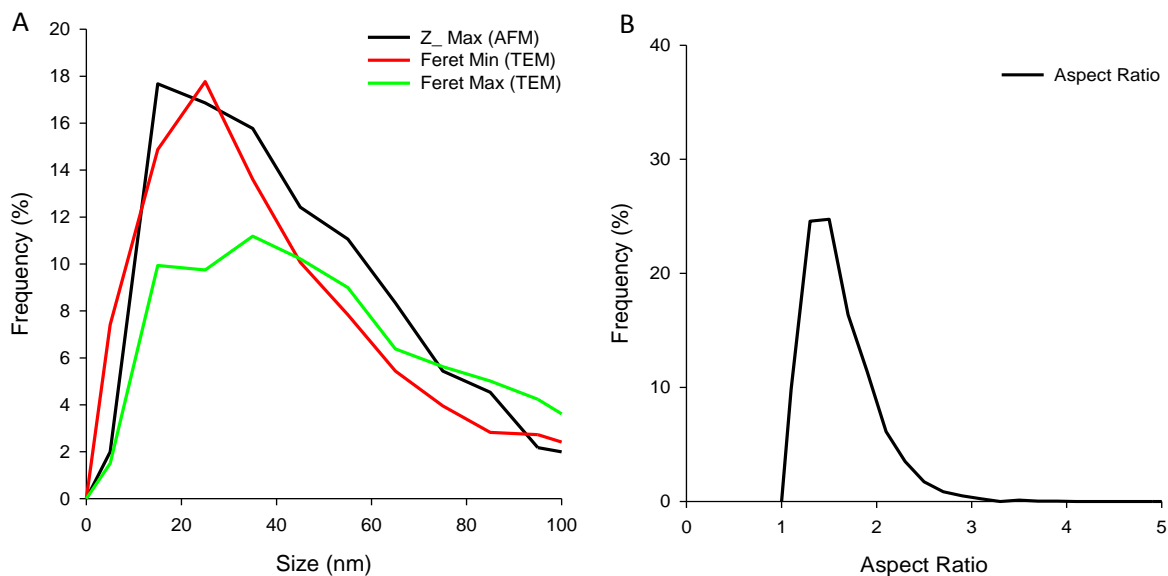
Figure 42 Characterization of the aggregates of SAS NM-202 in three-dimensions by combination of TEM and AFM. A) Number based size distributions of Feret Min, Feret max and Z-max. B) Number based distribution of the aspect ratio. Representative TEM (C) and AFM (D) micrographs visualizing the morphology of the aggregates.

Table 31 Characterization of SAS NM-203 in three dimensions

Lab	Technique	Parameter	Median (N)
CEA	AFM	Z max	24,2 (593)
CODA-CERVA	TEM	Feret Min	33,5 (4889)
CODA-CERVA	TEM	Feret Max	53,2 (4889)
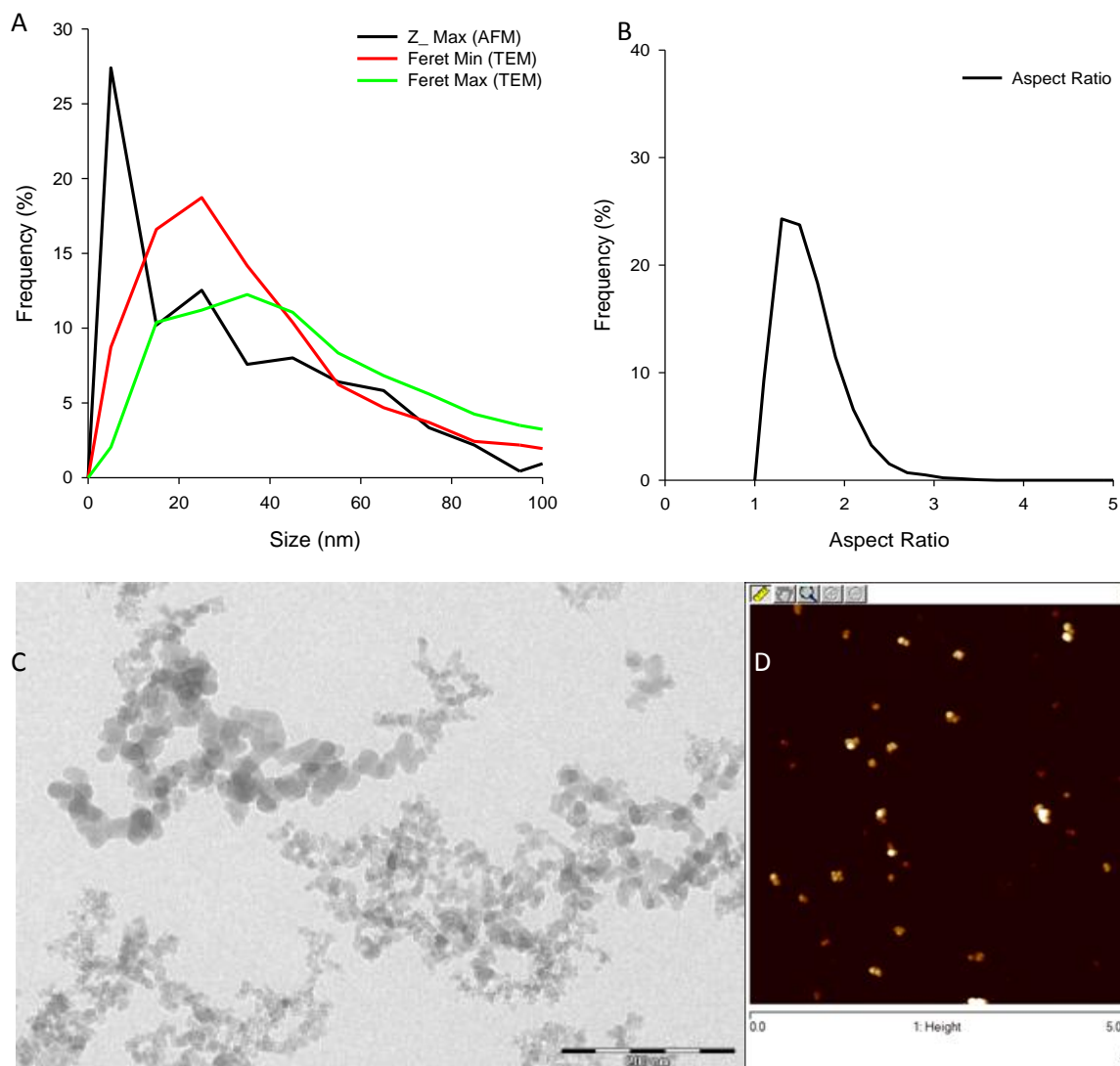
Figure 43 Characterization of the aggregates of SAS NM-203 in three-dimensions by combination of TEM and AFM. A) Number based size distributions of Feret Min, Feret max and Z_max. B) Number based distribution of the aspect ratio. Representative TEM (C) and AFM (D) micrographs visualizing the morphology of the aggregates.

For SAS nanomaterials, the suspension preparation protocols for AFM and TEM are very close (the only difference is 16 min sonication Vs. 20 min sonication which should no be of great influence since NM are already well dispersed after 16 min sonication), and nanoparticles interact with a surface

69

coated with alcian blue in both cases. This explains the very good correspondence between AFM and TEM values, and validate the comparison.

Particles which are unequiaxial have a preferential orientation versus the carrier grid, as was observed for NM-200 and NM-203 by electron tomography.

70

www.nanogenotox.eu

5 Discussion

5.1 Sample preparation

To characterize a NM, and for *in vivo* and *in vitro* toxicological testing, sonication is recommended as a standard preparatory step to disperse its large aggregates and agglomerates [34]. The sonication energy required to prepare a SAS and TiO_2 NM sample in its most disperse state was determined as suggested by Powers et al. [35]. This allowed optimization of the attachment of the NM to the grid.

To examine the intrinsic properties of SAS NM, samples were diluted in double distilled water because this medium allowed maximal adsorption of the fraction of nano-sized particles to the grid surface. Moderate salt concentrations as well as proteins resulted in a reduced number of particles per surface area, possibly indicating precipitation of NM-200. This is in agreement with the findings of [36]. MWCNTs were stabilized by BSA. This lowered the speed of precipitation increasing the stability of the suspension [37, 38].

5.2 Qualitative and quantitative analysis of NM based on TEM micrographs.

The general guidelines for image acquisition and analysis proposed by Pyrz and Buttrey [23] were adapted to the analysis of NM. TEM imaging conditions were chosen such that a compromise is reached that combines a sufficient number of particles per image with a resolution providing an acceptable number of pixels per image, while the useful range contained the large majority of the particles.

The preprocessing of images remains limited, only N x N averaging was essential, and is appropriate for all examined SAS and TiO_2 NM. This avoids loss of information and addition of artifacts associated with significant processing reducing errors into the analysis [23]. Automation allows measuring multiple and arithmetically complex parameters, described in Table 13 simultaneously on high numbers of detected particles. This reduces operator-induced bias and assures a statistically relevant number of measurements avoiding the tedious repetitive task of manual measurement. Primary particle measurements remained labor intensive and only 4 parameters could be measured.

Since this method contains no steps that are specific for a certain material, it can readily be adapted to characterize aggregates and agglomerates of a variety of NM, provided that they can be coated quantitatively to the EM-grid and distinguished from the background. For most metal oxides and for metallic NM, the latter poses no problem.

Access to multiple parameters allows selecting the optimal parameter in function of a specific material or purpose as exemplified hereafter. The mean diameter, and feret mean [39, 40] are the result of multiple diameters measured under different angles. Therefore, they can estimate the size of particles with complex surface topology, like SAS, more precisely than simple parameters, such as Feret min, Feret max, diameter min and diameter max. The measurement of the equivalent circle diameter (ECD), calculated from the projected surface area, assumes a spheroidal particle morphology like most separation and light scattering based techniques. Hence, ECD suits well from

71

comparison of results obtained by techniques such as disc centrifugation and dynamic light scattering. To define a material as a NM, the percentage of aggregates smaller than 100nm can be calculated from the number-based distribution of Feret min, an estimate for minimal size in one dimension. In the examined sonicated SAS and TiO_2, these percentages were much higher than 50% Table 14 and Table 16, defining them as NM according to [3]. Since *sensu stricto* not the aggregate size, but the size of the primary particles complying with this condition, the actual percentage can be assumed much higher (Table 4 and Table 5). The standard deviation of this measure ranging from 1 to 2% for SAS NM and from 0.4 to 2 % for titanium dioxide NM suggest that this method can also be useful in specific cases where, warranted by concerns for environment, health, safety or competitiveness, the number size distribution of 50% may be replaced by a threshold between 1 and 50% [3]. Size measures like the aggregate projected area (Area) and the aggregated maximum projected length (Feret Max) are suitable to assess fractal like NM comprising precipitated and pyrogenic SAS NM [41, 42]. Combined with the size and overlap coefficient of primary particles, the fractal dimensions can be inferred from these specific aggregate size measures according to [43]. These fractal dimensions are used to explain different phenomena in physics, chemistry, biology and medicine [44].

Principle component analysis demonstrated that the measured twenty-three parameters could be subdivided objectively for all SAS and for both examined titanium dioxide NM into three orthogonal classes representing size, shape and surface topology. Barrett et al. [20] proposed a fourth parameter for NM characterization, namely the surface texture. According to [45], this parameter be estimated from fractal dimension of the particles.

The characterization of a NM by at least one parameter of each of the three classes based on PCA is in line with the guidelines in [4, 16, 46] that parameters of these classes are essential for the characterization and identification of a NM, e.g. in the context of the risk assessment of the application of NMs in the food and feed chain. The findings of [17] corroborate this, showing that the size, physical form and morphology parameters determine the access of NM to human cells and cell organelles. In this context, the properties of individual particles measured in two dimensions can be more meaningful than one-dimensional parameters. Certain subpopulations cannot be distinguished based on one parameter but can be distinguished based on combinations of parameters for size, shape and surface topology, as described earlier by [20]

Differences in the production processes of SAS can result in differences in polydispersity, sphericity and shape factor, as illustrated for pyrogenic and precipitated SAS NM. Boldrige [41] proposed that for pyrogenic SAS the temperature variations occurring near the flame on a microscopic scale result in a greater variability in primary particle size as opposed to precipitated SAS where the primary particle size is more homogeneous.

5.3 Transmission electron tomography

As a proof of principle, it was shown that application of conventional BF ET allows 3D visualization of SAS NM. The examined SAS NM were shown to be amorphous and weak scattering such that their mass thickness is the dominant contrast mechanism. The BF images of the tilt series are thus essentially projections on which tomographic reconstructions can be based [5].

Titanium dioxide NM could not be visualized by BF-TEM combined with ET. Diffraction contributes to image formation and the projection requirement is not fulfilled for the entire tilt series. This

72

projection requirement states that for an image intensity to be usable for ET reconstruction, it has to be a monotonic function of a projected physical quantity [4]. A combination of scanning transmission electron microscopy (STEM) and high angle annular dark field imaging (HAADF) which is insensitive to Bragg diffraction would be preferable over bright field imaging to visualize these titanium dioxide NM at high resolution [11-13]. Because diffraction increases the background of the reconstruction and reduces its resolution, BF ET has been suggested to be of only limited value to analyze crystalline nanostructures [11,12].

For SAS NM, BF ET allows measuring their surface features and VSSA. This approach can hence contribute to bring the second and third condition of the definition of a nanomaterial proposed by the EC in practice [47]. Recent technical developments promise for the near future the possibility to analyze large numbers of particles [48] representative for the sample, a better reconstruction [49], less influence of missing wedge artifacts [48, 50-52] such that the characterization of nanomaterials by transmission electron tomography can become more precise and less time-consuming.

References

This report is based on the interim project reports and direct contributions from all co-authors. Most of the interim reports are available for the NANOGENOTOX consortium on the CIRCA web-page and not cited specifically in this report.

1. Jensen K, Clausen P, Birkedal R, Kembouche Y, Christiansen E, Levin M, Koponen I, Jacobsen N, Wallin H, De Temmeman P-J *et al*: **Standard operating procedures for characterization of the selected manufactured nanomaterials and dispersions thereof.** . In: *Standard operating procedures for characterization of the selected manufactured nanomaterials types.* Edited by Jensen K, Thieret N; 2011.
2. **Commission Recommendation on the definition of the term "nanomaterial"** [http://ec.europa.eu/environment/consultations/pdf/recommendation_nano.pdf]
3. **Commission Recommendation on the definition of nanomaterial** [http://ec.europa.eu/environment/chemicals/nanotech/pdf/commission_recommendation.pdf]
4. **Scientific Basis for the Definition of the Term "Nanomaterial"** [http://ec.europa.eu/health/scientific_committees/emerging/docs/scenihr_o_030.pdf]
5. ISO 14644-6: **Cleanrooms and associated controlled environments**. In: *Part 6: Vocabulary.* 2007.
6. ISO/TS 27687: **Terminology and definitions for nano-objects - Nanoparticle, nanofibre and nanoplate**. In: *Nanotechnologies.* 2008.
7. Roduner E: **Size matters: why nanomaterials are different**. *Chem Soc Rev* 2006, **35**(7):583-592.
8. Xu W, Xu F, Jones M, Keszthelyi B, Sedat J, Agard D, Mueller K: **High-performance iterative electron tomography reconstruction with long-object compensation using graphics processing units (GPUs)**. *J Struct Biol* 2010, **171**(2):142-153.
9. **Chemical Safety Report: Synthetic Amorphous Silica** [http://www.reach-sas.org/documents/synth%20amorph%20silica%20EC%20231-545-4%20uses.pdf]
10. Lin W, Huang YW, Zhou XD, Ma Y: **In vitro toxicity of silica nanoparticles in human lung cancer cells**. *Toxicol Appl Pharmacol* 2006, **217**(3):252-259.
11. Cervera Gontard L, Ozkaya D, Dunin-Borkowski RE: **A simple algorithm for measuring particle size distributions on an uneven background from TEM images**. *Ultramicroscopy* 2011, **111**(2):101-106.
12. Mast J, Demeestere L: **Electron tomography of negatively stained complex viruses: application in their diagnosis**. *Diagn Pathol* 2009, **4**:5.
13. Merkus HG: **Particle Size Measurements**, 1 edn. Pijnacker: Springer; 2009.
14. Tiede K, Boxall ABA, Tear SP, Lewis J, David H, Hassellöv M: **Detection and characterization of engineered nanoparticles in food and the environment**. *Food Additives & Contaminants: Part A: Chemistry, Analysis, Control, Exposure & Risk Assessment* 2008, **25**(7):795 - 821.
15. Masuda H, Gotoh K: **Study on the sample size required for the estimation of mean particle diameter**. *Advanced Powder Technology* 1999, **10**(2):159-173.
16. **Guidance on the risk assessment of the application of nanoscience and nanotechnologies in the food and feed chain** [http://www.efsa.europa.eu/en/efsajournal/doc/2140.pdf]

17. Chu Z, Huang Y, Tao Q, Li Q: **Cellular uptake, evolution, and excretion of silica nanoparticles in human cells**. *Nanoscale* 2011, **3**(8):3291-3299.
18. **European Comission Recomendation on the Term Nanomaterial** [http://ec.europa.eu/environment/consultations/pdf/recommendation_nano.pdf]
19. Van Doren E, De Temmerman P-J, Francisco M, Mast J: **Determination of the volume-specific surface area by using transmission electron tomography for characterization and definition of nanomaterials**. *Journal of Nanobiotechnology* 2011, **9**(1):17.
20. Barrett PJ: **The shape of rock particles, a critical review**. *Sedimentology* 1980, **27**(3):291-303.
21. **Synthetic Amorphous Silica and Silicates** [http://www.chem.unep.ch/irptc/sids/oecdsids/Silicates.pdf]
22. Hassellöv M, Readman J, Ranville J, Tiede K: **Nanoparticle analysis and characterization methodologies in environmental risk assessment of engineered nanoparticles**. *Ecotoxicology* 2008, **17**(5):344-361.
23. Pyrz WD, Buttrey DJ: **Particle Size Determination Using TEM: A Discussion of Image Acquisition and Analysis for the Novice Microscopist**. *Langmuir* 2008, **24**(20):11350-11360.
24. NIST 960-1: **Particle Size Characterization**. In*.*; 2001.
25. ISO 14887: **Dispersion procedures for powders in liquids**. In: *Sample preparation.* 2000.
26. ISO 14488: **Sampling and sample splitting for the determination of particulate properties**. In: *Particulate materials.* 2007.
27. ISO 13322-1: **Particle size analysis -Image analysis methods-**. In: *Part 1: Static image analysis methods.* 2004.
28. ISO 9276-2: **Calculation of average particle sizes/diameters and moments from particle size distributions**. In: *Representation of results of particle size analysis.* 2001.
29. ISO 9276-6: **Descriptive and quantitative representation of particle shape and morphology**. In: *Representation of results of particle size analysis.* 2008.
30. Krumbein WC, Sloss LL: **Stratigraphy and Sedimentation**. San Francisco; 1963.
31. ISO 9276-1: **Graphical representation**. In: *Representation of results of particle size analysis.* 1998.
32. Jensen K, Kembouche Y, Christiansen E, Jacobsen N, Wallin H: **The generic NANOGENOTOX dispersion protocol**. In: *Standard Operation Procedure (SOP) and background documentation Final Protocol for producing suitable manufactured nanomaterial exposure media* Edited by Jensen K, Thieret N; 2011.
33. Namork E, Johansen BV: **Surface activation of carbon film supports for biological electron microscopy**. *Ultramicroscopy* 1982, **7**(4):321-329.
34. **Preliminary Guidance notes on Sample Preparation and Dosimetry for the Safety Testing of Manufactured Nanomaterials** [http://www.oecd.org/officialdocuments/displaydocumentpdf?cote=ENV/JM/MONO%282010%2925&doclanguage=en]
35. Powers KW, Brown SC, Krishna VB, Wasdo SC, Moudgil BM, Roberts SM: **Research Strategies for Safety Evaluation of Nanomaterials. Part VI. Characterization of Nanoscale Particles for Toxicological Evaluation**. *Toxicol Sci* 2006, **90**(2):296-303.
36. Jiang J, Oberdörster G, Biswas P: **Characterization of size, surface charge, and agglomeration state of nanoparticle dispersions for toxicological studies**. *Journal of Nanoparticle Research* 2009, **11**(1):77-89.
37. Ji Z, Jin X, George S, Xia T, Meng H, Wang X, Suarez E, Zhang H, Hoek EMV, Godwin H *et al*: **Dispersion and Stability Optimization of TiO2 Nanoparticles in Cell Culture Media**. *Environmental Science & Technology* 2010:null-null.

38. Bihari P, Vippola M, Schultes S, Praetner M, Khandoga A, Reichel C, Coester C, Tuomi T, Rehberg M, Krombach F: **Optimized dispersion of nanoparticles for biological in vitro and in vivo studies**. *Particle and Fibre Toxicology* 2008, **5**(1):14.

39. Riley CM, Rose WI, Bluth GJS: **Quantitative shape measurements of distal volcanic ash**. *J Geophys Res* 2003, **108**(B10):2504.

40. Podczeck F, Mia Y: **The influence of particle size and shape on the angle of internal friction and the flow factor of unlubricated and lubricated powders**. *International Journal of Pharmaceutics* 1996, **144**(2):187-194.

41. Boldridge D: **Morphological Characterization of Fumed Silica Aggregates**. *Aerosol Science and Technology* 2010, **44**(3):182-186.

42. Bau S, Witschger O, Gensdarmes F, Rastoix O, Thomas D: **A TEM-based method as an alternative to the BET method for measuring off-line the specific surface area of nanoaerosols**. *Powder Technology* 2010, **200**(3):190-201.

43. Brasil AM, Farias TL, Carvalho MG: **A recipe for image characterization of fractal-like aggregates**. *Journal of Aerosol Science* 1999, **30**(10):1379-1389.

44. Nel AE, Madler L, Velegol D, Xia T, Hoek EM, Somasundaran P, Klaessig F, Castranova V, Thompson M: **Understanding biophysicochemical interactions at the nano-bio interface**. *Nat Mater* 2009, **8**(7):543-557.

45. ISO 9276-6: **Part 6: Descriptive and quantitative representation of particle shape and morphology**. In: *Representation of results of particle size analysis.* Geneva; 2008.

46. **Guidance Manual for the testing of Manufactured Nanomaterials** [http://www.oecd.org/officialdocuments/displaydocumentpdf/?cote=env/jm/mono%282009%2920/rev&doclanguage=en]

47. **European Comission recommendation on the definition of the term "nanomaterial"** [http://ec.europa.eu/environment/consultations/pdf/recommendation_nano.pdf]

48. Lengyel JS, Milne JL, Subramaniam S: **Electron tomography in nanoparticle imaging and analysis**. *Nanomedicine (Lond)* 2008, **3**(1):125-131.

49. Batenburg KJ, Bals S, Sijbers J, Kubel C, Midgley PA, Hernandez JC, Kaiser U, Encina ER, Coronado EA, Van Tendeloo G: **3D imaging of nanomaterials by discrete tomography**. *Ultramicroscopy* 2009, **109**(6):730-740.

50. Penczek P, Marko M, Buttle K, Frank J: **Double-tilt electron tomography**. *Ultramicroscopy* 1995, **60**(3):393-410.

51. Mastronarde DN: **Dual-axis tomography: an approach with alignment methods that preserve resolution**. *J Struct Biol* 1997, **120**(3):343-352.

52. Tong J, Arslan I, Midgley P: **A novel dual-axis iterative algorithm for electron tomography**. *J Struct Biol* 2006, **153**(1):55-63.

Appendix: Detailed Standard Operation Procedures for size analysis using TEM and sample preparation

Three different methods were applied for analyzing the particle size distribution by transmission electron microscopy.

Primary particle size distribution of TiO_2 and SiO_2 by TEM at INRS
Davy Rousset (INRS)

General description

The grids are directly observed by TEM (Zeiss EM 910 120 kV). For the determination of primary particles size distribution, particles are observed at a magnification of x 100 000. Images were digitized with a digital camera (ProgRes® JENOPTIK CF Scan Digital Microscope Camera Jenoptik – resolution 2k x 2k approx.) and associated software. The size distribution is based on 100 measurements (approx. 5 measurements x 20 images). Using a free processing image software (ImageJ, NIH), particles' outlines are manually drawn, so surface areas are reachable, and the diameter is calculated assuming primary particles spherical.

<u>Materials and Chemicals</u>

TEM Zeiss EM 910 120 kV operating at 100 kV
Ultrasonic bath (Annemasse)
ImageJ (free download at http://rsb.info.nih.gov/ij/)
Sputtering system: Balzers model SCD 040
TEM grid
Sterile pipette
Oven
2-propanol grade analysis
50 ml plastic vials
Spatula
For BSA see dispersion protocol
For aerosol see SOP Nanodustiness by the vortex shaker method

Sample preparation
<u>Dispersion in isopropanol</u>
A small amount of powder (spatula tip) is added to about 15ml isopropanol in a glass vial. The suspension is then sonicated during 10 min in ultrasonic bath to enhance NM's dispersion. Just at the end of sonication, about 3 to 10 droplets of suspension are put with disposable sterile pipettes onto pre-carboned TEM grids under vacuum (vacuum enhances droplet drying). Grids are then dried during few minutes in an oven at 50°C before TEM observation.

<u>Dispersion in BSA</u>

WP4 dispersion protocol is used. Just after sonification, drops of suspension are put with disposable sterile pipettes onto microscope glass slides. A pre-carboned TEM grid is then put onto the drop surface. After about 2 min, the grid is dried during few minutes in an oven at 50°C before TEM observation.

Data treatment

Regular spread-sheet or statistical program capable of calculating and plotting data for size distribution analysis. Size distribution data are presented in histogram.

Comments on use and applicability

This SOP is operator-dependant as it was not possible to computerize primary particles identification using our image processing software. This has to be hand-made.

Aggregate/agglomerate size distribution of TiO$_2$ and SiO$_2$ by TEM at INRS

Davy Rousset (INRS)

Description of method and data collection

The grids are directly observed by TEM (Zeiss EM 910 120 kV). For the determination of the aggregate/agglomerate size distribution, particles are observed at a magnification of x 25000 or x 50000 according to the size of the objects. Images were digitized with a digital camera (ProgRes® JENOPTIK CF Scan Digital Microscope Camera Jenoptik – resolution 2k x 2k approx.) and associated software. The size distribution is based on 100 measurements (approx. 20 images). Using a processing image software (Visilog, NOESIS), images are digitized and particles are identified automatically by the software which yields several morphological parameters for each aggregate/agglomerate, such as area, perimeter, Feret diameter… The unit of software is in pixel but could be easily converted in nm from internal calibration.

Materials and Chemicals

TEM Zeiss EM 910 120 kV operating at 100 kV
Ultrasonic bath (Annemasse)
Visilog (NOESIS)
Sputtering system: Balzers model SCD 040
TEM grid
Sterile pipette
Oven
2-propanol grade analysis
50 ml plastic vials
Spatula
For BSA see dispersion protocol

For aerosol see SOP Nanodustiness by the vortex shaker method

Sample preparation

Dispersion in isopropanol

A small amount of powder (spatula tip) is added to about 15ml isopropanol in a glass vial. The suspension is then sonicated during 10 min in ultrasonic bath to enhance NM's dispersion. Just at the end of sonification, about 3 to 10 droplets of suspension are put with disposable sterile pipettes onto pre-carboned TEM grids under vacuum (vacuum enhances droplet drying). Grids are then dried during few minutes in an oven at 50°C before TEM observation.

Dispersion in BSA

WP4 dispersion protocol is used. Just after sonification, drops of suspension are put with disposable sterile pipettes onto microscope glass slides. A pre-carboned TEM grid is then put onto the drop surface. After about 2 min, the grid is dried during few minutes in an oven at 50°C before TEM observation.

Data treatment

Size distribution (histogram)

Comments on use and applicability

Aggregate/agglomerate size distribution for aerosol to be done.

Need to check the influence of:

- Dispersion media (isopropanol, BSA-water, aerosol)
- Magnification

Semi-automatic detection and image analysis of nanoparticles at CODA-CERVA

Pieter-Jan de Temmerman & Jan Mast (CODA-CERVA)

General description

This protocol provides a step-by-step guide for semi-automatic detection and image analysis of nanoparticles that can be distinguished from the background based on their grey values corresponding with electron density. The protocol is conform with the ISO 13322-1:2004(E) "Particle size analysis – Part I: Image analysis methods. In principle the current method allows to detect and analyze any kind of nanoparticles and has successfully been applied for: Ag, Au, SiO_2, TiO_2, Fe_2O_3 and Fe_3O_4. However, on-going work suggests that even more information can be extracted from quantitative measurements than anticipated from the ISO norm.

During an automatic particle analysis, the image analysis program automatically detects particles on an image. The gray value, corresponding with electron density, is the criterion for the recognition of a particle. Therefore, in order to have successful particle detection, the particles must clearly stand out from the background. All detected particles can be semi-automatically measured. A wide array of measured parameters can be chosen.

A typical particle analysis consists of following steps:

- Image preparation
- Setting and adjusting the threshold value
- Defining the detection area
- Definition of the detection parameters and detection of the nanoparticles
- Selection of the particle parameters
- Defining the classification schemes
- Classification of the particles according the selected parameters
- Selection of the parameters for a class measurement
- Exporting of results in excel spreadsheets and storage of the images in the nanoparticles database

Equipment

In order to perform analyses, the 'Analysis solution' of the iTEM software (Version 5.0, Olympus, Münster, Germany) installed on a powerful computer is indispensable. The iTEM software can directly be integrated in a database in which relevant fields can be accessed. Alternatively separate files in TIF-format can be analysed if a correct calibration of pixel size can be assumed.

Instruction

Image preparation

- (Optional) Verify whether the image background (e.g. due to heterogeneous image illumination during image acquisition) is homogenous. The mean intensity profile should have no specific tendency.
- [Measure – Intensity Profile – Horizontal Mean]

Co-funded by
the Health Programme
of the European Union

- (Optional) Modify the gray values based on the graph displaying the frequencies of different gray values such that only relevant gray values are maintained.
- (Optional) Apply the Separator filter to separate neighbouring particles.
- Set the zoom level of the image in the viewport to 100%.
- Select the "Oper > Define Filter Separator..." command.
- Select the "Step option" in the "Boundary shape" group.
- Set both "Smooth" and "Fine/Coarse" slide controls to 1.
- Switch on the preview to be able to observe how adjusting settings alters the image.
- Move the Fine/Coarse slide control incrementally higher until you have found the optimal setting.
- If an image has a lot of noise, increase the value Smooth.
- Select the "Burn white option" in the Result group to be able to sketch white dividing lines on the original gray value image.
- Click the "Execute" button to separate particles.
- The resulting image in the target image buffer will display the image with the particles outlined in white (a gray value of 1).
- The separating line generated has a width of one pixel.
- Please keep in mind that the gray value range which defines the particles must not contain a gray value of "1".
- Introduce the obtained intermediate image into the nanoparticle database, attached to the original micrograph for later reference.

Setting thresholds

- Set the gray value range interactively and manually to define the particles so that they are distinguishable from the image background. The thresholds are comprised of the lowest and greatest gray values. Comment 1
- Load the image you wish to analyze into the active image buffer.
- Select the "Image > Set Thresholds..." command.
- Select the "Manual" tab. Define only one gray value phase.
- Select the "Histogram" entry from the "Diagram" group. The diagram now shows the gray-value distribution within the image frame you have set. The current threshold values are shown in the diagram as two perpendicular lines. The lower threshold is blue and the upper is red.
- Mark the "Current" option in the "Preview" group. The active phase is shown in color within the image so that you can view what affect your settings have.
- Define the gray value range directly in the diagram such that all particles belonging to that phase are shown in color. Move the mouse pointer over one of the two threshold lines. The mouse pointer will change into a double arrow. Hold down the left mouse button and pull the threshold to the desired value. The set gray value range will be colored within the image.
- Confirm the new threshold setting by clicking on "OK".

Defining detection area (ROI)

- Define the detection area. This is the region of interest (ROI) to which the particle analysis is restricted. Comment 2
- Select the "Analysis > Define ROI" command.

Co-funded by
the Health Programme
of the European Union

- To delete previously-set ROIs, click the Delete All button.
- Define the ROI selecting one of the shapes in Tools group.
- Make the ROI smaller than the picture, otherwise the Exclude border particles command will distort the result
- Right click to return to the dialog box. The new ROI will be numbered and added to the Active ROI list.
- Exit the Define ROIs dialog box via the "Close" button.
- Use the "Analysis > Draw ROIs > Into Overlay" command to have the defined ROIs displayed in the overlay.

Defining detection

- Set the parameters for detection in the "Define Detection" dialog box. Settings generally do not change between analysis for the same type of particles. Exclude border particles, limit the search area to the ROI, set the particle filter (minimal pixel size) to reduce background interferences. Indicate whether the analysis should be restricted to a range of any selected measurements. Indicate whether holes in particles should be taken in account. Select the type of pixel connectivity (adjacent borders versus include diagonals) that results in the best overall particle detection.
- Select the "Analysis > Define" Detection... command.
- The Define Detection dialog box has three tabs for defining detection and classification parameters.
- Select the "Detection" tab to set particle-detection parameters.
- Enter the minimum number of pixels which may be detected as comprising a particle into the Minimum field of the Particle filter group.
- This is an excellent way to exclude noise particles.
- Clear the Use ranges check box to detect all particles occurring within the thresholds set of measurements. The Total count field shows the number of particles which were detected during the previously-conducted detection.
- If particles have inclusions which are to be taken into account when calculating particle parameters, clear the "Fill holes" check box. This is necessary for particle holes to be recognized as such.
- Indicate that the ROI should be used for detection in the Search area group.
- Define that particles, which are not located entirely within the search area are excluded from analysis in the "Border particles" group.
- Define inter-particle connectivity in the "Connectivity" group. If the separation line between two particles is only one pixel in width (e.g. when using a separator filter), then select the Adjacent borders (4) option. Otherwise the separated particles will be considered one particle when detected.
- Click the "Execute" button to conduct particle detection.
- All particles detected will be shown in the image overlay in color. Determine how particles are shown in the Classification tab. Label the particles on the micrograph with their particle ID such that they also can be identified in the data sheet.
- The most recently-defined classification will be applied.
- Click on "OK" to close the dialog box.

<u>Selection of the particle parameters</u>

- Set the particle parameters in the "Define Measurements" dialog box. This dialog box contains three tabs for defining measurements of particles, classes and ROIs. First choose the "Particles" tab. Here all the parameters listed that can be measured. These are divided in categories: Area, Density, Dimension, Distance, Features, ID, Perimeter, Position and Shape some with their according subcategories.
- Select the "Analysis > Define Measurements..." command
- Select the "Particles" tab and select the parameters you want to include in your particle analysis. The easiest way to do this is to click on "All", hereby showing all parameters alphabetically. From the list that is now exposed on the right in the dialog box, you can include your desired parameters by clicking on the check boxes.
- In the middle part of the dialog box, the selected parameters are listed.
- By clicking on a parameter an upper and lower limit can be set in the Filter range area that becomes activated in the lower part of the dialog box).
- Click "OK" or "Detect" to perform analysis.
- (Optional) You can do the same for Classes and ROI.

<u>Definition of the classification schemes</u>

A classification scheme consists of a name, a unit and a class division. Particles are sorted via the classification scheme according to certain parameters (e.g. into 10 size classes). You can determine the number of particles per size class, for example. You define a new classification scheme in the Define Classification dialog box. You have numerous possibilities in opening the dialog box:

- Use the "Measure > Define Classification..." command.
- Click the "Define Classification" button located in the "Analysis" button bar.
- Use the "Analysis > Classify..." command. Click the "Classification..." button.

Automatic image analysis of nanoparticles at CODA-CERVA

Pieter-Jan de Temmerman & Jan Mast (CODA-CERVA)

The last used classification scheme will automatically be loaded when a new image is acquired in iTEM? Change the classification if it is not applicable to the new image. The last used classification scheme will be automatically saved.

Defining a classification scheme

- Select the "Measure > Define Classification..." command to define a suitable classification scheme.
- Select the "Show sample objects" check box to be able to evaluate classification.
  - o The current overlay will disappear from view and the analysis program will show a number of sample objects for visual reference purposes.
- Enter the name of the classification into the "New Classification" field. The "new" button will become available.
- Click the "New" button to create the new classification scheme.

- Click the "Unit..." button to select the unit desired for the classification. The unit you select will depend on the classification criterion. Classifying according to area is possible by select a unit of µm², for classification according to particle length, chose a length unit (e.g. m). Classify by particle characteristics is possible by selecting 'no unit'.
- Click the "Compute..." button to define the number and value range of each class. The value range is determined by the minimum and maximum particle parameters.
  - It is possible to automatically calculate a suitable classification. In the "Compute Classification" dialog box, enter the criteria and the amount of classes and click the "Auto" button.
- Click the "OK" button to return to the "Define Classification" dialog box.
- Go to the "Define Classification" dialog box to edit the class divisions interactively:
- To alter the color of a class select the line number of that class and select one of the 16 colors available in the "Set color" color palette.
  - To give names to classes, left click in the "Name" field of the class. Enter the class name into this field.
  - To interactively alter class divisions of a class, double click on one of the numeric values and enter a new one.
- Click on "OK" to exit the dialog box.

Classifying particles

Applying classification

- Select the "Analysis > Classify..." command to divide detected particles up into classes.
- Select the desired particle parameter for classification within the "Criterion" list in the "Classify" group (e. g., "Area").
- Select "No classification" in the list of classification criteria if no classification is desired. The class parameters will then refer to all detected particles. If the classification is not available in "Classification" check in "Define Classification" whether the appropriate unit is selected (e.g. nm for a length criterion, nm² for an area criterion, no unit for a characteristics criterion).
- Select the desired classification scheme in the "Classification" list. This list will show all classifications that can be used with the unit selected.
  - Should a suitable classification scheme not be available, click the "Classification..." button to create a new classification scheme or to edit an already existing one.
- Click the Execute button to have the classification applied to the image.
  - The particles in the overlay will be divided up into classes and shown in their class color. Any particles that do not belong to any of the classes will remain crosshatched.
- If "classification" does not produce the desired results then try out other classification schemes before generating a sheet for results.
- Click on OK to close the dialog box.

Select classification parameters and export results

- Select the "Analysis > Define Measurements..." command.
- Activate the Classes tab to determine the parameters to be include in the measurement sheet.

- Select the parameters desired: e. g., "ID Class" and "Particle Count". To do this, select the check box next to the parameter desired. It will appear in the "Selected Measurements" list.
  - The parameters selected will be moved to the "Selected Measurements" list and will appear in the results sheet for each class.
  - It is advisable to include the "ID Class" parameter in the results sheet to be able to see what results go with which classes.
  - The lower part of the dialog box shows a text and graphic definition of any parameter you select.
- Click on "OK" to close the dialog box.
- Select the "Analysis > Class" Results command.
  - A sheet containing the results of the class measurement will be generated.
- All particles which cannot be assigned to a class will be put in the "0" class and included in the sheet as well.

Exporting of results

After analysis is finished, iTEM shows the results in (a) spreadsheet(s), depending of the type of analysis which is performed. These include a sheet with particle results, a sheet with class results and a sheet with frame/ROI results. Furthermore, the pictures obtained (called annotated micrographs) can be stored in the database integrated in the software. Extra information can be indicated in the appropriate fields. One extra field with additional information about a particular picture is also included.

Comments on use and applicability

Regarding setting thresholds. A Particle is a quantity of connected pixels within a defined gray value range. This is why you must define a suitable gray or color value range before particle detection. Successful particle detection requires a clear correlation between gray or color values and particle structure.

Regarding defining the detection area. If no detection area is defined, the entire image is analyzed by default. The image analysis program provides various possibilities for restricting image analysis to a specific area within an image. Mostly regions of interest (ROI) are chosen. A ROI is an area of arbitrary shape within the image allowing to restrict the area for particle analysis.

Regarding analysis of NM, it was found that length dimensions of CNT could not be adequately measured using automatic or semi-automatic analysis.

Coating of dispersed nanoparticles in liquid on grids for TEM analysis at CODA-CERVA

Pieter-Jan de Temmerman and Jan Mast (CODA-CERVA)

General description

This procedure aims to coat nanoparticles suspended in a liquid on EM-grids. To be suitable for further TEM analyses, the NP should be evenly distributed over the grids, while the fraction of the attached NP represents the dispersed NP optimally. The method allows coating of dispersed nanoparticles in liquid on EM grids for further TEM analyses

85

Co-funded by
the Health Programme
of the European Union

- The nanoparticles can be metallic (Ag, Au), metal oxides (SiO_2, TiO_2, Fe_2O_3, Fe_3O_4 or other)
- The medium can be polar (water, phosphate buffered saline,..) or apolar (hexane, acetone,…).
- TEM analyses can be qualitative or quantitative.

Dispersed particulate NP are brought in contact with an EM-grid and are allowed to interact with its surface. When excess fluid is drained and grids are air-dried, a fraction of the NP remains attached to the grid by different types of interactions (electrostatic, apolar, van der Waals, …). The concentrations of NP, and the type and charge of the grid are chosen such that the fraction of nanoparticles attached to the grids optimally represents the dispersed NP, and that (aggregates of) nanoparticles can be detected individually.

Definition, abbreviations, references and norms

- Solution: Solutions are mixtures of dispersed particles, sizes lower then 2nm, in a liquid medium.
- Colloid: Colloids are mixtures of dispersed particles, sizes between 2 nm and 1000 nm, in a liquid medium.
- Suspension: Suspension are mixtures of dispersed particles, sizes greater than 1 µm, in a liquid medium.
- Primary- or single particle: An individual particle recognized by suitable physical means
- Aggregate: Primary particles assembled face-to-face; their surface area is smaller than the sum of the surface area of the primary particles (DIN 53206).
- Agglomerate: Primary particles and/or aggregates not permanently joined together but attached e.g. at the edges and corners. Their surface area does not differ markedly from the sum of that of the individual units (DIN 53206).
- Liquid: The state in which a substance exhibits a <u>characteristic</u> readiness to <u>flow</u> with <u>little</u> or no tendency to disperse and relatively high <u>incompressibility</u>.
- Medium: The liquid vehicle in which nanoparticles can be dispersed.
- PBS: Phosphate buffered saline
- TEM: Transmission electron microscopy
- NP: Nanoparticles
- NM: Nanomaterial

Materials and equipment

- Eppendorf microcentrifuge tubes
- Pioloform-coated and carbon-shaded copper grids 400 mesh (Agar Scientific Ltd., G2400C). Both home-made and commercially available grids can be used.
- Large (120 mm diameter) polyethylene petridish
- pipette tips of 200µl (Gilson Diamond) and 200-1000µl (VWR)
- Tweezers
- Filter papers Ø 70 mm (Whatman, 54 hardened) and tape
- 4" Parafilm M (American National Can, Freewich, CT06830)
- Permanent, waterproof marker or a ball point to indicate references on filter paper
- Water (double distilled), Hexane or PBS

- Alcian blue stock solution: 2 % in water
- Alcian blue working solution: Dilute the Alcian blue stock solution with an equal amount of water to obtain a 1 % working solution. The latter is stable for 1 month at 4 °C.
- Micropipettes of 20 µl, 200 µl and 1000 µl (Gilson)

Instruction for coating and preparation of TEM samples

Alcian blue pre-treatment of the grids

- Increase the hydrophilicity of EM-grids by pre-treating them with Alcian blue (Comment 1).
- Fix a strip of parafilm to a flat and clean surface by wetting the surface with some drops of water, press the parafilm with the film side to the surface and remove the protective cover carefully.
- Place an EM grid with the carbon-coated side on a drop of about 20 µl Alcian blue working solution and incubate for 10 minutes. Avoid air drying of the grids.
- Grip the grid carefully with a pair of tweezers and wash most of the blue stain away by transferring it to 5 drops of water placed on the parafilm. Remove excess fluid by blotting its edge on a strip of filter paper, leaving a rest of humidity.
- Use the grids immediately in the next step.

Coating the nanoparticles on the grid

- Homogenize the dispersed nanoparticles by shaking, vortexing stirring or pipetting.
- Dilute the dispersed NP by adding a suitable dilution medium (Comment 2).
    - Make a two to ten-fold dilution series by pipetting dispersed NP into an eppendorf-type microcentrifuge tube and dilute by adding medium.
    - Repeat this pipetting step with the last dilution another three times.
- Allow the NP to interact with the grid surface by either the drop-on-grid method, or the grid-on-drop method (Comment 3).

Grid-on-drop method: Place the EM-grid on a droplet of dispersed NP.

- Fix a strip of parafilm to a flat and clean surface by wetting the surface with some drops of water, press the parafilm with the film side to the surface and remove the protective cover carefully.
- Place a droplet of 2 to 50 µl of dispersed NP on the parafilm
- Transfer the grid to the droplet and indicate the appropriate references with a waterproof marker.
- Float the grids, with coated surfaces down, on the droplets for 1 to 10 minutes.
- Remove excess fluid by blotting its edge on a strip of filter paper, leaving a rest of humidity.

Drop-on-grid method: Place a droplet of dispersed NP on an EM-grid.

- Put the grid on the parafilm and then pipette a droplet of 2 to 50 µl of dispersed NP on the grid. Leave this for 1 to 10 minutes.
- Remove excess fluid by blotting its edge on a strip of filter paper, leaving a rest of humidity.

Extra rinse step (Comment 4)

Co-funded by
the Health Programme
of the European Union

- Rinse the grids, with coated surfaces down, by placing them on a droplet of water for 30 seconds to remove excess material
- Remove excess fluid by blotting its edge on a strip of filter paper, leaving a rest of humidity.

Storage of the grids

- Place the grids in a grid box or on a filter paper in a petri-dish.
- Make sure to always note the appropriate references in order to be able to recover the grids later on

Specific safety measures

- Because of the possible toxicity of the reagents and NP and the possible presence of unknown contaminants, it is highly recommended to wear gloves during this procedure.
- All waste materials generated during this procedure should be disposed in the suitable container for chemical waste.
- Hexane is explosive (see MSDS file)

Comments on use and applicability

Comment 1: The interaction of NP with an EM-grid is strongly determined by the charge of the grid. In general, carbon-coated coated grids are negatively charged, although dependent on the preparation of the grid these charges tend to disappear leaving a hydrophobic surface. The hydrophilicity of EM-grids can be increased by pre-treating them with Alcian blue. The resultant positive charge strongly increases attachment of negatively charged nanoparticles. In case the charge of the NP is unknown, it is wise to evaluate both Alcian blue and non-treated grids.

Comment 2: PBS can be diluted by water and vice versa. Dilution with water is preferred, to lower salt concentration. If the dispersability of the NP is not negatively altered.

Comment 3: A concentration of NP should be chosen such that the number of particles per picture is optimal. It should be taken into account that the NP do not touch or overlap each other. Optimal concentrations vary from sample to sample. A typical concentration for colloidal spherical unaggregated Silica NP is 0,05 mg/ml. For colloidal aggregated Silica NP a concentration of 0,5 mg/ml can be used. For non-colloidal aggregated Silica NP a concentration of 2,5 to 25 mg/ml can be used. Grid on drop provides good results for colloidal NP. For NP in suspension, apolar NP and NP in low concentration the drop-on-grid method is preferred since it improves contact between grids and NP.

Comment 4: The additional washing step reduces the background signal of the grid by removing excess salt and material of large aggregates. It also prevents the dry-out of the grid and the crystallization of the salts.

Co-funded by
the Health Programme
of the European Union

● Contact ●

Website:
www.nanogenotox.eu

E-mail:
nanogenotox@anses.fr

Coordinator: French Agency for Food, Environmental and Occupational Health & Safety (ANSES)

27-31, avenue du Général Leclerc
94701 Maisons-Alfort Cedex
France

Partners

French Agency for Food, Environmental and Occupational Health Safety (France)	ANSES	anses
Federal Institute of Risk Assessment (Germany)	BfR	BfR
French Atomic Energy Commission (France)	CEA	cea
Institute of Mineralogy and Crystallography (Bulgaria)	IMC-BAS	
Veterinary and Agrochemical Research Centre (Belgium)	CODA-CERVA	
Finnish Institute of Occupational Health (Finland)	FIOH	Finnish Institute of Occupational Health
Roumen Tsanev Institute of Molecular Biology Academy of Sciences (Bulgaria)	IMB-BAS	
Institut national de recherche et de sècurité (France)	INRS	inrs
National Health Institute Doutor Ricardo Jorge (Portugal)	INSA	
Scientific Institute of Public Health (Belgium)	IPH	isp WIV
Institut Pasteur of Lille (France)	IPL	Institut Pasteur de Lille
Istituto superiore di sanità (Italy)	ISS	
The Nofer institute of Occupational Medicine (Poland)	NIOM	
National Research Centre for the Working Environment (Denmark)	NRCWE	NATIONAL RESEARCH CENTRE FOR THE WORKING ENVIRONMENT
National Institute for Public Health and the Environment (The Netherlands)	RIVM	rivm
Universitat Autònoma de Barcelona (Spain)	UAB	UAB Universitat Autònoma de Barcelona

Co-funded by
the Health Programme
of the European Union

Grant Agreement n° 2009 21 01